INL/RPT-22-69214
Revision 0

# Multilevel Analysis, Design, and Modeling of Coupling Advanced Nuclear Reactors and Thermal Energy Storage in an Integrated Energy System

**September 2022**

Rami M. Saeed
Amey Shigrekar
Daniel Mikkelson
Aidan C.G. Rigby
Courtney M. Otani
Marisol Garrouste
Konor L. Frick
Shannon Bragg-Sitton

***Idaho National Laboratory***

IES
Integrated Energy Systems

INL/RPT-22-69214
Revision 0

# Multilevel Analysis, Design, and Modeling of Coupling Advanced Nuclear Reactors and Thermal Energy Storage in an Integrated Energy System

**Rami M. Saeed**
**Amey Shigrekar**
**Daniel Mikkelson**
**Aidan C.G. Rigby**
**Courtney M. Otani**
**Marisol Garrouste**
**Konor L. Frick**
**Shannon Bragg-Sitton**

**September 2022**

**Idaho National Laboratory**
**Integrated Energy Systems**
**Idaho Falls, Idaho 83415**

**http://www.ies.inl.gov**

**Prepared for the**
**U.S. Department of Energy**
**Office of Nuclear Energy**
**Under DOE Idaho Operations Office**
**Contract DE-AC07-05ID14517**

*Page intentionally left blank*

# ABSTRACT

This report discusses the different options for coupling thermal energy storage (TES) systems to advanced nuclear power plants (A-NPPs) in order to enable flexible and hybrid plant operation. An advanced light-water reactor (A-LWR), a high-temperature gas-cooled reactor (HTGR) and a liquid-metal fast reactor (LMFR) were selected as the initial use cases for demonstrating a thermally balanced energy storage coupling design for thermal power extraction.

The models presented herein showcase several design considerations, focusing on optimal deployment methodologies for achieving steady-state and transient-state operation with minimum disruption to the nuclear power cycle. This first part of the study presents steady-state models developed using Aspen HYSYS®, with the thermal energy bypass for NPP-TES coupling being varied at up to 50%. The various components were sized using the Aspen Process Economic Analyzer (APEA) and Aspen Exchanger Design and Rating (EDR), when applicable. Cost functions from these models were developed using the latest publicly available data obtained from APEA V11. The TES-coupled A-NPP steady-state models and cost functions then provided a baseline for dynamic operation and process optimization by using Idaho National Laboratory (INL)'s Framework for Optimization of Resources and Economics (FORCE) tools.

A stochastic optimization of the various energy storage systems coupled to the A-NPPs was then performed using the Risk Analysis Virtual Environment (RAVEN) and its dispatch optimization plugin, the Holistic Energy Resource Optimization Network (HERON). The signal processing and synthetic history capabilities of RAVEN were used to account for the unpredictable behavior of electricity markets. An autoregressive moving average (ARMA) model was used to analyze price signals from the Pennsylvania-New Jersey-Maryland (PJM) market and were applied to the HERON analysis in order to optimize a system with the best economics.

Transient modeling evaluation was then performed using Modelica models within the HYBRID repository, which was developed at INL for the Department of Energy Integrated Energy Systems program for the characterization of dynamic integrated system behavior and feedback. This includes evaluation of the TES-coupled A-LWR systems' impact on physical and thermal system response during imposed system demands. Additional TES-coupled reactor types, coupling approaches, markets, and TES technologies will be evaluated in future work.

*Page intentionally left blank*

# CONTENTS

## FIGURES

## TABLES

# ACRONYMS

| | |
|---|---|
| A-LWR | advanced light-water reactor |
| A-NPP | advanced nuclear power plant |
| APEA | Aspen Process Economic Analyzer |
| ARMA | autoregressive moving average |
| BOP | balance of plant |
| CAPEX | capital expenditure |
| CCV | charging control valve |
| C-IHX | charge intermediate heat exchanger |
| CSP | concentrated solar power |
| DCV | discharging control valve |
| D-IHX | discharge intermediate heat exchanger |
| EDR | Aspen Exchanger Design and Rating |
| FORCE | Framework for Optimization of Resources and Economics |
| FHV | feedwater heating valve |
| FWCP | feedwater control pump |
| FWH | feedwater heater |
| HERON | Holistic Energy Resource Optimization Network |
| HDR | Heat Diversion Ratio |
| HTGR | high-temperature gas-cooled reactor |
| IES | integrated energy systems |
| IHEX | intermediate heat exchanger |
| INL | Idaho National Laboratory |
| LMFR | liquid-metal cooled fast reactor |
| LWR | light-water reactor |
| MAPE | mean absolute percentage error |
| NPP | nuclear power plant |
| NREL | National Renewable Energy Laboratory |
| PRISM | Power Reactor Innovative Small Module |
| RAVEN | Risk Analysis Virtual Environment |
| SMR | small modular reactor |
| TBV | turbine bypass valve |
| TCV | turbine control valve |
| TES | thermal energy storage |

# Multilevel Analysis, Design, and Modeling of Coupling Advanced Nuclear Reactors and Thermal Energy Storage in an Integrated Energy System

## 1. INTRODUCTION

The Department of Energy (DOE) Office of Nuclear Energy (NE) Integrated Energy System (IES) Program is evaluating thermal energy storage (TES) systems in support of the current fleet of nuclear power plants (NPPs) as well as advanced NPPs (A-NPPs), with a focus on accommodating flexible power generation across multiple energy markets. A key component of these recent research efforts is exploring how nuclear energy can be used for purposes other than traditional electricity generation. A-NPPs may be tasked to operate in environments in which flexible power generation is more valuable than baseload generation. TES systems would enable NPPs to nimbly respond to market variability and could also enable A-NPPs to participate in multi-commodity markets, thus enhancing their economic competitiveness. Figure 1, which shows an example of a thermally coupled IES, represents one such possible IES architecture. In a thermally coupled IES configuration, the nuclear reactor provides baseload heat or power and operates at a high-capacity factor to cover operating and capital costs. TES is used to attenuate the dynamics of subsystems or defer energy delivery to a later time. This enables the reactor to operate at or near steady-state design conditions, enhancing performance and minimizing maintenance costs. Depending on the amount of heat dispatched to thermal storage, the amount of power generated from the balance of plant (BOP) can be ramped up or down, thus allowing for flexible generation. Heat recovered from storage can be used either directly and fed to the power generation cycle or sent to an industrial process when coupled within an IES. Note that this configuration represents one possible scenario, and that the specific need for and potential benefits of energy storage may differ in other IES architectures.

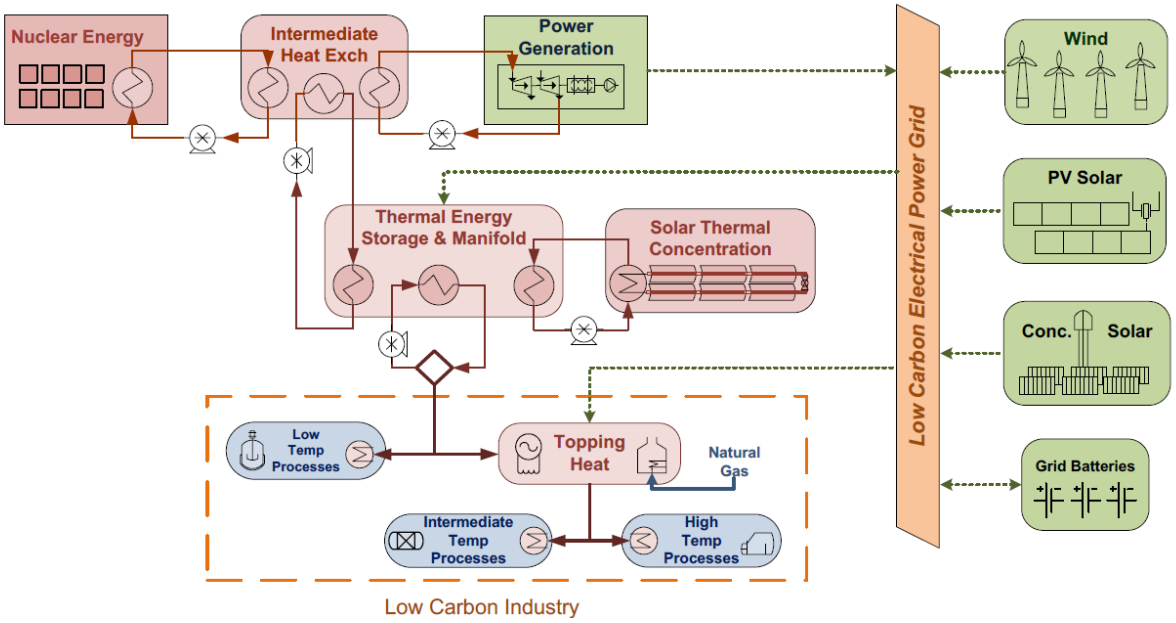


Figure 1. General architecture for a thermally coupled IES.

In previous work, Idaho National Laboratory (INL) evaluated the suitability of several TES technologies for coupling with A-NPPs, based on qualitative and merit indicators. Two-tank molten-salt, solid-media, and latent-heat TES systems were deemed well suited for coupling with a wide range of

A-NPPs featuring different reactor sizes and temperatures [1][2]. These findings, coupled with previous work in the field [3], provide the starting point for a more in-depth analysis.

This work focuses on analyzing the steady-state and component-level cost functions of NPP-TES coupling options for enabling flexible and hybrid plant operation. This is followed by a preliminary analysis of the transient controls and grid-wide economics of each coupling design. In a volatile market, an integrated setup of this kind would enable energy storage during periods of oversupply, dispatching it to produce electricity during periods of high demand or for use as heat by industrial users. To date, model development has included the following:

1. Creation of steady-state Aspen HYSYS® systems-level BOP models of two advanced nuclear reactors (an advanced light-water reactor [A-LWR] and a high-temperature gas-cooled reactor [HTGR]), each for three TES coupling methods, with three different thermal energy bypass ratios (i.e., heat diversion ratios [HDRs]). To date, liquid-metal fast reactor (LMFR) model development has included systems-level BOP models for TES coupling at one HDR, in addition to one coupling method.
2. Creation of cost functions derived from the fully balanced A-LWR and HTGR models as a function of different system sizes.
3. Creation of Aspen HYSYS® systems-level BOP models for a LMFR for one TES coupling method, with upward of 50% thermal energy bypass.
4. Development of a stochastic optimization approach that includes (a) evaluation of price signals from the Pennsylvania-New Jersey-Maryland (PJM) market, using an autoregressive moving average (ARMA) model, and (b) use of the ARMA model to perform stochastic optimization of the nuclear coupled energy storage system by utilizing the Risk Analysis Virtual Environment (RAVEN) tool and its dispatch optimization plugin, the Holistic Energy Resource Optimization Network (HERON). Initial runs are currently being performed for the TES-coupled A-LWR and HTGR use cases in order to optimize their technoeconomic viability.
5. Development of transient state and characterization of dynamic integrated system behavior and feedback by using Modelica models within the HYBRID repository, focusing on implementing the three coupling methods for the light-water-type small modular reactor (SMR) candidate systems.

The different thermal energy bypass ratios, or HDRs, were analyzed to understand how thermal power extraction impacts overall system efficiency, and to perform parametric studies by varying the HDRs away from the turbine.

Holistic Energy Resource Optimization Network (HERON) is a software framework for constructing workflows to solve complex resource allocation problems and meet target economic goals [4]. As a modeling toolset, it is used as a RAVEN plugin to accelerate stochastic technoeconomic assessment of the economic viability of various grid-energy system configurations, especially with application to electrical grids and IES.

Dynamic modeling evaluation uses Modelica IES models constructed from components in the HYBRID repository [5]. The HYBRID repository primarily contains Modelica models designed at INL for characterizing dynamic integrated system behavior and feedback. Through the use of HYBRID modeling, various control and integration strategies can be implemented to evaluate their impact on physical and thermal system response, maximize ramping capabilities, and support both quantitative and qualitative analysis of the impact of dynamic operation.

## 2. BACKGROUND

TES technologies accumulate and release energy by heating, cooling, melting, or solidifying a storage medium so the stored energy can later be used for various applications (i.e., power generation) by simply reversing the process. When coupled with NPPs, TES technologies store excess thermal energy not being used for power production. This energy is later recovered to generate heat or electrical power during

periods of high demand/pricing for grid electricity. In this manner, NPPs can operate at maximum capacity without having to load follow to match market demands, thereby improving their economics, increasing their efficiency, and reducing mismatches between the energy supply and the demand.

While TES technologies can be classified in many ways, such classifications are generally based on three common approaches to energy storage: sensible heat, latent heat, and thermochemical energy. In previous work, two-tank molten-salt energy storage systems were studied in detail for integration with NPPs [3],[5]. Due to this technology's low-cost potential, high technology readiness level, and ability to be integrated with existing or future power plants (e.g., NPPs), and because this technology has already been widely studied and deployed, it was selected in this work as a prime candidate for coupling with A-NPPs. Other thermal storage technologies will be evaluated similarly in future work.

The two-tank system is considered the most common form of sensible heat storage technology for medium- and high-temperature (200–600°C) applications that require hours of storage capacity. This TES technology has already been deployed on a large scale in concentrated solar power (CSP) plants. Operation of this TES system involves using two large tanks, each capable of storing the entire mass of the storage medium; a heat source to charge the TES system; and a power block to discharge it. Figure 2 shows schematics of a two-tank TES system coupled to two different CSP plant configurations.

For the two-tank TES designs, further classification can be made as to whether the heat storage medium is heated directly by the heat source or indirectly via a heat transfer fluid. During the charge cycle in the indirect heating setup, the storage medium is pumped from the cold tank, through an intermediate heat exchanger (IHEX) that couples the TES system to the heat source, and into the hot tank for storage. During the discharge cycle, the system operates in reverse by depositing its heat to a fluid that is then sent to the power block. The power block uses the heated fluid to produce steam, which is then expanded in a turbine to generate electricity. The direct heating setup differs only in the charging phase, since the storage medium is directly heated by the heat source prior to transfer to the cold tank. Figure 2 shows a schematic of a coupling between concentrated solar power collectors and a two-tank TES design. A similar representation of a potential two-tank TES system coupled to a NPP is also shown in Figure 3. A light-water reactor (LWR)-design-based NPP-TES coupling would use steam as the working fluid to charge the tanks. During the discharge, feedwater could be used to produce steam that could then be sent to a later stage in the turbine train to produce additional power.

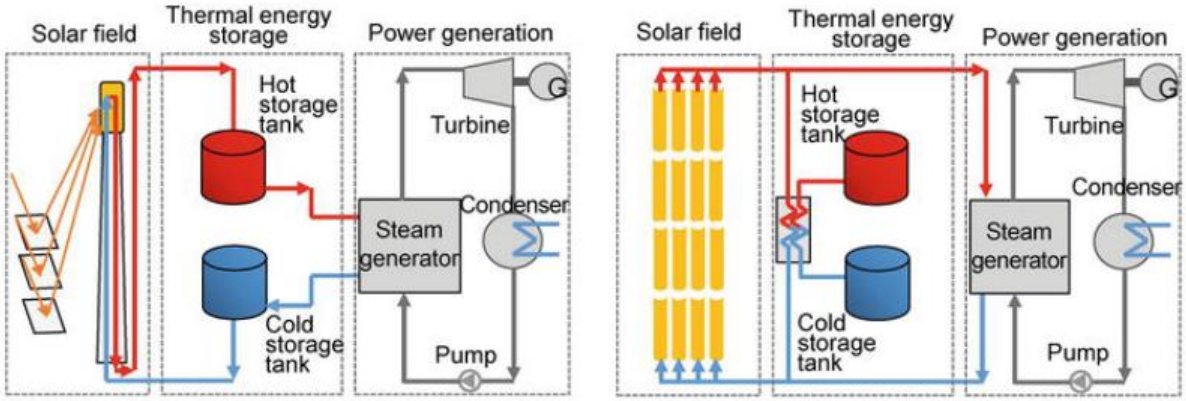


Figure 2. Schematics of a two-tank TES system connected to a solar-power- and a trough-based CSP [7].

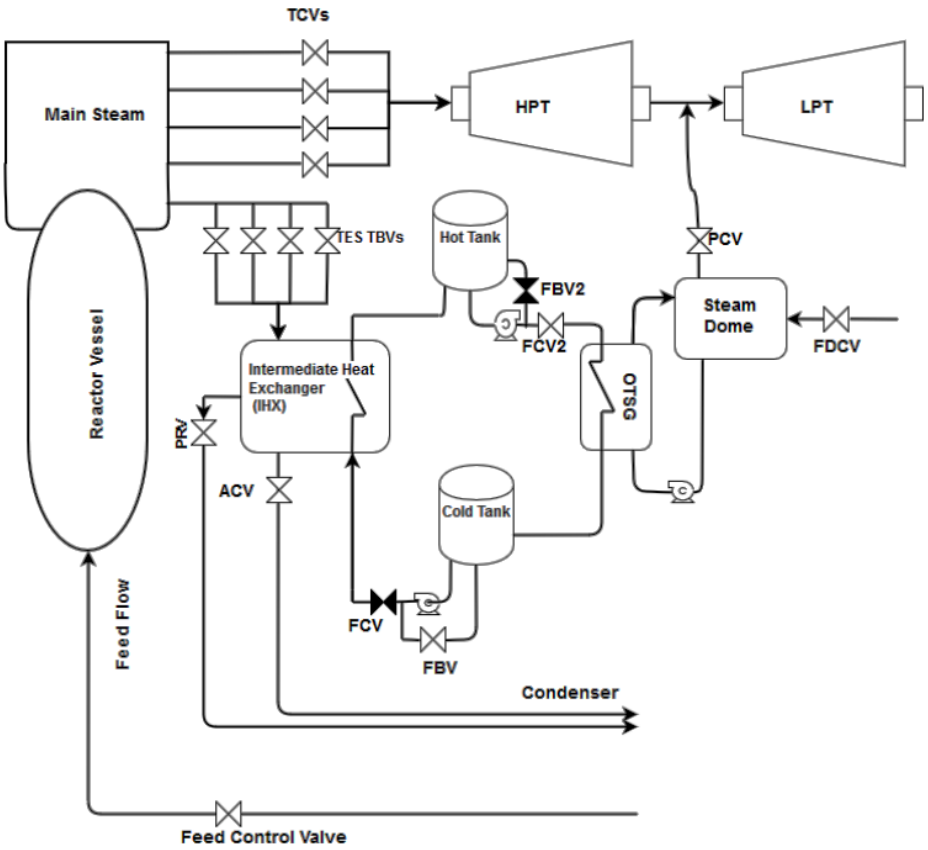


Figure 3. Schematic demonstrating a coupling between a nuclear reactor and a two-tank TES system [3].

Molten salts are prime candidates for heat storage, as they are very well understood and possess useful characteristics (e.g., low vapor pressure and high thermal conductivity). They are also low in cost and present a low degree of risk during accidents, as they solidify when they leak and cool down. Hitec and solar salt were selected as the heat transfer fluid and storage mediums for the two-tank TES systems in this study. Due to the reactor outlet temperatures for the two reactor types analyzed herein, Hitec was chosen for the A-LWR case, while solar salt was chosen as the medium for the HTGR case. Molten salts were chosen over other synthetic and organic fluids for the following reasons: (1) they are stable at the operating temperatures of the reactors selected for this study, (2) they remain liquid under atmospheric pressure at near the reactor coolant temperatures, and (3) they are very competitively priced compared to other energy storage materials well suited to this storage temperature (e.g., thermal oil). Additional details on why Hitec salt was chosen for the A-LWR and solar salt was chosen for the HTGR are given in Sections 2.1.1 and 4, respectively.

Table 1. Thermophysical properties of Hitec salts [8].

| Energy Storage Material | Melting point [ºC] | Stability limit [ºC] | Sensible heat storage [kJ/kg.K] | Density (solid) [kg/m$^3$] | Density (liquid) [kg/m$^3$] |
|---|---|---|---|---|---|
| $NaNO_3$-$KNO_3$-$NaNO_2$ (7-49-44 mol%) (7-53-40 wt%) | 142 | 535 | 1.38 @180°C | 2007 @100°C | 1945 @180°C |
| $NaNO_3$-$KNO_3$ (60-40 wt%) | 222 | 600 | 1.47 @180°C | | 1908 @260 °C |

## 2.1 Advanced Nuclear Power Plant – Case Studies

As mentioned, the goal of this case study was to analyze the coupling of TES technologies featuring high technology readiness levels to various A-NPP options that operate over a wide temperature range. Three advanced nuclear reactor technologies were considered for achieving this target: (1) A-LWR, (2) HTGR, and (3) LMFR.

### 2.1.1 Advanced Light-Water Reactor (A-LWR)

The first NPP design investigated in this study is a light-water-based SMR. As the operating conditions of the NuScale SMR are readily available, they served as a baseline for developing the BOP models in Aspen HYSYS®. The primary loop of the NuScale reactor module contains saturated liquid water, which transfers heat to feedwater via the steam generators to produce steam, which is then dispatched for electricity generation. This steam was chosen as the primary heat transfer fluid during the charging cycles in the A-LWR cases.

Using the design certification application that NuScale submitted to the U.S. Nuclear Regulatory Commission, a detailed steady-state model of its BOP was developed in Aspen HYSYS® [11]. However, to reduce the complexity of the analysis carried out in this work, an equivalent simplified model of the steam and power conversion system was also developed (see Figure 4). For better readability, the detailed model is presented in landscape format in Appendix A. The simplified model applies the same operating conditions to its major components (e.g., steam generator, turbine, and condenser). Although the pumping power slightly differed due to the simplified model's lack of a feedwater heater (FWH) train, the system's overall thermal efficiency was maintained.

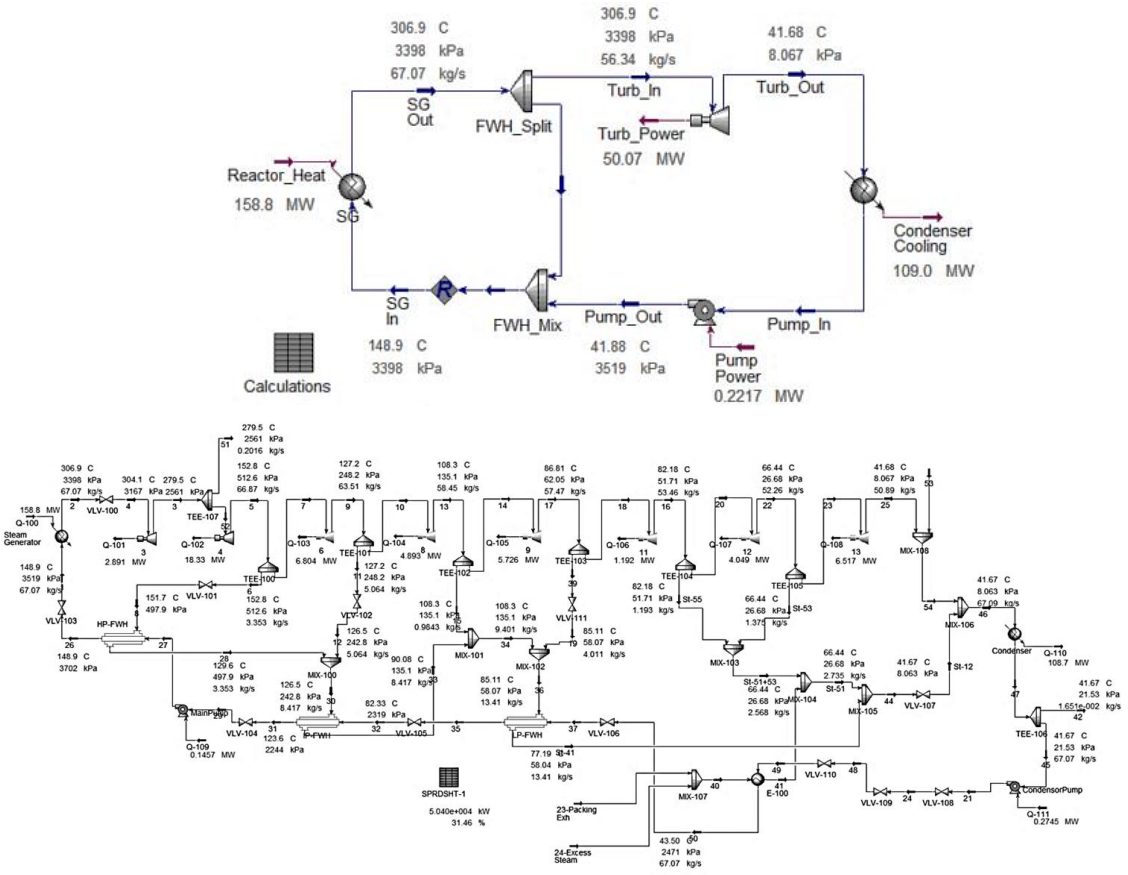


Figure 4. Aspen HYSYS® models of the detailed (bottom) and simplified (top) NuScale BOP system (also presented in larger landscape format in Appendix A).

To ensure that this simplification did not affect the technoeconomic evaluation carried out in the next steps, a cost analysis of both these designs was conducted by sizing each component within the two models and then using the Aspen Process Economic Analyzer (APEA) to acquire their costs. The two models showed less than a 2.8% difference with each other in terms of installed costs.

To establish a basis for developing the steady-state models, the NuScale BOP and operating conditions used in this study are listed in Table 2. These conditions were extracted from the NuScale Standard Plant Design Certification Application that NuScale submitted to the U.S. Nuclear Regulatory Commission [14].

Table 2. Operating conditions of the NuScale power conversion system [14].

| Component | Power (MW) | Mass flow rate (kg/s) | Inlet temperature (°C) | Inlet pressure (kPa) |
|---|---|---|---|---|
| Steam generator | 158.8 | 67.07 | 148.9 | 3519 |
| Turbine | 49.02 | 55.15 | 306.9 | 3398 |
| Condenser | 110 | 55.15 | 41.68 | 7 |
| Condenser feedwater pump | 0.396 | 2349 | 26.67 | 101.3 |
| BOP pump | 0.216 | 55.15 | 27.11 | 7 |

As opposed to HTGRs, the NuScale steam generator has a steam outlet temperature of about 307°C and a pressure of 3398 kPa. However, due to the limitations imposed by the steam saturation point, it can only heat the Hitec salt to a maximum of 240°C (i.e., ~100° above its melting point). The design considerations discussion in Section 4 explains this technical limitation in greater detail. The fact that the cold storage tank temperature must be maintained at ~40° above the melting point of Hitec salt allows for a maximum of ~100° between the cold and hot tank temperatures. Such a small difference necessitates a large mass of molten salt in order to store a given amount of heat, as opposed to cases involving storage media with lower melting points or reactors with higher outlet temperatures—cases that will be explored in future studies.

Synthetic oils are also good heat storage media candidates. In previous work, several storage media (Hitec [$NaNO_3$-$KNO_3$-$NaNO_2$: 142°C melting point] Hitec XL [$NaNO_3$-$KNO_3$-$Ca[NO_3]_2$: 120°C melting point], Therminol-66, and Dowtherm A) were evaluated over temperature ranges similar to those considered in this study. Of these, a simple technoeconomic analysis (TEA) revealed that Hitec salt affords the lowest levelized cost of storage for both short (6 hours) and long (12 hours) durations [9]. The results of this comparison are summarized in Table 3, based on a discharge capacity of 500 MWe and a charging cost of $30/MWh.

Table 3. Comparison of energy storage options for a power arbitrage discharge capacity of 500 MWe and a charging cost of $30/MWh.

| Storage Option | Melting Point (°C) | Cost ($/kg) | Capital Cost per Unit of Stored Energy ($/kWh) | Levelized Cost of Storage (breakeven) ($/MWh-e) |
|---|---|---|---|---|
| Hitec | 142 | 0.93 | 212 (6h)<br>174 (12h) | 109 (6h)<br>97 (12h) |
| Hitec XL | 120 | 1.19 | 218 (6h)<br>181 (12h) | 111 (6h)<br>99 (12h) |
| Therminol-66 | -32 | 6.72 | 533 (6h)<br>496 (12h) | 209 (6h)<br>197 (12h) |
| Dowtherm A | 15 | 3.96 | 401 (6h)<br>361 (12h) | 168 (6h)<br>156 (12h) |

### 2.1.2 High-temperature Gas-cooled Reactor (HTGR)

The second NPP design investigated is a HTGR. As the operating conditions of the X-energy reactor (Xe-100) are readily available, they served as a baseline for developing the Aspen HYSYS® BOP models. To establish a basis for developing the steady-state models, the operating conditions are listed in Table 4.

Table 4. Operating conditions of the Xe-100 power conversion system [15].

| Component | Power (MW) | Mass flow rate (kg/s) | Inlet temperature (°C) | Inlet pressure (kPa) |
|---|---|---|---|---|
| Steam generator | 203 | 76.87 | 193.3 | 19800 |
| Turbine | 87.01 | 61.77 | 565 | 16500 |
| Condenser | 116.6 | 61.77 | 39.01 | 3.24 |
| Condenser feedwater pump | 0.453 | 2685 | 26.67 | 101.3 |
| BOP pump | 1.369 | 61.77 | 39.01 | 3.24 |

HTGRs could potentially offer a larger ΔT between the maximum hot tank storage temperature and the cold tank temperature. As opposed to LWRs, the steam generator in a HTGR (taking Xe-100 as a case study) has a steam outlet temperature of about 565°C and a pressure of 16500 kPa. Under these conditions, the design limitation imposed by the steam saturation point is more forgiving, as it can heat the storage material up to 400°C without causing a temperature cross (further explained in section 4) in the TES charge IHX (C-IHX). The design considerations discussion in the "Molten salt maximum design temperature" section in Section 4 explains this technical limitation in greater detail. These operating conditions enable the use of molten salts with higher melting temperatures and operating temperature thresholds. For this particular case, an ideal storage material candidate is solar salt, which is a two-component mixture of potassium nitrate and sodium nitrate and has a melting point of about 222°C for $NaNO_3$-$KNO_3$ (60–40 wt%). Another advantage is that, historically, solar salt is cheaper (0.49 $/kg) than Hitec (0.93 $/kg) [16]. A more detailed discussion on the current and historical costs of various energy storage materials is provided in the cost functions analysis given in Section 5.

### 2.1.3 Liquid-Metal Fast Reactors (LMFRs)

The third NPP design investigated is the LMFR. As the operating conditions of the GE Hitachi Nuclear Energy reactor, known as Power Reactor Innovative Small Module (PRISM), are readily available, this reactor served as a baseline for developing the BOP models in Aspen HYSYS® for the LMFR use case. PRISM is one of only a few designs for which sufficient information on its power conversion cycle is available in the public domain. To establish a basis for developing the steady-state models, the data available on the operating condition for PRISM were taken from the Preliminary Safety Information Document that General Electric prepared for the U.S. Department of Energy [17][18]. The BOP and operating conditions of PRISM are listed in Table 5.

Table 5. Operating conditions of the PRISM power conversion system [17][18].

| Component | Power (MW) | Mass flow rate (kg/s) | Inlet temperature (°C) | Inlet pressure (kPa) |
|---|---|---|---|---|
| Steam generator | 1680 | 759 | 221.8 | 14720 |
| Turbine | 622 | 563 | 452.2 | 14720 |
| Condenser | 1067 | 563 | 40.60 | 7.619 |
| Condenser feedwater pump | 0.439 | 25500 | 26.65 | 101.3 |
| BOP pump | 9.277 | 563 | 40.22 | 7.467 |

In future work, the steady-state models at various HDRs and under different coupling options will be created in Aspen HYSYS®. These models will then be used to create cost functions for use in HERON, and to provide the initial conditions and optimum dispatch profiles for the transient process models and control schemes that will be created using HYBRID.

As in the HTGR cases, the LMFR will offer a larger ΔT between the maximum hot tank storage temperature and the cold tank temperature. As opposed to LWRs, the steam generator in a LMFR (taking PRISM as a case study) has a steam outlet temperature of about 452.2°C and a pressure of 14720 kPa. Under these conditions, the design limitation imposed by the steam saturation point is more forgiving, as it can heat the storage material up to 363°C without causing a temperature cross in the TES C-IHX. The design considerations discussion in the "Molten salt maximum design temperature" section in Section 4 explains this technical limitation in greater detail. These operating conditions enable the use of molten salts with higher melting temperatures and operating temperature thresholds. For this particular case, the ideal storage material candidate is solar salt, which offers cost advantages over Hitec. A more detailed discussion on the current and historical costs of various energy storage materials is provided in the cost functions analysis given in Section 5.

## 2.2 NPP-TES Coupling Options

All three NPP-TES coupling options covered in this study were selected in order to minimize the impacts on the NPP, such that nuclear reactor operations can continue without affecting the NPP or its operating license. In each of the coupling options, the TES molten-salt system was designed to maintain the working fluid temperatures in the cold tank at 180 and 260°C for the LWR and HTGR, respectively (at least 38° above the melting point of each). During the charge cycle, superheated steam was used to heat the molten salt to 240 and 400°C for the LWR and HTGR, respectively (i.e., the technical heating limits for each reactor type), and the molten salt was then transferred to the hot tank for storage. The TES loop operates at a pressure of 120 kPa. During the discharge, the hot molten-salt fluid is run through a different heat exchanger that converts a stream of feedwater into saturated steam for heat dispatch to industrial users or for power generation (as is the case in the three scenarios covered in this study).

A key attribute of the two-tank TES system is that it can discharge molten salt at a constant temperature, indicating the ability to maintain constant power delivery or thermal energy dispatch in real-world applications, as reflected in the current steady-state Aspen HYSYS® models. The three coupling options investigated in this work are:

- Option 1 – Standalone NPP-TES coupled with a secondary power generation cycle
- Option 2 – Directly coupled NPP-TES system
- Option 3 – Integrated NPP-TES coupled with an oversized primary turbine.

### 2.2.1 Option 1 – Standalone NPP-TES Coupled with a Secondary Power Generation Cycle

The first option entails diverting heat from the primary BOP during the charge cycle to heat the fluid flowing from the cold tank to the hot tank. During the discharge cycle, a secondary steam Rankine power generation setup is employed. Figure 5 shows simplified process flow diagrams of the first coupling option.

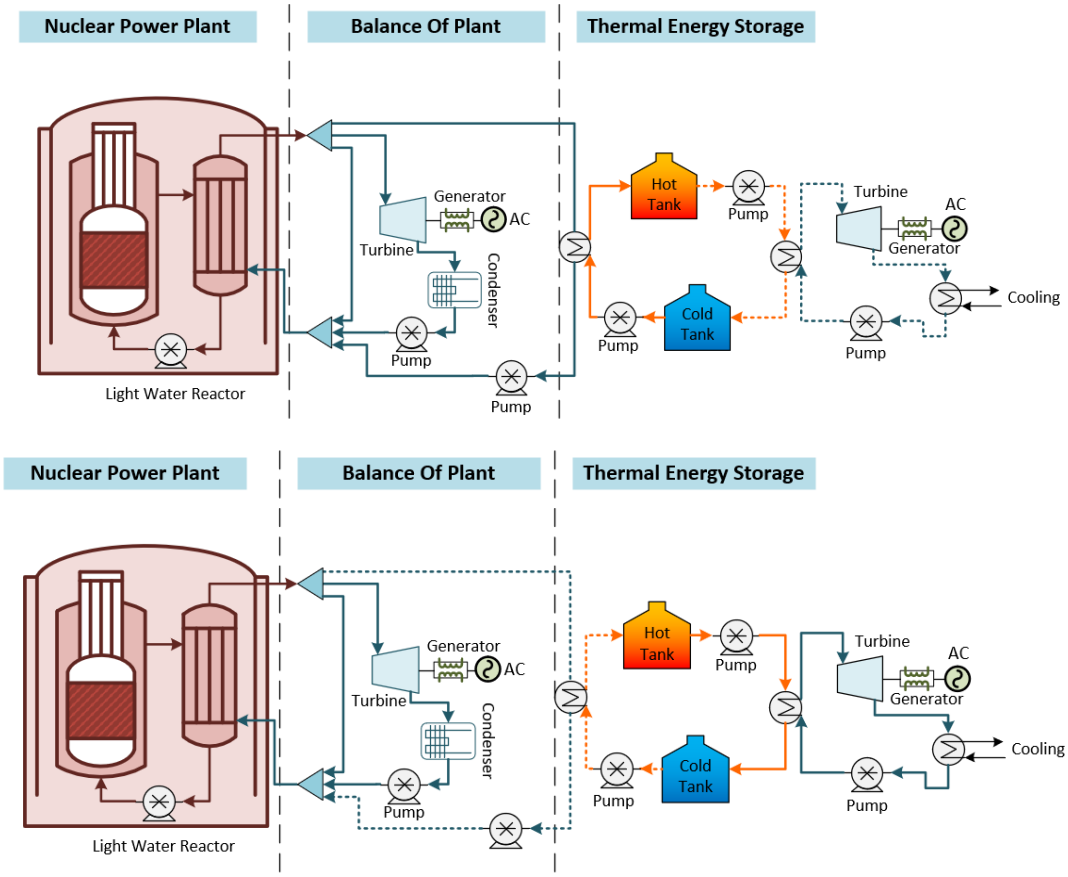


Figure 5. Simplified process flow diagrams of the first coupling option, showing the charge (top) and discharge (bottom) cycles (solid lines represent active streams and dashed lines represent standby cycles).

### 2.2.2 Option 2 – Directly Coupled NPP-TES System

The second coupling option involves direct heat transfer from the NPP to the TES system, which independently and directly discharges thermal energy to the BOP and feeds the primary Rankine power generation. A simplified process flow diagram of the second option is shown in Figure 6.

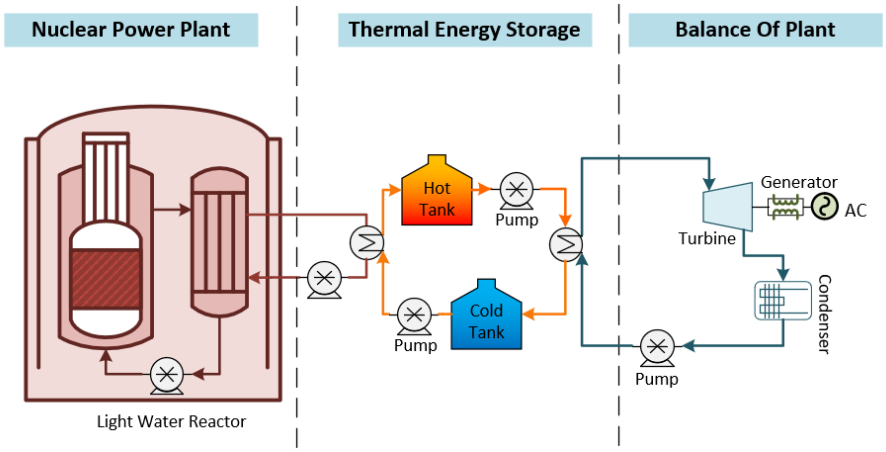


Figure 6. Simplified process flow diagram of the second coupling option, showing the combined operation of the charge and discharge cycles.

### 2.2.3 Option 3 – Integrated NPP-TES Coupled with an Oversized Primary Turbine

The third coupling option involves heat diversion from the NPP to the TES system during the charge cycle. During the discharge cycle, thermal energy is utilized to deliver steam to one of the low -pressure turbines in the primary turbine train assembly (details not shown here). Simplified process flow diagrams of this coupling option are shown in Figure 7.

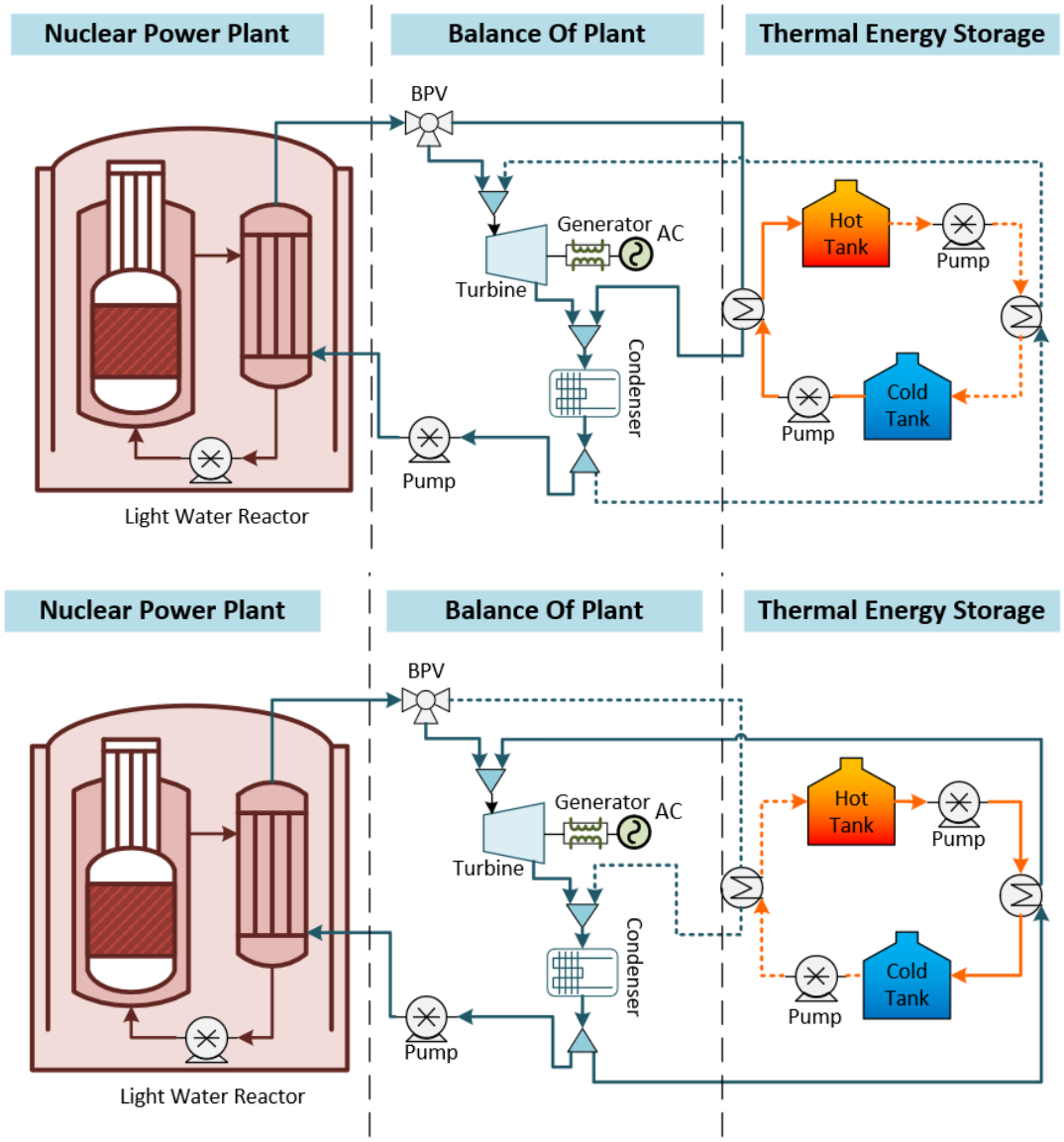


Figure 7. Simplified process flow diagrams of the third coupling option, showing the charge (top) and discharge (bottom) cycles.

It should be noted that although Figure 5, Figure 6, and Figure 7 show the coupling for the A-LWR case, this coupling is similar to that of the HTGR system.

# 3. DEVELOPMENT OF ASPEN HYSYS® STEADY-STATE MODELS

To enable TES integration with A-NPPs, this work analyzed three different coupling options—with various amounts of thermal power extraction—via Aspen HYSYS®. The following sections provide details on each of the three coupling options, along with the LWR and HTGR reactor technologies serving as their primary heat source, the assumptions made in creating the models, and the results that were generated.

## 3.1 Advanced Light-Water Reactor

In all three methods of coupling TES with A-LWRs, the charge and discharge cycles were presented separately. In the following three subsections, a heat diversion of ~50% of the total steam production was chosen as the baseline for discussing the models. However, three thermal energy dispatch ratios (or HDRs)—50%, 25%, and 10%—were also created for the first and third coupling options and are summarized in Sections 3.1.1 and 3.1.3. All models and coupling methods were created with the goal of making the charge and discharge cycles last for 6 hours each.

To establish a basis for developing the steady-state models, steam from the steam generator was used as the heat transfer fluid to heat the storage medium during the charge cycle. The NuScale steam generator operating conditions used for this analysis are listed in Table 6.

Table 6. NuScale steam generator operating conditions.

| Parameter | Value |
|---|---|
| Mass flow rate (kg/hr) | $2.415 \times 10^5$ |
| Exit pressure (MPa) | 3.398 |
| Exit temperature (°C) | 306.9 |

As Hitec is not readily available as a fluid for use in Aspen HYSYS®, it was added to the Aspen library as a hypothetical fluid, based on the thermophysical properties acquired from the literature [19]. The Peng-Robinson equation of state was used to calculate the enthalpy and entropy of this newly added hypothetical fluid, whereas the NBS Steam package was used for the heat transfer fluid. The polynomial function and constants used for calculating Hitec's enthalpy, heat capacity, viscosity, thermal conductivity, and density are listed below. Here, $X$ is the temperature is degrees Celsius.

$$Property = a + b * X + c * X^2 + d * X^3 + e * X^4$$

Table 7. Polynomial function constants for Hitec thermophysical properties.

| Property: | Density | Thermal Conductivity | Viscosity | Heat Capacity | Enthalpy |
|---|---|---|---|---|---|
| Constants | (kgmole/m3) | (W/m-K) | (cP) | (kJ/kgmole-C) | (kJ/kgmole) |
| a | 8.9385E+00 | 7.8000E-01 | 1.4991E+02 | 4.6764E+02 | 7.4459E+04 |
| b | -2.8734E-03 | -1.2500E-03 | -5.8262E+03 | -2.5510E-01 | 1.1029E+03 |
| c | 5.1775E-17 | 1.6000E-06 | -2.2391E+01 | -2.8371E-15 | -1.0054E+00 |
| d | -6.6530E-20 | -1.8601E-21 | 1.1253E-05 | 3.2481E-18 | -1.0310E-03 |
| e | 3.1735E-23 | 7.6568E-25 | 0 | -1.3875E-21 | 3.7585E-07 |

To standardize the analyses of all three coupling options, the following assumptions were made when creating steady-state Aspen HYSYS® models for the LWR use cases:

- There is no heat loss from any of the BOP components, streams, or TES tanks.

- The cold tank temperature is 180°C, and the hot tank temperature is 240°C.
- The discharge power cycle is maintained in hot standby mode when not being utilized. The same applies to the charge cycle components when only the discharge cycle is active. Hot standby mode is achieved by diverting ~1% of the primary cycle's original mass flow needed to operate each cycle.
- The turbomachinery components were each operated at 90% isentropic and adiabatic efficiencies.
- The heat exchangers had a minimum approach temperature limit and pinch point (minimum difference between hot and cold at a given location) limit of 5°C, as shown in Figure 8. This also determines the maximum molten salt temperature possible for each scenario (more on this technical limitation in Section 4).
- The pressure drop across the heat exchangers is calculated based on the pressure drop value from the Aspen Exchanger Design and Rating (EDR).
- Molten-salt heat exchangers are sized using EDR with molten salt on the tube side and a heat source (high-pressure steam and condensation) on the shell side.
- Condensers are modeled as heat exchangers, with feedwater on the shell side and low-pressure condensate on the tube side. This is contrary to the convention of modeling them as surface condensers with the cooling water in the tubes and steam condensing on the tube surfaces. However, such a setting did not allow the condenser sizing algorithm to converge, thus preventing its cost analysis.

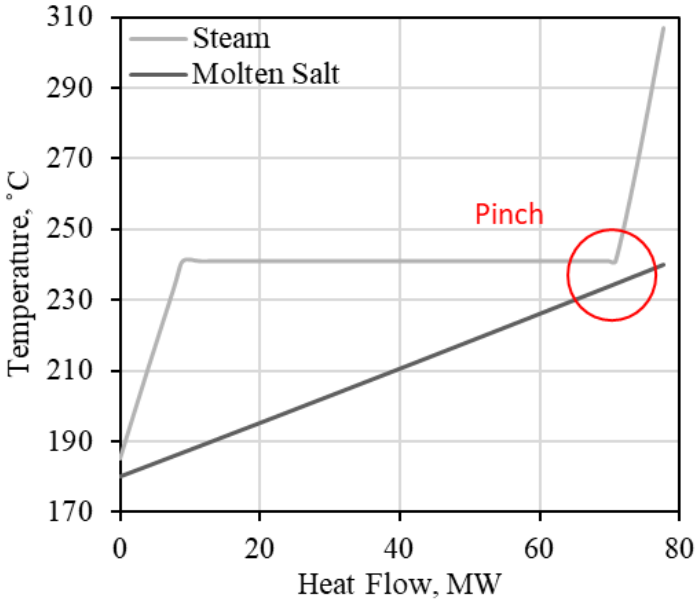


Figure 8. Intermediate heat exchanger temperature profile for the LWR case study.

### 3.1.1 Option 1: Standalone NPP-TES Coupled with a Secondary Power Generation Cycle

The overall setup of this model is based on drawing superheated steam from the main steam header, running it through the C-IHX, and condensing it into a subcooled liquid at ~195°C. This condensate is then returned to a mixer that simulates the FWH train in the BOP. Note that most BOP systems feature multiple FWHs, drawing steam from the turbine train at various stages. However, for the sake of simplicity, a steam mixer was used in this study. On the secondary side of the C-IHX, molten salt pumped from the cold tank absorbs the heat of the steam's condensation and is itself heated to ~240°C during

transfer to the hot tank for storage. For the charge cycle at a 50% HDR, the amount of steam diverted from the main steam header equals 50% of the total mass flow, whereas during the discharge cycle, the diversion only accounts for ~1% in order to maintain the inactive charge components/streams in hot standby mode. Based on the operating conditions of the steam, as well as the limitations imposed on the Hitec heat storage medium, the C-IHX had a charge power of ~72.57 $MW_{th}$. Thus, the total storage capacity of the TES system for the 6 hours of storage was calculated to be ~435.4 $MWh_{th}$. Similarly, other models under different HDRs (25% and 10%) were created and are summarized at the end of this section.

Figure 9 shows a process flow diagram of an active charge cycle (under coupling option 1) with a HDR of 50%, alongside the corresponding discharge cycle in hot standby mode (as developed in Aspen HYSYS®).

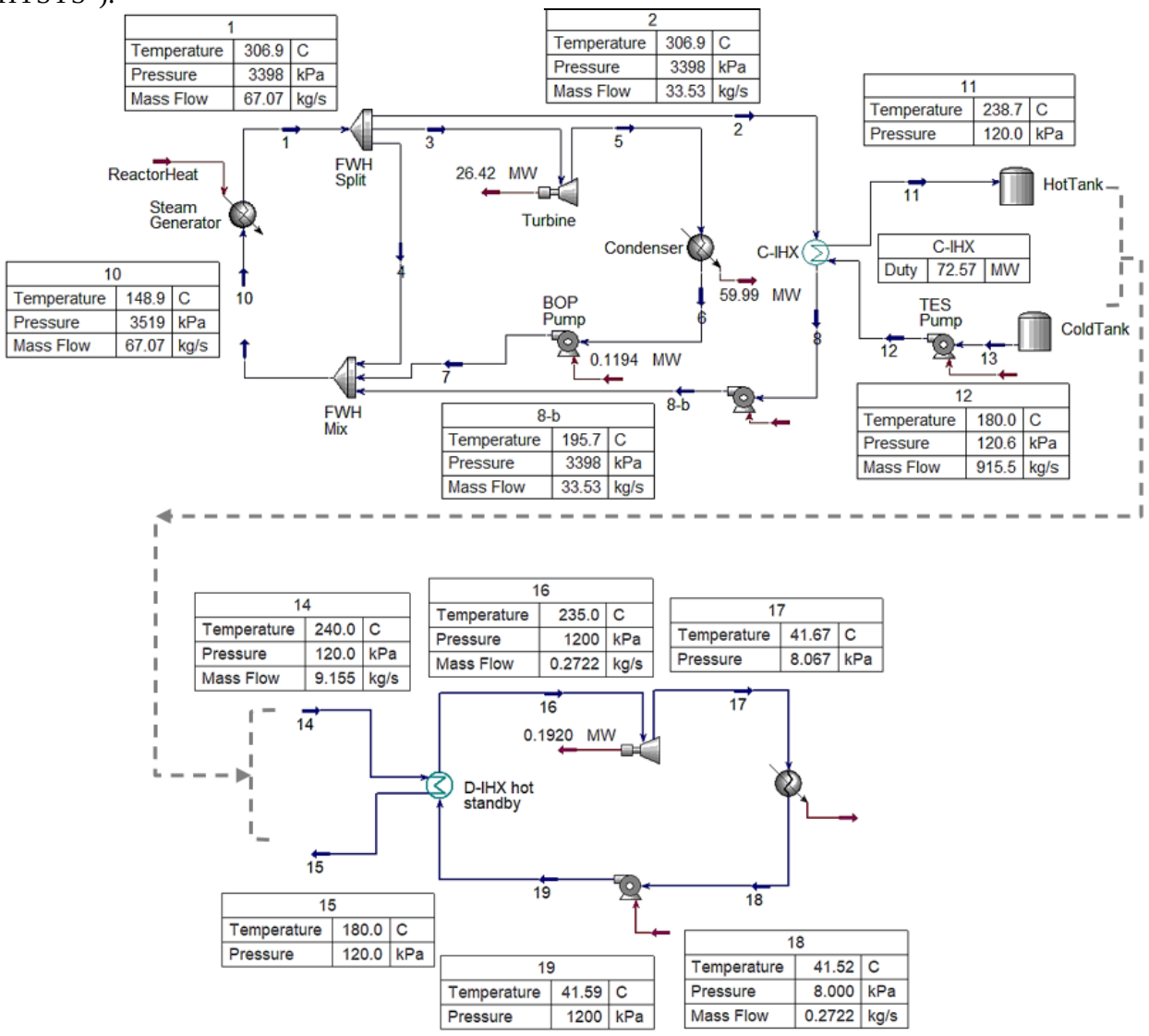


Figure 9. Process flow diagram of an advanced LWR-TES coupling with a standalone secondary TES power generation cycle (first coupling method) and a HDR of 50%, showing the active charge cycle (top) and inactive hot standby discharge cycle in hot standby mode (bottom).

A secondary discharge IHX (D-IHX) was designed to produce steam from feedwater during the discharge cycle, using the heat storage medium from the hot tank. During this process, hot salt is pumped

from the hot tank and through the D-IHX, at which point it deposits its heat into the feedwater before being transferred to the cold tank. This heat exchange process converts the feedwater into steam, which is then used to produce electricity via the secondary power cycle.

Figure 10 shows process flow diagrams of the BOP and active discharge cycle for the 50% HDR case.

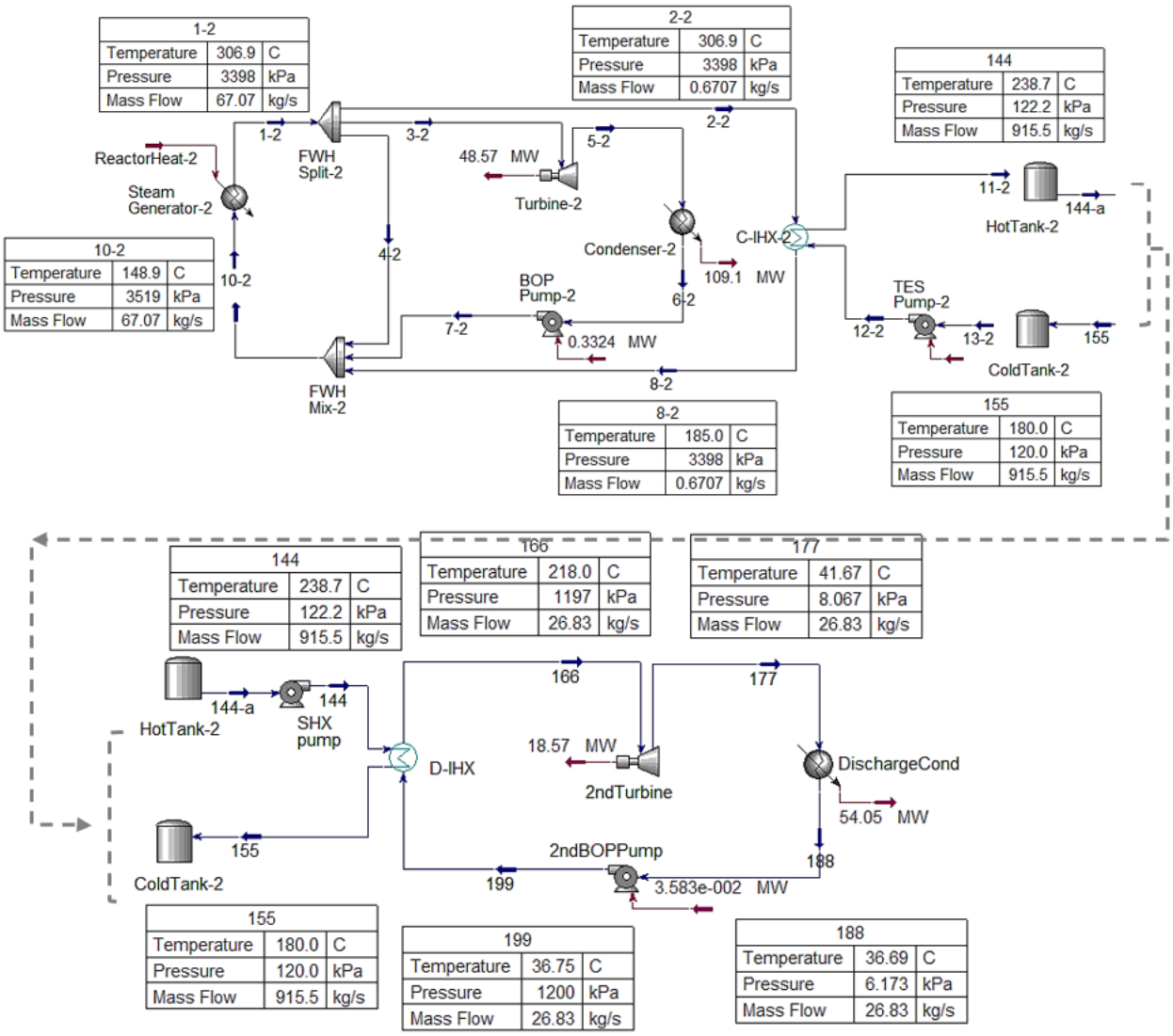


Figure 10. Process flow diagrams of an advanced LWR-TES coupling with a standalone secondary TES power generation cycle (first coupling method), showing the primary power generation cycle with an inactive charging cycle (top), as well as the active discharge cycle and secondary power generation cycle (bottom).

Now that the first coupling option has been discussed in detail for the 50% HDR case, the results in Table 8–Table 10 show the BOP and operating conditions for the different HDRs (50%, 25%, and 10%). The operation and overall structure of the models under these other HDRs are very similar to those seen in the 50% case discussed above. It should be noted that when the system is operating in power production mode (no charge or discharge), the TES components are in a standby mode, with a minimum flow of ~1% through the systems to maintain temperature. Section 4 and Figure 22 discuss and provide

the minimum flow split from the turbine stages to the FWH in order to maintain the steam generator inlet design point for all the HDRs.

Table 8. BOP and operating conditions of an A-LWR-TES coupling with a secondary power generation cycle and a HDR of 50%.

| Equipment | Cycle | Equipment size | Mass flow rate (kg/s) | Inlet temperature (°C) | Exit temperature (°C) |
|---|---|---|---|---|---|
| Charge HX (C-IHX) | Charge | 72.57 $MW_{th}$ | 33.53 (steam)<br>915.5 (salt) | 306.9 (steam)<br>180 (salt) | 195.7 (water)<br>238.7 (salt) |
| Discharge HX (D-IHX) | Discharge | 72.57 $MW_{th}$ | 26.83 (steam)<br>915.5 (salt) | 36.7 (water)<br>238.8 (salt) | 218 (stream)<br>180 (salt) |
| Cold tank pump | Charge | 0.00031 MW | 915.5 | 180 | 180 |
| Hot tank pump | Discharge | 0.00117 MW | 915.5 | 238.7 | 238.7 |
| TES power cycle pump | Discharge | 0.03580 MW | 26.83 | 36.69 | 36.75 |
| FWH pump | Charge | 0.00626 MW | 33.53 | 195.7 | 195.7 |
| NPP BOP pump | Charge | 0.11940 MW | 30.39 | 36.86 | 37.05 |
| BOP condenser | Charge | 59.99 MW | 30.39 | 41.68 | 36.86 |
| BOP condenser pump | Charge | 0.2075 MW | 1230 | 26.67 | 26.67 |
| TES condenser | Discharge | 54.05 MW | 26.86 | 41.67 | 36.69 |
| TES condenser pump | Discharge | 0.2195 MW | 1300 | 26.66 | 26.67 |
| BOP turbine | Charge | 26.42 $MW_e$ | 30.39 | 306.9 | 41.68 |
| BOP turbine | Discharge | 48.57 $MW_e$ | 55.81 | 306.9 | 41.68 |
| TES turbine | Discharge | 18.57 $MW_e$ | 26.83 | 218 | 41.67 |
| Molten salt | - | 19,774,800 kg | - | 238.7 (cold) | 180 (hot) |
| Cold/hot tanks | - | 435.42 $MWh_{th}$ | - | 238.7 (cold) | 180 (hot) |

Table 9. BOP and operating conditions of an A-LWR-TES coupling with a secondary power generation cycle and a HDR of 25%.

| Equipment | Cycle | Equipment size | Mass Flow rate (kg/s) | Inlet temperature (°C) | Exit temperature (°C) |
|---|---|---|---|---|---|
| Charge HX (C-IHX) | Charge | 36.35 $MW_{th}$ | 16.77 (steam)<br>547.8 (salt) | 306.9 (steam)<br>180 (salt) | 194.8 (water)<br>238.8 (salt) |
| Discharge HX (D-IHX) | Discharge | 36.35 $MW_{th}$ | 13.47 (steam)<br>547.8 (salt) | 40.34 (water)<br>238.8 (salt) | 217.9 (stream)<br>180 (salt) |
| Cold tank pump | Charge | 0.000165 MW | 457.8 | 180 | 180 |
| Hot tank pump | Discharge | 0.000133 MW | 457.8 | 238.8 | 238.8 |
| TES power cycle pump | Discharge | 0.0180 MW | 13.47 | 39 | 39.06 |
| FWH pump | Charge | 0.00312 MW | 16.77 | 194.8 | 194.8 |
| NPP BOP pump | Charge | 0.1633 MW | 43.06 | 35.59 | 35.77 |
| BOP condenser | Charge | 85.28 MW | 43.06 | 41.68 | 35.59 |
| BOP condenser pump | Charge | 0.3138 MW | 1860 | 26.66 | 26.67 |
| TES condenser | Discharge | 26.99 MW | 13.47 | 41.68 | 39 |
| TES condenser pump | Discharge | 0.0957 MW | 595 | 40.28 | 40.34 |
| BOP turbine | Charge | 37.44 $MW_e$ | 43.06 | 306.9 | 41.68 |
| BOP turbine | Discharge | 48.53 $MW_e$ | 55.81 | 306.9 | 41.68 |
| TES turbine | Discharge | 9.319 $MW_e$ | 13.47 | 217.9 | 41.68 |
| Molten salt | - | 9,888,480 kg | - | 238.8 (cold) | 180 (hot) |
| Cold/hot tanks | - | 218.1 $MWh_{th}$ | - | 238.8 (cold) | 180 (hot) |

Table 10. BOP and operating conditions of an A-LWR-TES coupling with a secondary power generation cycle and a HDR of 10%.

| Equipment | Cycle | Equipment size | Mass Flow rate (kg/s) | Inlet temperature (°C) | Exit temperature (°C) |
|---|---|---|---|---|---|
| Charge HX (C-IHX) | Charge | 14.11 $MW_{th}$ | 6.77(steam)<br>180 (salt) | 306.9 (steam)<br>180 (salt) | 209 (water)<br>238 (salt) |
| Discharge HX (D-IHX) | Discharge | 14.11 $MW_{th}$ | 5.243 (steam)<br>180 (salt) | 37.98 (water)<br>238 (salt) | 227.4 (stream)<br>180 (salt) |
| Cold tank pump | Charge | 0.0000616 MW | 180 | 180 | 180 |
| TES power cycle pump | Discharge | 0.0000525 MW | 180 | 238 | 238 |
| FWH pump | Discharge | 0.0070 MW | 5.243 | 37.92 | 39.98 |
| NPP BOP pump | Charge | 0.00127 MW | 6.77 | 209 | 209 |
| BOP condenser | Charge | 0.1975 MW | 50.39 | 29 | 29.17 |
| BOP condenser pump | Charge | 101.1 MW | 50.39 | 41.68 | 29 |
| TES condenser | Charge | 0.388 MW | 2300 | 26.66 | 26.67 |
| TES condenser pump | Discharge | 10.61 MW | 5.243 | 41.68 | 37.92 |
| BOP turbine | Discharge | 0.0388 MW | 230 | 26.67 | 26.66 |
| BOP turbine | Charge | 43.82 $MW_e$ | 50.39 | 306.9 | 41.68 |
| TES turbine | Discharge | 48.53 $MW_e$ | 55.81 | 306.9 | 41.68 |
| Molten salt | Discharge | 3.667 $MW_e$ | 5.243 | 227.4 | 41.68 |
| Cold/hot tanks | - | 3,888,000 kg | - | 238 (cold) | 180 (hot) |
| TES power cycle pump | - | 84.66 $MWh_{th}$ | - | 238 (cold) | 180 (hot) |

### 3.1.2 Option 2: Directly Coupled NPP-TES System

The overall setup of this coupling option is similar to that of TerraPower's Natrium reactor and the BOP model, both of which directly couple a TES system to the NPP before depositing its heat to the power generation cycle. The difference between the Natrium reactor model and this one is that, in this model, heat transfer to the thermal storage salt occurs via an intermediate steam/water loop, as is more representative of the baseline NuScale reactor system. In an actual Natrium design, heat transfer to thermal storage salt occurs directly via the reactor coolant molten salt. Figure 11 shows the model developed in Aspen HYSYS®. The operating conditions for the steam generator are similar to those seen in options 1 and 3, as are the operating temperature limits for the storage tanks.

The drawback of such a coupling in the A-LWR case is that the saturation temperature of the steam becomes a limiter to achieve higher salt temperature for thermal storage. Because of the pinch point that occurs in the steam-to-salt heat exchanger, useful heat is lost, and the terminal temperature on the hot end (turbine inlet) is 72°C lower than a traditional no-TES case (the temperature difference between stream #1 and #10). Section 4 provides more information on this limitation. As this is not an optimal coupling, the dynamic analyses and dispatch optimizations of this case using the Framework for Optimization of Resources and Economics (FORCE) tools were not conducted. In future work, the limitation of such two-phase heat transfer when steam is used as the source of heat for TES can be overcome by using one of the reactor-coolant loops (liquid metal or salt, when applicable), instead of using steam extraction as the source of heat, thus enabling a single-phase-to-single-phase heat transfer between the primary fluid and the storage medium used in the TES.

The charge and discharge cycles for this setup look identical—the sole difference arising during cycle operations. This difference—namely, that the dynamics of charging/discharging cannot be modeled separately—becomes obvious in light of the current steady-state model. In a dynamic setup, the hot tank's discharge rate varies in accordance with the demand of the power cycle, thus changing the storage media level within the tank. For example, during periods of lower demand, fluid from the hot tank flows at a lower rate through the D-IHX and into the cold tank, while the opposite is true during periods of higher demand. The charge cycle, however, operates at a constant rate, absorbing heat from the steam generator and maintaining baseload operation in the nuclear reactor.

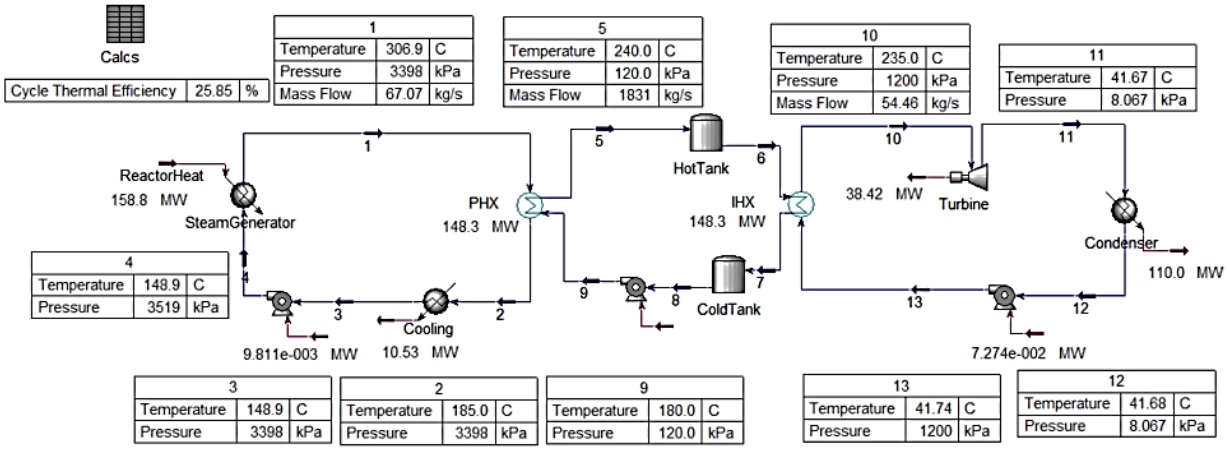


Figure 11. Process flow diagram of the directly coupled NPP-TES setup for the A-LWR use case.

### 3.1.3 Option 3: Integrated NPP-TES Coupled with an Oversized Primary Turbine

The overall setup of this coupling option is similar to that seen in option 1, in which conventional operation transitions from 100% of thermal power being used to generate electricity to a hybrid operation in which 50% of thermal power is dispatched to a TES system that delivers thermal energy at times of higher demand in order to increase the level of power generation or deliver flexible thermal energy in the form of heat (i.e., steam) to industrial users. The setup and sizing of the charge and storage systems (C-IHX, D-IHX, molten salt, hot/cold tanks, and hot/cold tank pumps) in this coupling option are identical to those in option 1, with the following exceptions: (1) the turbine receiving additional thermal energy from the TES loop is an oversized turbine in the BOP, as opposed to a standalone turbine in a dedicated power cycle for TES; and (2) there is no dedicated condenser in a TES power cycle, as an oversized BOP condenser is utilized. When the data from this coupling option are combined with data generated from the three HDRs from the first coupling option, these models provide enough resolution to create the cost functions for the various component and system sizes.

During the charge cycle, the 50% heat diversion strategy is achieved by routing saturated steam from the main steam header to be condensed in the C-IHX, while simultaneously heating the molten-salt loop. As specified in the conventional operation outlined in Section 3.1, the steam flow rate in the main steam header is 67.07 kg/s. In the current model, because steam is extracted from the main steam header (where its enthalpy is highest), the percentage of total steam extracted equals the percentage of thermal energy extracted. Hence, 50% thermal energy extraction equates to 50% of flow rates being diverted to the TES side (33.53 kg/s at 306.9°C) through the C-IHX. On the secondary side of the C-IHX, the molten salt pumped from the cold tank absorbs the heat from the steam's condensation and rises in temperature from 180 to 238.7°C during transferal to the hot tank for storage. The steam on the primary side of the C-IHX is condensed to subcooled liquid at 195.7°C, then returned to a mixer that simulates the FWH train in the primary NPP power cycle.

Figure 12 shows a process flow diagram of an active charge cycle under coupling option 3 and a HDR of 50%, alongside the corresponding discharge cycle in hot standby mode (as developed in Aspen HYSYS®).

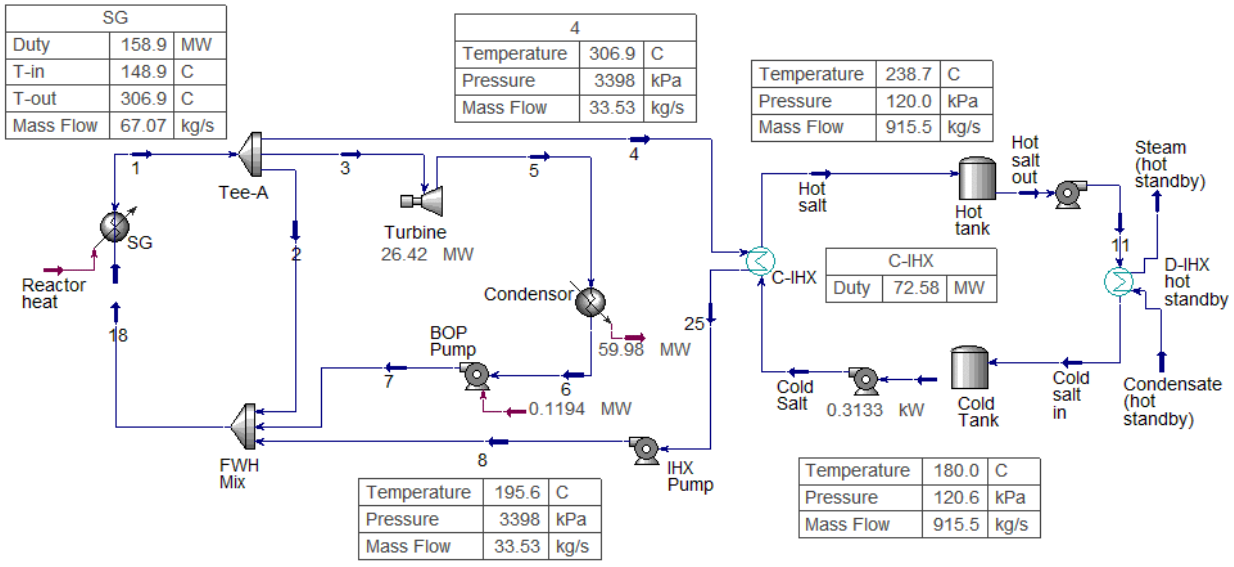


Figure 12. Process flow diagram of an A-LWR-TES coupling with an oversized BOP cycle (the third coupling method) and a HDR of 50%, showing the active charge cycle (left of the hot/cold tanks) and part of the inactive hot standby discharge cycle in hot standby mode (right of the hot/cold tanks).

It should be noted that one alternative approach is to route the condensate from C-IHX to the condenser. However, the proposed design offers the benefit of utilizing additional available heat in the condensate (C-IHX exit) to support the FWH train, such that the condensate leaving C-IHX at 195.7°C adds heat to the FWHs, thus more efficiently achieving the steam generator fixed inlet design point (149°C). This reduces the heat and mass flow that the FWH train originally draws from the FWH split (Tee-A in the figure above) in the form of high-quality steam from the turbine train at various stages, or from the main steam header to the steam generator inlet. This process, under various HDRs, is discussed in more detail in Section 4.

Although the discharge cycles discussed in this report are more focused on dispatching thermal energy for power generation purposes, the cycles presented for coupling options 1 and 3 can also be utilized as valid use cases whose end goal is to dispatch thermal energy to an industrial user. For example, Figure 12 shows a D-IHX modeled as a steam generator for a simple demonstration case. In theory, this heat exchanger can convert a stream of condensate or water at room temperature (20°C, 104 $m^3$/hr, 29 kg/s) into saturated steam (out) at 150°C, producing up to 624 $m^3$ of steam during the complete 6-hour discharge duration, while simultaneously maintaining the 240 and 180°C design temperatures for the hot and cold tanks, respectively, at a flow rate of 915.5 kg/s on the molten-salt loop side. A more complicated use case for the discharge cycle (discussed in the following paragraph) focuses on increasing the power generation capacity of the NPPs.

A secondary D-IHX (shown in Figure 13) is designed to produce steam from feedwater (condenser exit) during the discharge cycle, using the heat storage medium from the hot tank. During this process, hot salt is pumped from the hot tank and through the D-IHX, where it deposits its heat into the feedwater prior to transferal into the cold tank. This heat exchange converts the feedwater into saturated steam that is then routed to one of the low-pressure turbines in the primary NPP turbine assembly. The impact of increased flow rate, or heightened power generation capacity, on the low-pressure turbine is beyond the scope of the current analysis; however, additional details are discussed in Section 6 as part of the dynamic models of this case using Dymola. In Figure 13, Turbine_2 (LPT) represents only the additional power generated by the low-pressure turbine stage(s) thanks to adding a TES-dispatched steam load to the system, whereas the total power generated from the BOP turbine train during the discharge cycle is the sum of the power generated by Turbine_1 and Turbine_2 (LPT).

Figure 13 shows a process flow diagram of the discharge cycle and TES loop for this coupling option within Aspen HYSYS®.

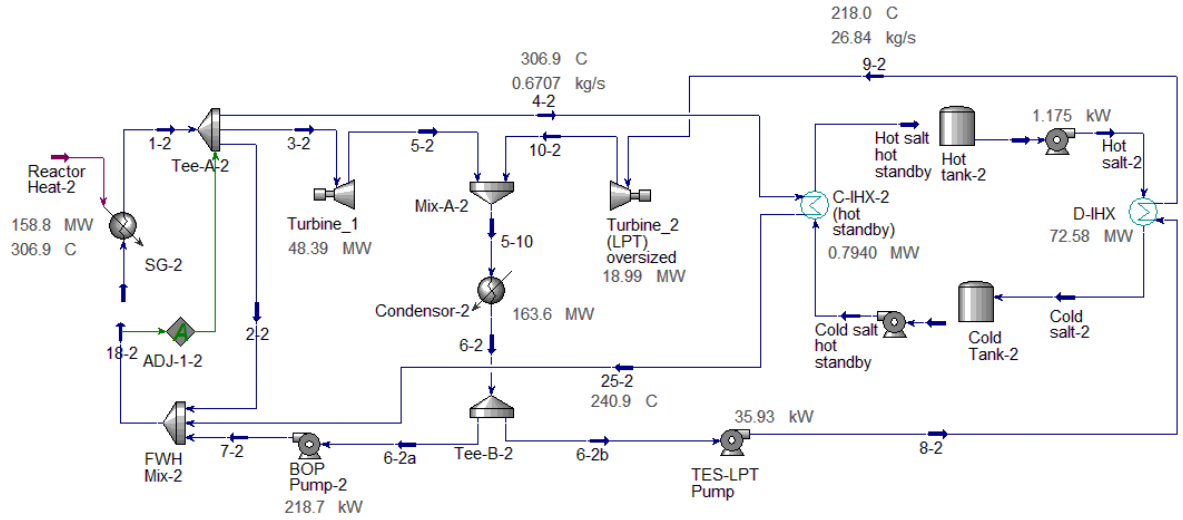


Figure 13. Process flow diagram of an A-LWR-TES coupling with an oversized BOP cycle (the third coupling method) and a HDR of 50%, showing the BOP condition during the discharge cycle (left of C-IHX-2), inactive charge cycle (left of the hot/cold tanks and right of C-IHX-2), and active discharge cycle (streams entering and leaving the D-IHX).

In the conventional case (i.e., full electrical power generation), the net electricity at 100% power is 49.5 MWe. At 50% thermal energy bypass (during the charge cycle), the turbine's power generation drops to 26.42 MWe (approximately 53.9% of the full-power capacity). During discharge, the addition of the TES -dispatched steam load to the system increased the net power to 67.38 MWe (approximately a 37.5% increase over the full-power electrical capacity in the conventional case).

Now that the third coupling option has been discussed in detail for the 50% HDR, the results in Table 11 show the BOP and operating conditions. It should be noted that when the system is operating in power production mode (no charge or discharge), the TES components are in a standby mode, with a minimum flow of ~1% through the systems to maintain temperature. The setup in this coupling option is identical to that seen in option 1, except that the heat dispatched from TES is fed to the main BOP turbine train (Turbine_2 [LPT] in Figure 13).

Table 11. BOP and operating conditions of an A-LWR-TES coupling with an oversized BOP cycle at a HDR of 50%.

| Equipment | Cycle | Equipment size | Mass Flow rate (kg/s) | Inlet temperature (°C) | Exit temperature (°C) |
|---|---|---|---|---|---|
| Charge HX (C-IHX) | Charge | 72.57 $MW_{th}$ | 33.53 (steam)<br>915.5 (salt) | 306.9 (steam)<br>180 (salt) | 195.7 (water)<br>238.7 (salt) |
| Discharge HX (D-IHX) | Discharge | 72.57 $MW_{th}$ | 26.83 (steam)<br>915.5 (salt) | 36.75 (water)<br>278.87 (salt) | 218 (stream)<br>180 (salt) |
| Cold tank pump | Charge | 0.00031 MW | 915.5 | 180 | 180 |
| Hot tank pump | Discharge | 0.00117 MW | 915.5 | 238.7 | 238.7 |
| NPP BOP pump | Discharge | 0.2187 MW | 55.65 | 36.69 | 36.75 |
| FWH pump | Charge | 0.00512 MW | 33.53 | 195.7 | 195.7 |
| NPP BOP pump | Charge | 0.11940 MW | 30.39 | 36.86 | 37.05 |
| BOP condenser | Charge | 59.98 MW | 30.39 | 41.68 | 36.86 |
| BOP condenser pump | Charge | 0.2075 MW | 1230 | 26.67 | 26.67 |
| BOP condenser | Discharge | 136.7 MW | 82.49 | 41.67 | 36.69 |
| BOP condenser pump | Discharge | 0.6365 MW | 3733 | 26.66 | 26.67 |
| BOP turbine | Charge | 26.42 $MW_e$ | 30.39 | 306.9 | 41.68 |
| BOP turbine_1* | Discharge | 48.39 $MW_e$ | 55.65 | 306.9 | 41.68 |
| BOP turbine_2 (LPT)** | Discharge | 18.99 $MW_e$ | 26.84 | 218 | 41.67 |
| Molten salt | - | 19,774,800 kg | - | 238.7 (cold) | 180 (hot) |
| Cold/hot tanks | - | 435.42 $MWh_{th}$ | - | 238.7 (cold) | 180 (hot) |

* The total power generated from the BOP turbine during the discharge cycle is 67.38 Mwe (the sum of BOP Turbine_1 and BOP Turbine_2 [LPT]).
** BOP Turbine 2 (LPT) represents only additional power generated from the BOP turbine train due to the additional heat dispatched from TES.
** Steam sent from TES to BOP Turbine_2 (LPT) during discharge is delivered at 1200 kPa.

## 3.2 High-temperature Gas-cooled Reactor (HTGR)

In the current HTGR case study, the charge and discharge cycles were modeled separately, as they require different streams and components. The HTGR use case was studied for the first coupling option (standalone NPP-TES coupling) and third coupling option (integrated NPP-TES coupling). A heat diversion of ~50% of the total steam production was chosen as the baseline for discussing the HTGR use case. Two additional thermal energy dispatch ratios (or HDRs) of 25% and 10% were created. All models and coupling methods were created with the goal of making the charge and discharge cycles last 6 hours each.

To establish a basis for developing the steady-state models, steam from the steam generator was used as the heat transfer fluid to heat the storage medium during the charge cycle. The Xe-100 steam generator operating conditions used for this analysis are listed in Table 12.

Table 12. Xe-100 steam generator operating conditions.

| Parameter | Value |
|---|---|
| Mass flow rate (kg/hr) | $2.767 \times 10^5$ |
| Exit pressure (MPa) | 1.65 |
| Exit temperature (°C) | 565.0 |

As discussed in Section 4, the higher steam temperature and pressure produced by the steam generator in a HTGR design allow for a larger ΔT between the maximum hot tank storage temperature and the cold tank temperature. This results in a higher $MWh_{th}$ of storage than that afforded by LWRs with the same storage size (i.e., molten salt mass). Hence, HTGRs require 16,533 kgs of molten salt for 1 $MWh_{th}$ of storage, whereas LWRs require 45,415 kgs. Additionally, heat storage at a higher temperature (higher quality) is more attractive than low-quality heat to support coupling with industrial process heat applications.

Based on the HTGR (i.e., Xe-100) operating conditions, solar salt—a two-component mixture (NaNO3-KNO3, 60–40 wt%) with a melting point of 222°C—was selected as the storage material candidate for the HTGR case study. As solar salt is not readily available as a fluid for use in Aspen HYSYS®, it was added to the Aspen library as a hypothetical fluid, based on the thermophysical properties acquired from the literature [19]. The Peng-Robinson equation of state was used to calculate the enthalpy and entropy of this newly added hypothetical fluid, whereas the NBS Steam package was used for the heat transfer fluid. The polynomial function used for calculating the enthalpy, heat capacity, viscosity, thermal conductivity, and density of solar salt is similar in form to that of Hitec, as described in Section 3.1. The constants of this polynomial for solar salt properties are listed below.

Table 13. Polynomial function constants for solar salt thermophysical properties.

| Property: | Density | Thermal Conductivity | Viscosity | Heat Capacity | Enthalpy |
|---|---|---|---|---|---|
| Constants | (kgmole/m3) | (W/m-K) | (cP) | (kJ/kgmole-C) | (kJ/kgmole) |
| a | 2.5154E+01 | 6.3250E-01 | 1.1480E+02 | -1.0702E+03 | 9.4036E+04 |
| b | -9.0448E-03 | -3.1300E-04 | -5.1567E+03 | 9.0878E+00 | 7.5944E+01 |
| c | 1.6795E-16 | 1.4132E-18 | -1.6768E+01 | -2.5663E-02 | -6.0885E-02 |
| d | -2.0775E-19 | -1.8442E-21 | 5.7103E-06 | 3.2139E-05 | -2.6387E-04 |
| e | 9.5444E-23 | 8.8490E-25 | 0 | -1.5035E-08 | 4.6218E-08 |

To standardize the analyses of all three coupling options, the following assumptions were made when creating the steady-state Aspen HYSYS® models for the HTGR use cases:

- There is no heat loss from any of the BOP components, streams, or TES storage tanks.
- The cold tank temperature is 260°C, and the hot tank temperature is 400°C.
- The discharge power cycle is maintained in hot standby mode when not being utilized. The same applies to the charge cycle components when only the discharge cycle is active. Hot standby mode is achieved by maintaining ~1% of the original mass flow needed to operate each cycle.
- The turbomachinery components were each operated at 90% isentropic and adiabatic efficiencies.
- The heat exchangers had a minimum approach temperature limit and pinch point limit of 5°C, as shown in Figure 14. This also determines the maximum hot molten salt temperature for each scenario (more on this technical limitation is found in Section 4).
- The pressure drop across the heat exchangers is calculated based on the pressure drop value from Aspen EDR.
- The molten-salt heat exchangers are sized using EDR, with molten salt on the tube side and a heat source (high-pressure steam and condensation) on the shell side.
- The condensers are modeled as a heat exchanger, with feedwater on the shell side and low -pressure condensate on the tube side.

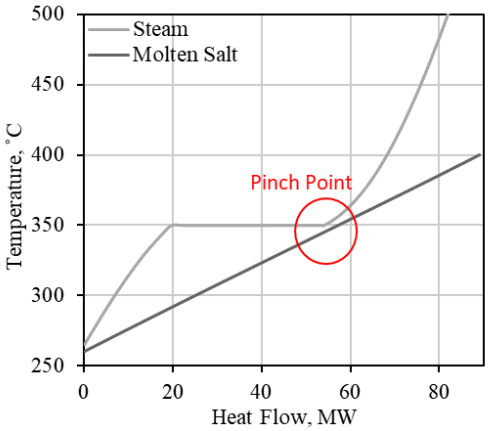


Figure 14. Intermediate heat exchanger temperature profile for the HTGR case study.

### 3.2.1 Option 1: Standalone NPP-TES Coupled with a Secondary Power Generation Cycle

For the first coupling option, the overall setup of this model is similar to that seen in the LWR use case. Supercritical steam is drawn from the main steam header, run through the C-IHX, and condensed into a subcooled liquid at ~266°C. This condensate is then returned to a mixer that simulates the FWH train. On the secondary side of the C-IHX, molten salt is pumped from the cold tank at 260°C, absorbs the heat of the steam's condensation and is itself heated to ~400°C during transfer to the hot tank for storage. The amount of steam diverted from the main steam header equals 50% of the total mass flow. Based on the operating conditions of the steam and molten-salt loops, the C-IHX had a charge power of ~88.95 $MW_{th}$. Thus, the total storage capacity of the TES system for the 6 hours of storage was calculated to be ~534 $MWh_{th}$. In future work, other models with different HDRs (25% and 10%) will be created and their cost functions developed.

Figure 15 shows a process flow diagram of an active charge cycle under coupling option 1, with a HDR of 50%, alongside the corresponding discharge cycle in hot standby mode (as developed in Aspen HYSYS®). The inactive TES discharge cycle is not shown.

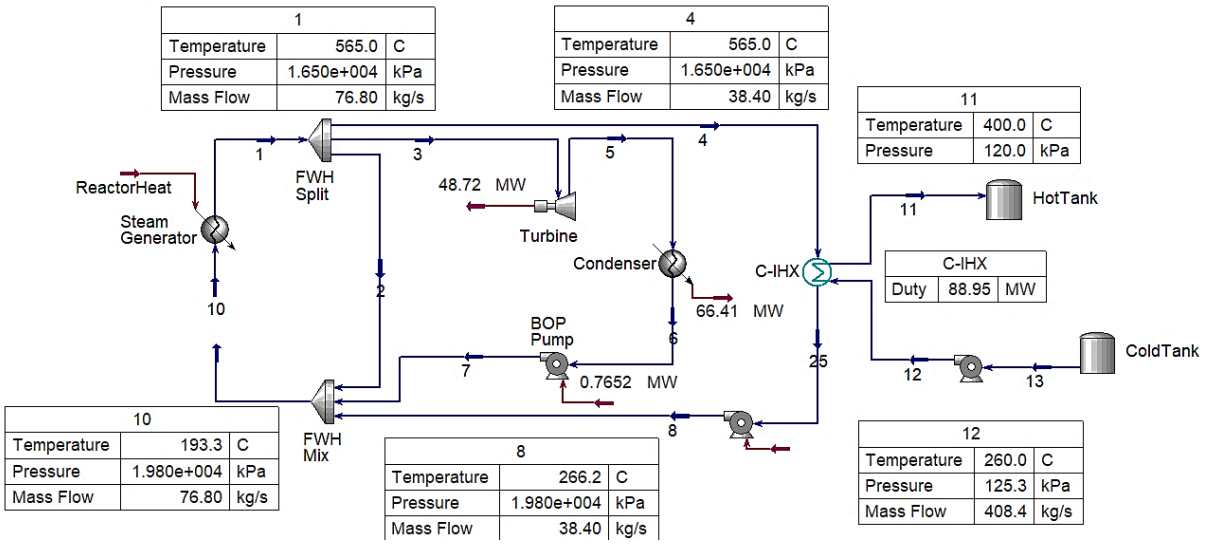


Figure 15. Process flow diagram of an advanced HTGR-TES coupling with a standalone secondary TES power generation cycle (first coupling method) and a HDR of 50%, showing the active charge cycle.

As with the models developed for the LWR case studies, the D-IHX was designed to produce steam from feedwater during the discharge cycle, using the heat storage medium from the hot tank, which produces electricity in the secondary TES power cycle.

Figure 16 shows process flow diagrams of the BOP and active discharge for the 50% HDR case.

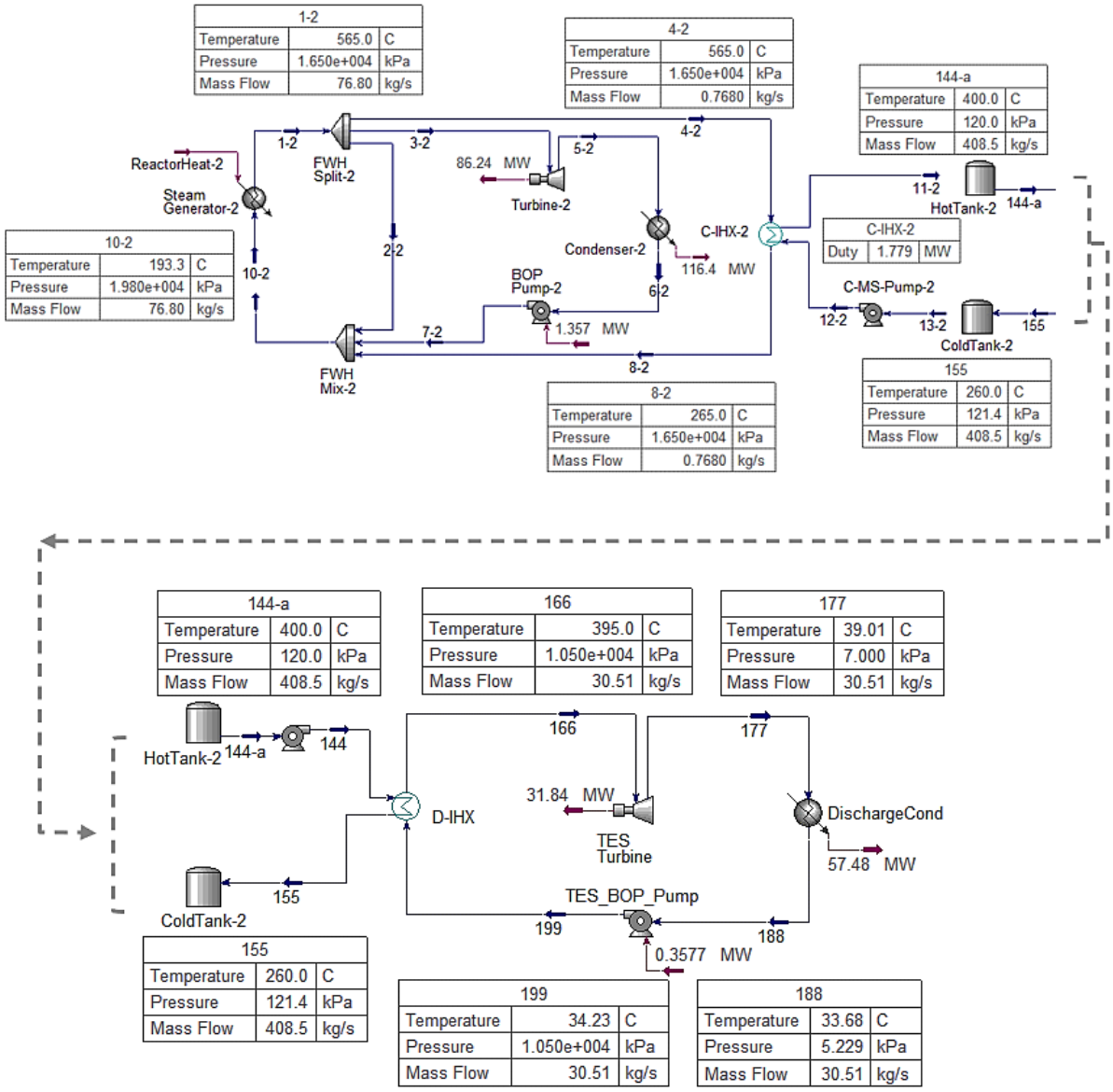


Figure 16. Process flow diagrams of an advanced HTGR-TES coupling with a standalone secondary TES power generation cycle (first coupling method) and a HDR of 50%, showing the primary power generation cycle (top), active discharge cycle, and secondary power generation cycle (bottom).

Now that the HTGR-TES coupling use case has been discussed in detail regarding the 50% HDR, the results in Table 14–Table 20 show the operating conditions for the different HDRs (50%, 25%, and 10%). The operation and overall structure of the models under other HDRs are very similar to those seen in the 50% case discussed above. It should be noted that when the system is operating in power production mode (no charge or discharge), the TES components are in a standby mode, with a minimum flow of ~1% through the systems to maintain temperature. Figure 22 in Section 4 discusses and shows the minimum flow split from the turbine stages to the FWH to maintain the steam generator inlet design point.

Table 14. BOP and operating conditions of an HTGR-TES coupling with a secondary power generation cycle at a HDR of 50%.

| Component | Cycle | Component size | Mass Flow rate (kg/s) | Inlet temperature (°C) | Exit temperature (°C) |
|---|---|---|---|---|---|
| C-IHX | Charge | 88.95 $MW_{th}$ | 38.4 (steam)<br>408.5 (salt) | 565 (steam)<br>260 (salt) | 265 (water)<br>400 (salt) |
| D-IHX | Discharge | 88.95 $MW_{th}$ | 30.51 (steam)<br>408.5 (salt) | 34.23 (water)<br>400 (salt) | 395 (stream)<br>260 (salt) |
| Cold tank pump | Charge | 0.000307 MW | 408.4 | 260 | 260 |
| Hot tank pump | Discharge | 0.000158 MW | 408.4 | 400 | 400 |
| TES power cycle pump | Discharge | 0.3577 MW | 30.51 | 36.68 | 34.23 |
| FWH pump | Charge | 0.2137 MW | 38.4 | 265 | 267.6 |
| NPP BOP pump | Charge | 0.7652 MW | 34.59 | 32.66 | 35.68 |
| BOP condenser | Charge | 66.41 MW | 34.59 | 39.01 | 34.61 |
| BOP condenser pump | Charge | 0.220 MW | 1564 | 26.65 | 26.66 |
| TES condenser | Discharge | 57.48 MW | 30.51 | 39.01 | 36.68 |
| TES condenser pump | Discharge | 0.235 MW | 1392 | 26.66 | 26.67 |
| BOP turbine | Charge | 48.72 $MW_e$ | 34.52 | 565 | 39.01 |
| BOP turbine | Discharge | 86.24 $MW_e$ | 61.22 | 565 | 39.01 |
| TES turbine | Discharge | 31.84 $MW_e$ | 30.51 | 395 | 39.01 |
| Molten salt | - | 8,821,440 kg | - | 400 (Hot) | 260 (Cold) |
| Cold/hot tanks | - | 533.7 $MWh_{th}$ | - | 400 (Hot) | 260 (Cold) |

Table 15. BOP and operating conditions of an HTGR-TES coupling with a secondary power generation cycle and a HDR of 25%.

| Component | Cycle | Component size | Mass flow rate (kg/s) | Inlet temperature (°C) | Exit temperature (°C) |
|---|---|---|---|---|---|
| C-IHX | Charge | 44.48 $MW_{th}$ | 19.2 (steam)<br>204.2 (salt) | 565 (steam)<br>260 (salt) | 265 (water)<br>400 (salt) |
| D-IHX | Discharge | 44.48 $MW_{th}$ | 15.26 (steam)<br>204.2 (salt) | 34.23 (water)<br>400 (salt) | 395 (stream)<br>260 (salt) |
| Cold tank pump | Charge | 0.0001537 MW | 204.2 | 260 | 260 |
| Hot tank pump | Discharge | 0.0000789 MW | 204.2 | 400 | 400 |
| TES power cycle pump | Discharge | 0.179 MW | 15.26 | 36.68 | 34.23 |
| FWH pump | Charge | 0.1074 MW | 19.2 | 265 | 267.6 |
| NPP BOP pump | Charge | 1.059 MW | 47.88 | 34.61 | 35.68 |
| BOP condenser | Charge | 92.34 MW | 47.88 | 39.01 | 34.61 |
| BOP condenser pump | Charge | 0.3121 MW | 2218 | 26.65 | 26.66 |
| TES condenser | Discharge | 28.75 MW | 15.26 | 39.01 | 33.68 |
| TES condenser pump | Discharge | 0.1155 MW | 684.1 | 26.66 | 26.67 |
| BOP turbine | Charge | 67.45 $MW_e$ | 47.88 | 565 | 39.01 |
| BOP turbine | Discharge | 86.24 $MW_e$ | 61.22 | 565 | 39.01 |
| TES turbine | Discharge | 15.93 $MW_e$ | 15.26 | 395 | 39.01 |
| Molten salt | - | 1,764,504 kg | - | 400 (Holt) | 260 (Cold) |
| Cold/hot tanks | - | 106.7 $MWh_{th}$ | - | 400 (Hot) | 260 (Cold) |

Table 16. BOP and operating conditions of an HTGR-TES coupling with a secondary power generation cycle and a HDR of 10%.

| Component | Cycle | Component size | Mass flow rate (kg/s) | Inlet temperature (°C) | Exit temperature (°C) |
|---|---|---|---|---|---|
| C-IHX | Charge | 17.79 $MW_{th}$ | 7.68 (steam)<br>81.69 (salt) | 565 (steam)<br>260 (salt) | 265 (water)<br>400 (salt) |
| D-IHX | Discharge | 17.79 $MW_{th}$ | 6.123 (steam)<br>81.69 (salt) | 36.76 (water)<br>400 (salt) | 395 (stream)<br>260 (salt) |
| Cold tank pump | Charge | 0.0000569 MW | 81.69 | 260 | 260 |
| Hot tank pump | Discharge | 0.0000202 MW | 81.69 | 400 | 400 |
| TES power cycle pump | Discharge | 0.07186 MW | 6.123 | 36.19 | 36.76 |
| FWH pump | Charge | 0.0429 MW | 7.68 | 265 | 265 |
| NPP BOP pump | Charge | 1.241 MW | 56.1 | 39.01 | 40.14 |
| BOP condenser | Charge | 107.6 MW | 56.1 | 39.01 | 39.01 |
| BOP condenser pump | Charge | 0.3496 MW | 2485 | 26.65 | 26.66 |
| TES condenser | Discharge | 11.49 MW | 6.123 | 39.01 | 36.19 |
| TES condenser pump | Discharge | 0.0459 MW | 271.8 | 26.66 | 26.67 |
| BOP turbine | Charge | 79.03 $MW_e$ | 56.1 | 565 | 39.01 |
| BOP turbine | Discharge | 86.24 $MW_e$ | 61.22 | 565 | 39.01 |
| TES turbine | Discharge | 6.39 $MW_e$ | 6.123 | 395 | 39.01 |
| Molten salt | - | 1,764,504 kg | - | 400 (Hot) | 260 (Cold) |
| Cold/hot tanks | - | 106.7 $MWh_{th}$ | - | 400 (Hot) | 260 (Cold) |

### 3.2.2 Option 2: Directly Coupled NPP-TES System

The overall setup of this coupling option is similar to that discussed in Section 3.1.2, in which the TES system is directly coupled to the NPP before depositing its heat to the power generation cycle. Figure 17 shows the model developed in Aspen HYSYS®. The operating conditions for the steam generator are similar to those seen in options 1 and 3, as are the operating temperature limits for the storage tanks.

The drawback of such a coupling in the HTGR case is that the saturation temperature of the steam becomes a limiter for the achievable upper-limit temperature of the salt. Because of the pinch point that occurs in the steam-to-salt heat exchanger, useful heat is lost, and the maximum steam temperature at the inlet of the turbine is reduced from 565 to 400°C. As this is not an optimal coupling, the dynamic analyses and dispatch optimizations (using the FORCE tools) for this case were not conducted. In future work, the limitation of such two-phase heat transfer when steam is used as the heat source for TES can be overcome by using one of the reactor coolant loops (liquid metal or salt, as applicable), instead of using stream extraction as the heat source, thus enabling single-phase-to-single-phase heat transfer between the primary fluid and the storage medium used in the TES.

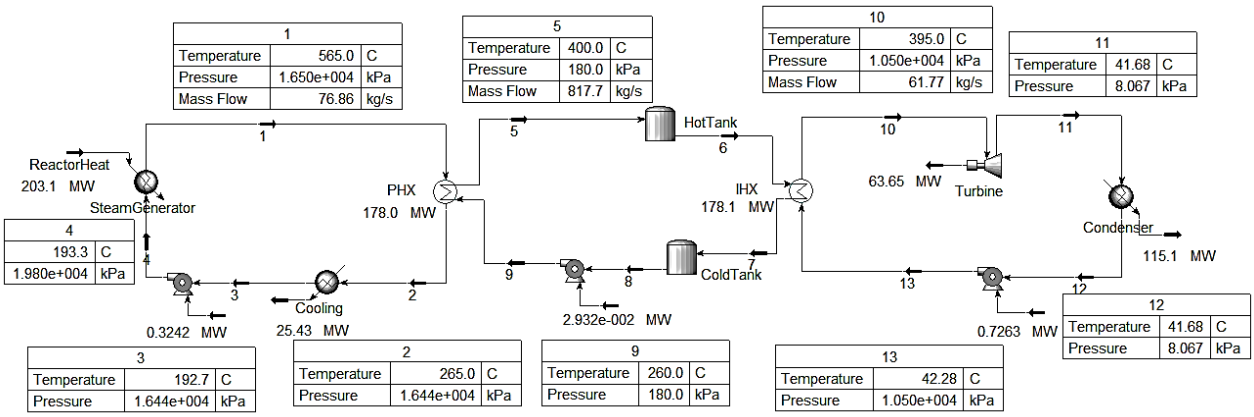


Figure 17. Process flow diagram of the directly coupled NPP-TES setup for the HTGR use case.

### 3.2.3 Option 3: Integrated NPP-TES Coupled with an Oversized Primary Turbine

The overall setup of this coupling option is similar to that seen in option 1, in which conventional operation transitions from 100% of thermal power being used to generate electricity to a hybrid operation in which 50% of thermal power is dispatched to a TES system that delivers thermal energy at times of higher demand in order to increase the level of power generation or deliver flexible thermal energy in the form of heat (i.e., steam) to industrial users. The setup and sizing of the charge and storage systems (C-IHX, D-IHX, molten salt, hot/cold tanks, and hot/cold tank pumps) in this coupling option are identical to those in option 1, with the following exceptions: (1) the turbine receiving additional thermal energy from the TES loop is an oversized turbine in the BOP, as opposed to a standalone turbine in a dedicated power cycle for TES; and (2) there is no dedicated condenser in a TES power cycle, as an oversized BOP condenser is utilized instead. When the data from this coupling option are combined with data generated from the three HDRs from the first coupling option, these models provide sufficient resolution to create the cost functions for the various component and system sizes.

During the charge cycle, the 50% heat diversion strategy is achieved by routing saturated steam from the main steam header to be condensed in the C-IHX, while simultaneously heating the molten-salt loop. As specified in the conventional operation outlined in Section 3.2, the steam flow rate in the main steam header is 76.8 kg/s. In the current model, because steam is extracted from the main steam header (where its enthalpy is highest), the percentage of total steam extracted equals the percentage of thermal energy extracted. Hence, 50% thermal energy extraction equates to 50% of the flow rates being diverted to the TES side (38.4 kg/s at 565°C) through the C-IHX. On the secondary side of the C-IHX, the molten salt pumped from the cold tank absorbs the heat from the steam's condensation and rises in temperature from 260 to 400°C during transferal to the hot tank for storage. The steam on the primary side of the C-IHX is condensed to subcooled liquid at 265°C, then returned to a mixer that simulates the FWH train in the primary NPP power cycle.

Figure 18 shows a process flow diagram of an active charge cycle under coupling option 3 and a HDR of 50%, alongside the corresponding discharge cycle in hot standby mode (as developed in Aspen HYSYS®).

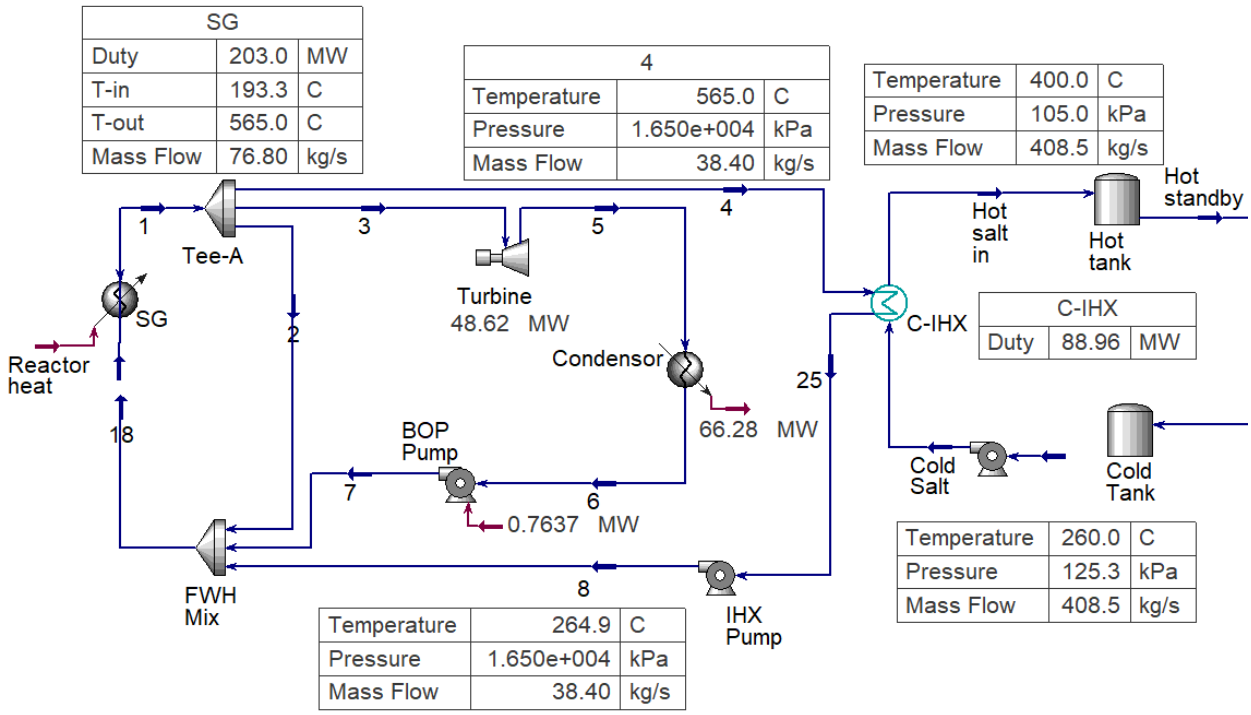


Figure 18. Process flow diagram of an HTGR-TES coupling with an oversized BOP cycle (the third coupling method) and a HDR of 50%, showing the active charge cycle (left of the hot/cold tanks) and part of the inactive hot standby discharge cycle in hot standby mode (right of the hot/cold tanks).

As in the case of LWR use cases, one alternative approach is to route the condensate from the C-IHX to the condenser. However, the proposed design offers the benefit of utilizing additional available heat in the condensate (C-IHX exit) to support the FWH train, such that the condensate leaving the C-IHX at 264.9°C adds heat to the FWHs, thus more efficiently achieving the steam generator fixed inlet design point (193.3°C). This reduces the heat and mass flow that the FWH train originally draws (FWH split Tee-A in the figure above) in the form of high-quality steam from the turbine train at various stages, or from the main steam header to the steam generator inlet. This process, under various HDRs, is discussed in more detail in Section 4.

Although the discharge cycles discussed in this report are more focused on dispatching thermal energy for power generation purposes, the cycles presented for coupling options 1 and 3 can also be utilized as valid use cases whose end goal is to dispatch thermal energy to an industrial user. Based on the design conditions described above for the 50% HDR case, the heat in the hot molten-salt tank can be used to convert a stream of condensate or water at room temperature (20°C, 119.3 $m^3$/hr, 33.1 kg/s) into saturated steam (out) at 150°C, producing up to 716 $m^3$ of steam during the complete 6-hour discharge duration, while simultaneously maintaining the 240 and 180°C design temperatures for the hot and cold tanks, respectively, at a flow rate of 408.5 kg/s on the molten-salt loop side. A more complicated use case for the discharge cycle (discussed in the following paragraph) focuses on increasing the power generation capacity of the NPPs.

A secondary D-IHX (shown in Figure 19) is designed to produce steam from the feedwater (condenser exit) during the discharge cycle, using the heat storage medium from the hot tank. During this process, hot salt is pumped from the hot tank and through the D-IHX, where it deposits its heat into the feedwater prior to transferal into the cold tank. This heat exchange converts the feedwater into saturated steam that is then routed to one of the low-pressure turbines in the primary NPP turbine assembly. The impact of increased flow rate, or heightened power generation capacity, on the low-pressure turbine is beyond the scope of the current analysis. In Figure 13, Turbine_2 (LPT) represents only the additional power generated by the low-pressure turbine stage(s) thanks to adding a TES-dispatched steam load to the system, whereas the total power generated from the BOP turbine train during the discharge cycle is the sum of the power generated by Turbine_1 and Turbine_2 (LPT).

Figure 19 shows a process flow diagram of the discharge cycle and TES loop for this coupling option within Aspen HYSYS®.

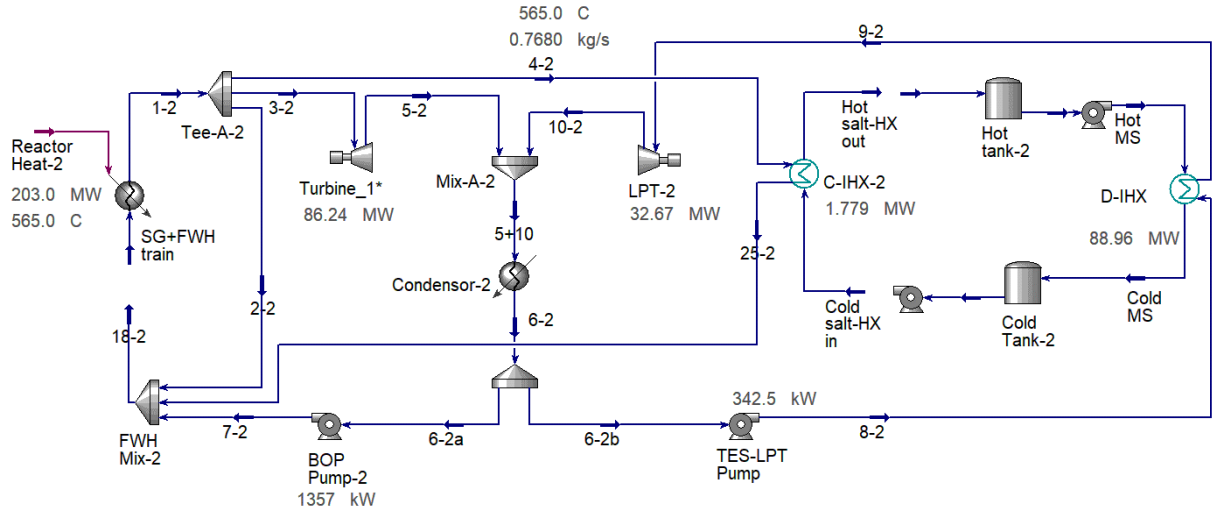


Figure 19. Process flow diagram of the HTGR-TES coupling with an oversized BOP cycle (the third coupling method) and a HDR of 50%, showing the BOP condition during the discharge cycle (left of C-IHX-2), inactive charge cycle (left of the hot/cold tanks and right of C-IHX-2), and active discharge cycle (streams entering and leaving D-IHX).

In the conventional case (i.e., full electrical power generation), the net electricity at 100% power is ~85.9 MWe. At 50% thermal energy bypass (during the charge cycle), the turbine's power generation drops to 48.6 MWe (approximately 56.6% of the full-power capacity, or a 43.4% power drop). During the discharge, addition of the TES-dispatched steam load to the system increased the net power to 118.4 MWe (approximately a 38% increase over the full-power electrical capacity in the conventional case).

Now that the third coupling option has been discussed in detail for the 50% HDR, the results in Table 17 show the BOP and operating conditions. It should be noted that when the system is operating in power production mode (no charge or discharge), the TES components are in a standby mode, with a minimum flow of ~1% through the systems to maintain temperature. The setup in this coupling option is identical to that seen in option 1, except that the heat dispatched from TES is fed to the main BOP turbine train (Turbine_2 [LPT] in Figure 19).

Table 17. BOP and operating conditions of an HTGR-TES coupling with an oversized BOP cycle at a HDR of 50%.

| Equipment | Cycle | Equipment size | Mass flow rate (kg/s) | Inlet temperature (°C) | Exit temperature (°C) |
|---|---|---|---|---|---|
| Charge HX (C-IHX) | Charge | 88.96 $MW_{th}$ | 38.4 (steam)<br>408.5 (salt) | 565 (steam)<br>260 (salt) | 265 (water)<br>400 (salt) |
| Discharge HX (D-IHX) | Discharge | 88.96 $MW_{th}$ | 30.47 (steam)<br>408.5 (salt) | 39.57 (water)<br>400 (salt) | 395 (stream)<br>260 (salt) |
| Cold tank pump | Charge | 0.0000569 MW | 408.4 | 260 | 260 |
| Hot tank pump | Discharge | 0.0000202 MW | 408.4 | 400 | 400 |
| NPP BOP pump | Discharge | 1.394 MW | 60.96 | 35.64 | 36.73 |
| FWH pump | Charge | 0.2907 MW | 38.4 | 265 | 267.6 |
| NPP BOP pump | Charge | 0.7637 MW | 34.59 | 34.61 | 35.68 |
| BOP condenser | Charge | 66.28 MW | 34.59 | 39.01 | 34.61 |
| BOP condenser pump | Charge | 0.220 MW | 1564 | 26.65 | 26.66 |
| BOP condenser | Discharge | 173.6 MW | 91.43 | 39.01 | 35.64 |
| BOP condenser pump | Discharge | 0.743 MW | 5286 | 26.66 | 26.67 |
| BOP turbine | Charge | 48.62 $MW_e$ | 34.52 | 565 | 39.01 |
| BOP turbine_1* | Discharge | 85.88 $MW_e$ | 60.96 | 565 | 39.01 |
| BOP turbine_2 (LPT)** | Discharge | 32.51 $MW_e$ | 30.47 | 395 | 39.01 |
| Molten salt | - | 8,821,440 kg | - | 400 (Hot) | 260 (Cold) |
| Cold/hot tanks | - | 533.7 $MWh_{th}$ | - | 400 (Hot) | 260 (Cold) |

* The total power generated from the BOP turbine during the discharge cycle is 118.4 Mwe (the sum of BOP Turbine_1 and BOP Turbine_2 [LPT]).
** BOP Turbine 2 (LPT) represents only the additional power generated from the BOP turbine train due to the additional heat dispatched from TES.
** Steam sent from TES to BOP Turbine_2 (LPT) during discharge is delivered at 1200 kPa.

## 3.3 Liquid-Metal Fast Reactors (LMFRs)

In the current LMFR case study, the charge and discharge cycles will be modeled separately, as they require different streams and components. As with the HTGR, the LMFR use case will be studied for the first coupling option (standalone NPP-TES coupling) and third coupling option (integrated NPP-TES coupling). A heat diversion of ~50% of the total steam production was chosen as the baseline for discussing the LMFR use case. Two additional thermal energy dispatch ratios (or HDRs) of 25% and 10% will be presented in follow-up work. All models and coupling methods were created with the goal of making the charge and discharge cycles last 6 hours each.

To establish a basis for developing the steady-state models, steam from the steam generator was used as the heat transfer fluid to heat the storage medium during the charge cycle. The PRISM steam generator operating conditions used for this analysis are listed in Table 18.

Table 18. PRISM steam generator operating conditions.

| Parameter | Value |
|---|---|
| Mass flow rate (kg/hr) | $2.732 \times 10^6$ |
| Exit pressure (MPa) | 14.72 |
| Exit temperature (°C) | 452.2 |

As discussed in Section 2.1.3 the higher steam temperature and pressure produced by the steam generator in a LMFR design allow for a larger ΔT between the maximum hot tank storage temperature and the cold tank temperature. This results in a higher $MWh_{th}$ of storage than that afforded by LWRs with the same storage size (i.e., molten salt mass). Conversely, LMFRs require 22,344 kgs of molten salt for 1 $MWh_{th}$ of storage, whereas LWRs require 45,415 kgs and HTGRs require 16,533 kgs. Additionally, heat storage at a higher temperature (higher quality) is more attractive than low-quality heat to support coupling with industrial process heat applications.

Based on the LMFR (i.e., PRISM) operating conditions, solar salt—a two-component mixture (NaNO3-KNO3, 60–40 wt%) with a melting point of 222°C—was selected as the storage material candidate for the LMFR case study. As solar salt is not readily available as a fluid for use in Aspen HYSYS®, it was added to the Aspen library as a hypothetical fluid (see Section 3.2 for additional details on creating the user-defined thermophysical properties and polynomial functions of solar salt).

To standardize the analyses of all three coupling options, the same assumptions adopted for the HTGR cases (detailed in Section 3.2) were also adopted for the LMFR, with the exception that the cold tank temperature was set to 260°C and the hot tank temperature was set to 400°C.

### 3.3.1 Option 1: Standalone NPP-TES Coupled with a Secondary Power Generation Cycle

As stated previously, additional thermal energy dispatch ratios, or HDRs, will be evaluated for the LMFR use case in future work. In the present study, the first coupling option is evaluated following an overall setup similar to that seen in the LWR and HTGR use cases. Supercritical steam is drawn from the main steam header, run through the C-IHX, and condensed into a subcooled liquid at 265°C. This condensate is then returned to a mixer that simulates the FWH train. On the secondary side of the C-IHX, molten salt pumped from the cold tank at 260°C absorbs the heat of the steam's condensation and is itself heated to ~363°C during transfer to the hot tank for storage. The amount of steam diverted from the main steam header equals 50% of the total mass flow. Based on the operating conditions of the steam and molten-salt loops, the C-IHX had a charge power of ~763.2 $MW_{th}$. Thus, the total storage capacity of the TES system for the 6 hours of storage was calculated to be ~4579 $MWh_{th}$.

Figure 20 shows a process flow diagram of an active charge cycle under coupling option 1 and with a HDR of 50%, alongside the corresponding discharge cycle in hot standby mode (as developed in Aspen HYSYS®). The inactive TES discharge cycle is not shown.

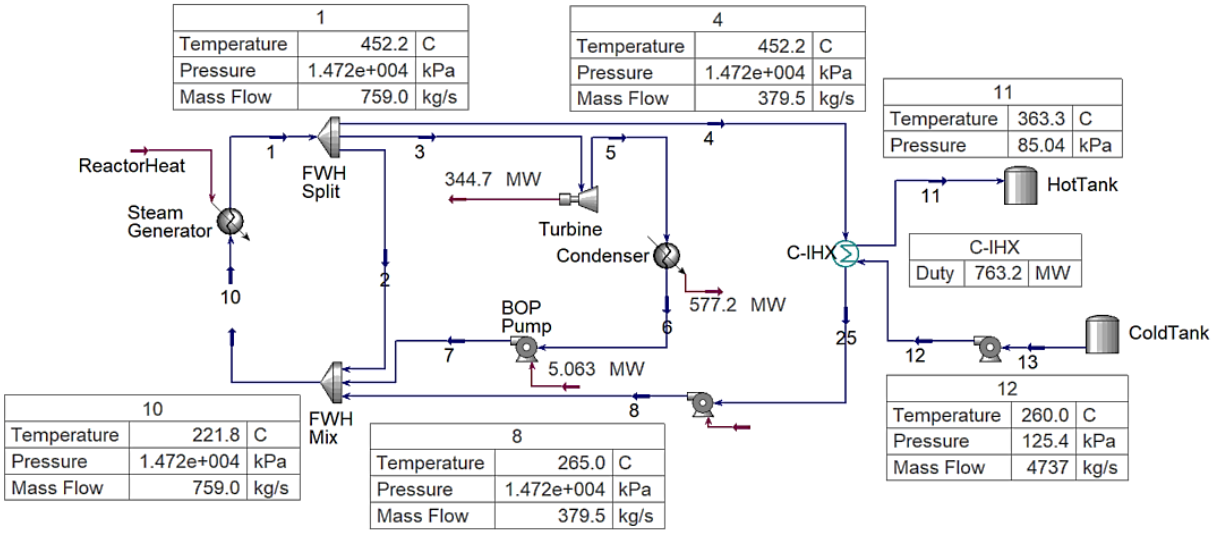


Figure 20. Process flow diagram of an advanced LMFR-TES coupling with a standalone secondary TES power generation cycle (first coupling method) and a HDR of 50%, showing the active charge cycle.

As with the models developed for the LWR case studies, the D-IHX was designed to produce steam from the feedwater during the discharge cycle, using the heat storage medium from the hot tank, which is utilized to produce electricity in the secondary TES power cycle.

Figure 21 shows process flow diagrams of the BOP and active discharge cycle for the 50% HDR case.

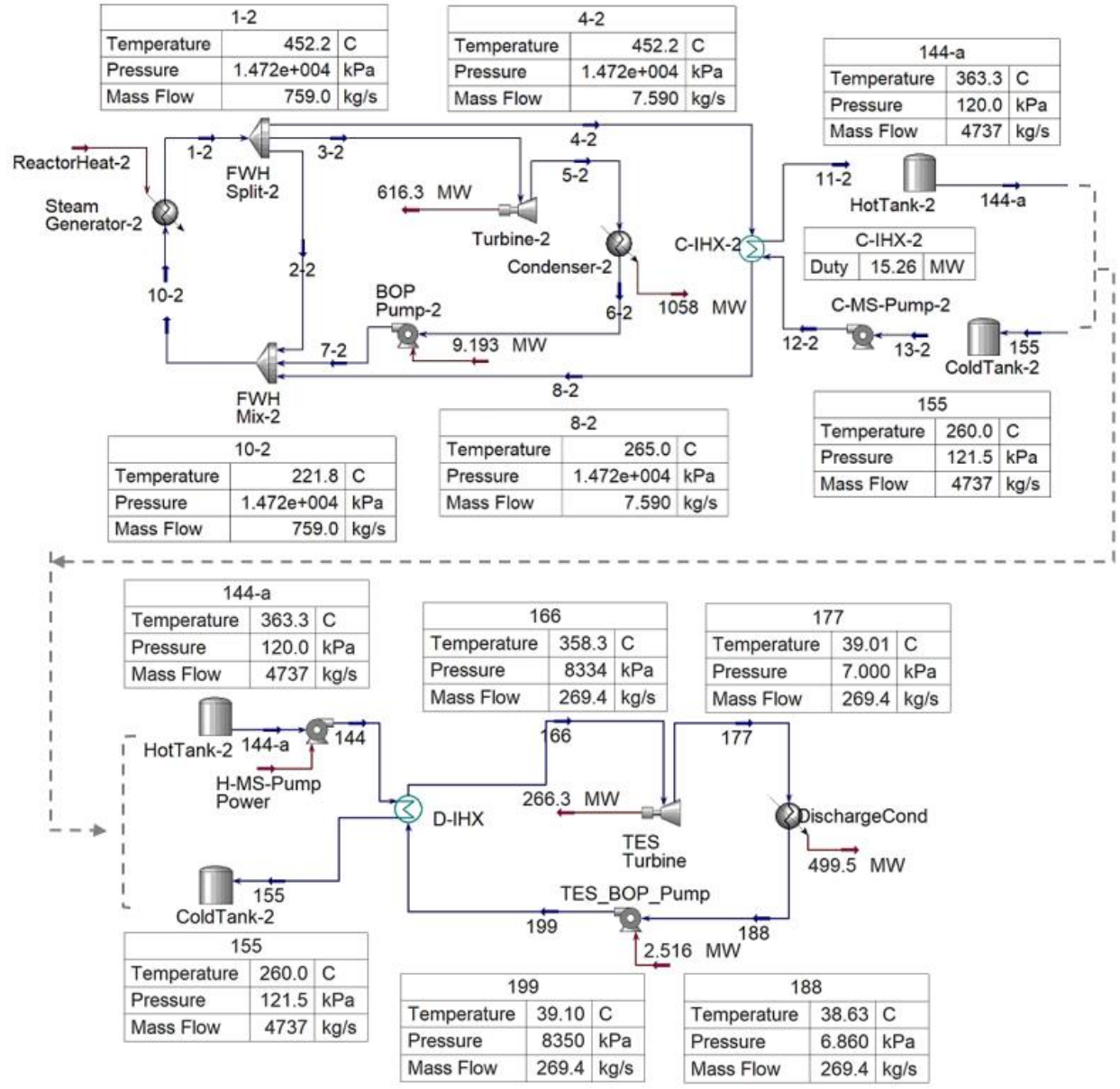


Figure 21. Process flow diagrams of an advanced LMFR-TES coupling with a standalone secondary TES power generation cycle (first coupling method) and a HDR of 50%, showing the primary power generation cycle (top), active discharge cycle, and secondary power generation cycle (bottom).

Now that the LMFR-TES coupling use case has been discussed in detail for the 50% HDR, the results in Table 19 show the BOP and operating conditions for all of the components.

Table 19. BOP and operating conditions of a LMFR-TES coupling with a secondary power generation cycle at a HDR of 50%.

| Component | Cycle | Component size | Mass flow rate (kg/s) | Inlet temperature (°C) | Exit temperature (°C) |
|---|---|---|---|---|---|
| C-IHX | Charge | 763.2 $MW_{th}$ | 379.5 (steam)<br>4737 (salt) | 452.2 (steam)<br>260 (salt) | 265 (water)<br>363.3 (salt) |
| D-IHX | Discharge | 763.2 $MW_{th}$ | 269.4 (steam)<br>4737 (salt) | 39.1 (water)<br>363.3 (salt) | 358.3 (steam)<br>260 (salt) |
| Cold tank pump | Charge | 0.01523 MW | 4737 | 260 | 260 |
| Hot tank pump | Discharge | 0.000036 MW | 4737 | 363.3 | 363.3 |
| TES power cycle pump | Discharge | 2.516 MW | 269.4 | 38.63 | 39.10 |
| FWH pump | Charge | 0.07704 MW | 379.5 | 265 | 265 |
| NPP BOP pump | Charge | 5.603 MW | 307.3 | 40.22 | 41.06 |
| BOP condenser | Charge | 577.2 MW | 307.3 | 40.60 | 40.22 |
| BOP condenser pump | Charge | 2.565 MW | 15500 | 26.65 | 26.66 |
| TES condenser | Discharge | 649.2 MW | 269.4 | 39.01 | 38.63 |
| TES condenser pump | Discharge | 3.488 MW | 21079 | 26.65 | 26.66 |
| BOP turbine | Charge | 344.7 $MW_e$ | 307.3 | 452.2 | 40.60 |
| BOP turbine | Discharge | 616.3 $MW_e$ | 557.9 | 452.2 | 40.60 |
| TES turbine | Discharge | 266.3 $MW_e$ | 269.4 | 358.3 | 39.01 |
| Molten salt | - | 102,320,771 kg | - | 363.3 (hot) | 260 (cold) |
| Cold/hot tanks | - | 4579 $MWh_{th}$ | - | 363.3 (hot) | 260 (cold) |

In future work, LMFR models of the first coupling option with different HDRs (25% and 10%), as well as the third coupling option at HDRs of 50%, 25%, and 10%, will be created and their cost functions developed. The optimal system size and heat dispatch results will be generated via HERON, followed by transient-state modeling and optimized control schemes using HYBRID.

# 4. DESIGN CONSIDERATIONS AND ANALYSIS

During the charge and discharge cycles, the addition of a new steam load to the system necessitates a change in how overall thermal efficiency is calculated. This can be expressed by calculating two efficiency indicators for the NPP: (1) the power generation efficiency, in which only the nuclear reactor heat and the resulting turbine power output are considered, and (2) the overall plant energy utilization efficiency, which is calculated based on how energy is utilized across the entire NPP, including TES -stored/dispatched energy.

**Conventional case (no TES):**

- Power generation efficiency: $\eta_{power} = \frac{E_{net}}{Q_{in-into\ turbine}}$
- Plant energy utilization efficiency = Power generation efficiency

**Thermal storage case (coupling option 3):**

- Power generation efficiency (charge): $\eta_{power\_TES\_C} = \frac{E_{net}}{Q_{in}}$
- Plant energy utilization efficiency (charge) = $\eta_{NPP\_TES\_C} = \frac{E_{net} + Q_{TES}}{Q_{in}}$
- Power generation efficiency (discharge): $\eta_{power\_TES\_D} = \frac{E_{net}}{Q_{in}}$
- Plant energy utilization efficiency (discharge) = $\eta_{NPP\_TES\_D} = \frac{E_{net}}{Q_{in+}Q_{TES}}$

where

$E_{net}$ is the net electricity produced by the NPP (including the storage unit)
$Q_{in}$ is the thermal power input to the system from the nuclear reactor (158.9 $MW_{th}$)
$Q_{TES}$ is the TES system's thermal energy input/output.

The electric and thermal power dispatch values and overall thermal efficiency indicators for the conventional case and the LWR TES uses case are summarized in Table 20. The TES use case values are based on the average values for coupling option 1 and option 3, which were nearly identical. Similarly, Table 21 shows the calculations for the HTGR use cases.

Table 20. Electric and thermal power dispatch and thermal efficiency indicators for the LWR use cases.

| Thermal power dispatch % | Net electricity (MWe) | TES heat dispatch ($MW_{th}$) | Plant energy utilization efficiency (%) | Plant power generation efficiency (%) |
|---|---|---|---|---|
| Conventional (0%) | 48.80 | 0 | 30.7% | 30.7% |
| Charge (-50%) | 26.30 | 72.57 | 62.2% | 11.4% |
| Discharge (+50%) | 67.16 | 72.57 | 29.0% | 42.3% |

Table 21. Electric and thermal power dispatch and thermal efficiency indicators for the HTGR use cases.

| Thermal power dispatch % | Net electricity (MWe) | TES heat dispatch ($MW_{th}$) | Plant energy utilization efficiency (%) | Plant power generation efficiency (%) |
|---|---|---|---|---|
| Conventional (0%) | 85.64 | 0 | 42.2% | 42.2% |
| Charge (-50%) | 47.73 | 88.95 | 67.3% | 16.3% |
| Discharge (+50%) | 116.35 | 88.95 | 39.9% | 57.3% |

Certain design considerations, limitations, and critical knowledge were acquired from each case. The key design considerations captured from this case are summarized as follows:

- ***Steam generator inlet temperature and flow split from the turbine train to the FWHs.*** The proposed coupling methods offer the benefit of utilizing additional available heat in the condensate (i.e., C-IHX exit) to support the FWH train, such that the condensate leaving the C-IHX at high temperatures (190–210 and 260°C for the LWR and HTGR cases, respectively) is utilized to add heat to the FWHs, thus more efficiently achieving the steam generator inlet design point (i.e., 148.9 and 193.3°C for LWR and HTGR, respectively), which remains equivalent to that for the no-TES case. This reduces the heat and mass flow that the FWH train originally drew in the form of high-quality steam from the turbine train at various stages, or from the main steam header. Figure 22 shows the minimum required flow-split mass flow rate from the turbine train to the FWH as a function of different HDRs for the LWR use case.

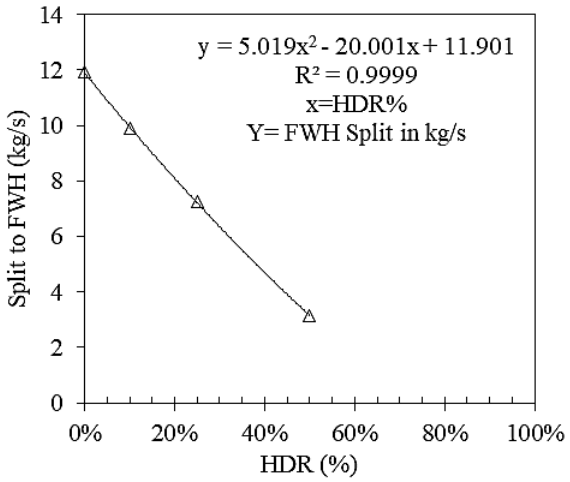


Figure 22. Minimum flow split to the FWH, as a function of HDR, to TES for the LWR use case in order to maintain the steam generator inlet design point. 0% HDR represents the reference case (i.e., no TES).

- ***Thermal extraction to an industrial user:*** Although the current models focus on extracting thermal energy from TES for power generation purposes, another option is to extract thermal energy and then divert it to an industrial user (i.e., D-IHX in coupling option 3 [for steam generation]). In this case, note that the total thermal power ($MW_{th}$) may even exceed that implied by the initial extraction percentage (i.e., HDR during the charge). For example, the industrial user may require thermal energy at a faster discharge rate—or steam at a lower temperature—than in the power generation case presented herein.
- ***Hot standby operation:*** During the discharge cycle, all the components used by the various streams during the charge cycle (e.g., the steam entering the C-IHX and the cold molten-salt stream to the C-IHX) are maintained in hot standby mode. During this process, about 0.8 $MW_{th}$ is retrieved at the charge cycle C-IHX to produce additional hot molten salt for transferal to the hot tank during the discharge cycle. In this manner, hot standby operation mode can be maintained while still capturing useful heat. Similarly, during the charge cycle, a small amount of feedwater condensate (~1% of the corresponding mass flow when the discharge cycle is active) is extracted from the condenser exit and diverted to the discharge streams (i.e., D-IHX) to maintain them in hot standby mode. This causes an approximately 1% decrease in turbine power output. The advantage of maintaining the TES loop in hot standby mode even when not in use is that thermal power from the NPP can be dispatched rapidly and upon demand to industrial users, and operation can smoothly switch from charge mode to 100% discharge mode for power delivery. This is important for an IES meant to operate in markets in which spinning reserves generate large amounts of revenue.
- ***Molten salt maximum design temperature***: During the charge cycle, the maximum temperature (i.e., 240 and 400°C for the LWR and HTGR use cases, respectively) of the hot molten salt was chosen such that a minimum approach temperature of 5°C could be maintained in IHEX-1. The temperatures within C-IHX are shown in Figure 8 and Figure 14 for the LWR and HTGR use cases, respectively. The LWR and HTGR C-IHX conditions are overlayed in Figure 23.

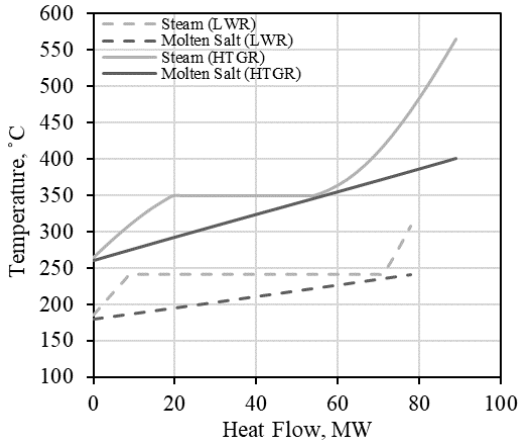


Figure 23. Steam saturation temperature threshold and molten-salt temperature curve for the TES C-IHX from the LWR and HTGR use cases (dashed lines: LWR; solid lines: HTGR).

- ***Molten salt minimum design temperature***: The minimum cold tank temperature (i.e., 180°C for the LWR and 260°C for the HTGR use cases, respectively) was chosen such that the molten salt for each case is maintained at a temperature of at least 38°C above its melting point.
- ***Storage media flow rate***: The flow rate of the molten salt is calculated to meet three design targets: (1) the temperature of the resulting condensed steam (C-IHX exit) is 5° higher than that of the cold salt (180°C), thus avoiding a temperature cross at the heat exchanger terminals; (2) the C-IHX molten salt exit temperature (hot tank inlet) is maintained at a specific maximum (i.e., 240 and 400°C for the LWR and HTGR, respectively).
- ***Heat dispatch and steam pressure during discharge for the third coupling option:*** The delivery pressure of the discharge-cycle pump (i.e., the TES LPT Pump in Figure 13), which determines the steam pressure supplied to the low-pressure turbine, is often limited. In such cases, the maximum pressure is 1200 and 10,000 kPa for the LWR and HTGR use cases, respectively. This pressure relates to the maximum saturation temperature the steam can achieve without causing a temperature cross within the heat exchanger. This pressure threshold is calculated such that a minimum of 5°C is maintained between the steam saturation temperature in the steam-temperature-heat-flow curve and the molten salt temperature at any location within the D-IHX in order to avoid a temperature cross. An example of the steam saturation curve for the TES D-IHX, based on the LWR (left figure) and HTGR (right figure) use cases, is shown in Figure 24. Such limitations are also driven by the cold molten-salt storage temperature.

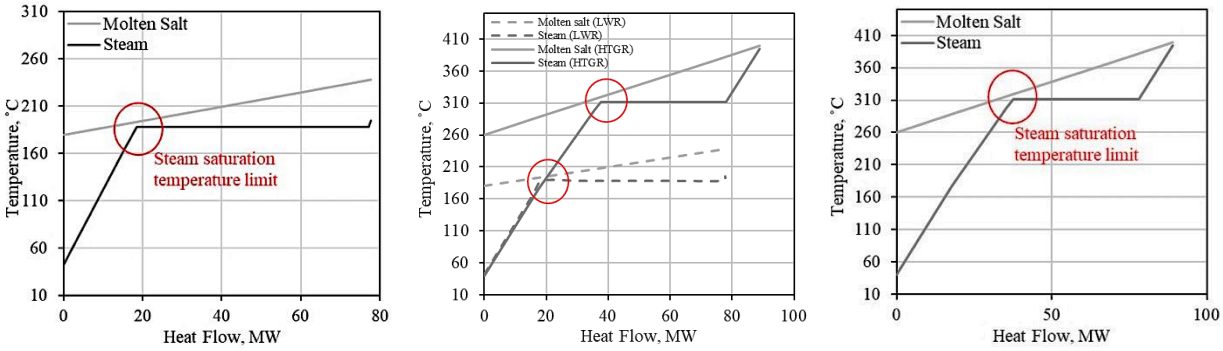


Figure 24. Steam saturation temperature threshold and molten-salt temperature curve for the TES D-IHX (left figure: LWR use case; right figure: HTGR use case; middle figure: both examples combined).

# 5. DEVELOPMENT OF COST FUNCTIONS AND SYSTEM DISPATCH OPTIMIZATION

This section discusses the cost functions developed for the different use cases. With the current information from the steady-state models developed for LWR and HTGR cases based on different HDRs and coupling options, there is enough resolution in the data to create cost functions for the various component and system sizes for both reactor types. To date, cost function development includes the creation of cost functions derived from the fully balanced A-LWR and HTGR models as a function of varying system size. In future work, the resolution of data for the LMFR use case will be increased by creating additional use cases at different HDRs and a separate set of cost functions for the LMFR case.

## 5.1 Methodology

This section discusses the methodologies used for cost functions development and equipment sizing. Cost functions were developed using the latest publicly available data obtained from APEA-V11.

### 5.1.1 Cost Functions

The most helpful economic drivers for IES cases are the fixed and variable costs, and how they scale with changing constructed unit size. Hence, the cost functions were developed using the following equation:

$$Y = A \,.\, (D / D')^{x}$$

where

*Y* is the installed cost of the equipment of interest
*A* is the reference installed cost for the equipment corresponding to capacity or size *D'*
*D* is the scaled equipment size determined in the optimization or that must be costed
*D'* is the reference equipment size that will be fixed and assigned to each piece of equipment
*x* is the exponential scaling factor (<1 implies economy of scale).

In developing cost functions, *A*, *D'*, and *x* are assigned as constants for each piece of equipment, therefore the installed cost (*Y*) of the equipment at any scaled size (*D*) can be derived.

Using the equation below, the mean absolute percentage error (MAPE) for each cost function was also calculated to indicate the accuracy of cost forecasts based on each cost function. MAPE is the most common measure for forecasting error and works best when there are no extremes in the data and no zeros.

$$MAPE = \frac{1}{n} \sum_{t=1}^{n} \left| \frac{A_t - F_t}{A_t} \right|$$

where

*n* is the number of fitted points (different-sized equipment) used to generate the cost function
$A_t$ is the actual value "cost" for each fitted point
$F_t$ is the forecast (calculated) value for each fitted point, using the cost function equation
Σ refers to the summation of the absolute values of the relative errors.

Cost functions based on these models were developed using the latest publicly available data obtained from APEA-V11. Once the costing data were acquired from APEA, the cost functions were developed via the following steps:

1. The equipment and installed costs for all components that appeared in the current models (e.g., turbine, heat exchangers, condensers, pumps, tanks, and energy storage materials) were acquired from APEA to generate a database of cost as a function of equipment size.

Note: The installed cost for each piece of equipment includes the estimate for the following cost elements: equipment and setting, piping, civil, structural steel, instrumentation, electrical, insulation, and paint.

2. A separate cost function for each component type was created (installed cost as a function of equipment size). These cost functions are discussed in Section 5.2.1.
3. Whenever the data resolution (cost as a function of equipment size) from the steady-state models was not varied sufficiently to create a regressed cost function for a particular piece of equipment, additional cost datapoints (i.e., additional pieces of equipment) were sized, modeled, and added to the database for that particular equipment type. This enhances the accuracy and reliability of the cost functions.
4. The individual equipment subsets were grouped to form three major TES (superset) models (Figure 25):
    a. Charge model: group of charge-loop-specific equipment (C-IHX, FWH pump), with a reference system size (*D'*) that relates to the charging power in $MW_{th}$
    b. Storage model: group of storage-loop-specific equipment (hot tank pump, cold tank pump, molten salt, holding tanks), with a reference system size (*D'*) that relates to the storage capacity in $MWh_{th}$
    c. Discharge model: group of discharge-loop-specific equipment (D-IHX, turbine, condenser, condenser feedwater pump, TES power cycle pump), with a reference system size (*D'*) that relates to the thermal power consumed by the turbine in $MW_{th}$
5. A cost function was created for each of the three superset models by using the individual cost functions for each piece of equipment falling under that superset model. The cost functions of the three superset models can indicate the additional cost realized by adding TES as a function of system size. These cost functions are discussed in Section 5.2.2.

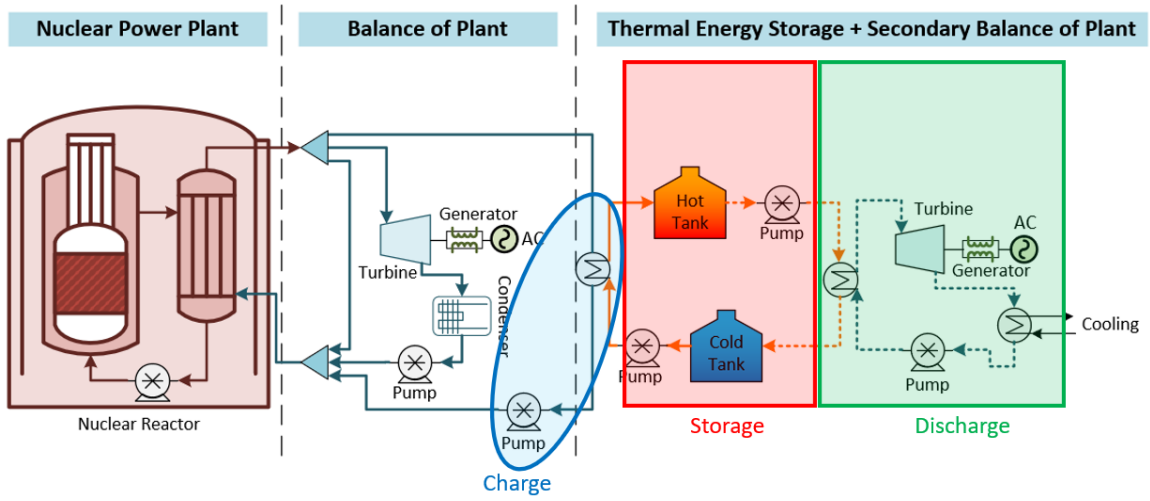


Figure 25. Component groupings to derive the superset cost functions.

### 5.1.2 Equipment Sizing

Some equipment (e.g., pumps and turbines [<20 MWe]) costs can be acquired directly from APEA runs. However, some equipment requires special consideration, or additional steps, before the equipment cost and installed cost can be directly acquired from APEA, or before their cost functions can be created. These components include the heat exchanger, turbines (>20 MWe), condensers, molten-salt storage media, and tanks.

- **Heat exchangers**: Heat exchangers must be sized before their equipment cost and installed cost can be acquired from APEA. This applies for the charge and discharge heat exchangers (C-IHX and D-IHX), as well as the condensers, which are modeled as heat exchangers in Aspen HYSYS. The sizing of the heat exchangers is accomplished via Aspen EDR using the rigorous shell and tube model. The operating conditions at two inlet streams of the heat exchanger and one exit stream are defined, and sizing is accomplished by continuing to vary the allowable pressure drop for the hot and cold sides until four technical targets are met: (1) limiting the resulting pressure drop ratio to <10% of the total inlet pressure for each stream, (2) the lowest and most optimal cost, (3) limiting the (Excess Surface Area) in the EDR geometry window to 0–5%, and (4) limiting the Dp-ratio shell side/tube side in the EDR geometry window to 0.85–1. All heat exchangers in this work were modeled and sized using Tubular Exchanger Manufacturers Association (TEMA)-type BEM heat exchangers. The BEM heat exchangers are shell and tube heat exchangers with a tube bundle constructed in a fixed manner for easy mounting onto a skid, with "B" referring to bonnet design for the front head, "E" referring to a one pass shell for the core or middle section, and "M" referring to fixed tube sheet rear head design..
- **Turbines**: Turbine equipment also require additional sizing steps before their cost can be acquired from APEA. The maximum size that can be modeled within APEA is 22.3 MWe. Hence, turbines with a capacity exceeding 22.3 MWe were each divided into multiple turbine stages of 20 MWe or less. When a turbine is downsized, the operating conditions are matched and the mass flow rate reduced. The scaling constant ($x$) generated from the fitted points of turbines with 20 MWe output or less was then applied to forecast the cost of turbines featuring >20 MWe output, using the cost function from the fitted points.
- **Storage tanks:** Cost function analysis of the storage tanks (molten salt holding tanks) was completed outside of Aspen HYSYS. To acquire the cost of the storage tanks, the cost data were retrieved from the 2011 National Renewable Energy Laboratory (NREL) study [11], which was based on the capital cost estimate for two-tank storage at a 100 MWe parabolic trough power plant with 6 hours of TES. The average cost for the low-temperature tank (<450˚C) was 7.08 $/kWh$_{th}$, which includes the cost of the entire storage tank system (holding tanks, tank supports, foundations, site work, electrical and instrumentation, piping, valves, and fittings). These numbers are consistent with the cost numbers found in other reports, including an INL study [9], a Sandia report based on two large-scale utility studies [10], and the 2011 NREL study [11].
- **Molten-salt storage media**: For Hitec® molten salts (the LWR use case), the cost functions were completed outside Aspen HYSYS by using actual quotes, historical pricing data, and costing numbers from previous projects. Recall that the LWR use case involves Hitec® as a storage material. Figure 26 shows the cost of Hitec® molten salt as a function of year, quantity, and grade/purity. Small quantities on the x-axis represent quantities of 10M kg or less. Industrial grades represent molten salt grades typically used in industrial and large-scale thermal storage systems, whereas higher grades represent the higher purity typically needed for medical/food applications or laboratory tests. The ideal zone in which most large-scale NPP-coupled TES systems would operate is in the higher quantity and industrial-grade zone (bottom-right corner of Figure 26). The "small quantities-high purity" dataset represents cost numbers from actual quotes and datapoints provided by the main U.S. supplier and owner of the Hitec® trademark (i.e., Coastal Chemical Co., LLC—a Brenntag company) for the years 1990–2021. The historical molten salt pricing data for "large quantity-industrial grade" are based on proportional cost numbers reported in the INL ($0.93/kg, 2003 project) and NREL ($1.23/kg, 2011 project) reports [9],[11]. The 2003 and 2011 cost numbers for the "large quantity-industrial grade" dataset were found to be reasonably proportional to the 2011 data points received from vendors for the "small quantity-industrial grade" dataset. To expand the data range, data based on actual quotes and data from the vendor for the "small quantities, high purity/grade" dataset were then used to generate time-dependent price trends and extrapolate the 2021 prices for the "large quantities, industrial grade" dataset. The data extrapolated via this method show an average annual increase of 4.38% year-over-year from 2011–2021, which is not too far from the 2.81% average global inflation

rates for the same period, based on the Producer Price Index for the Chemical Manufacturing as per the Federal Reserve Economic Data [12]. Any extrapolated data in the current database will be replaced with actual quotes/data points from vendors as they become available. The cost functions for solar salt were obtained by following the same approach; their cost per kg is provided in Figure 27.

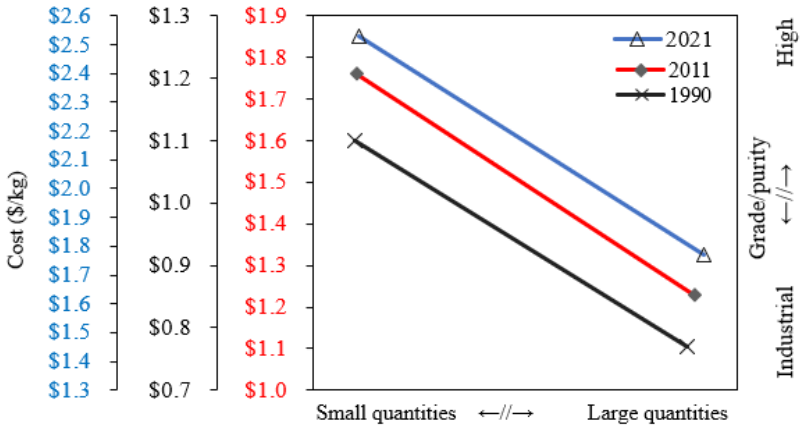


Figure 26. Cost of Hitec® molten salt as a function of year, quantity, and grade/purity.

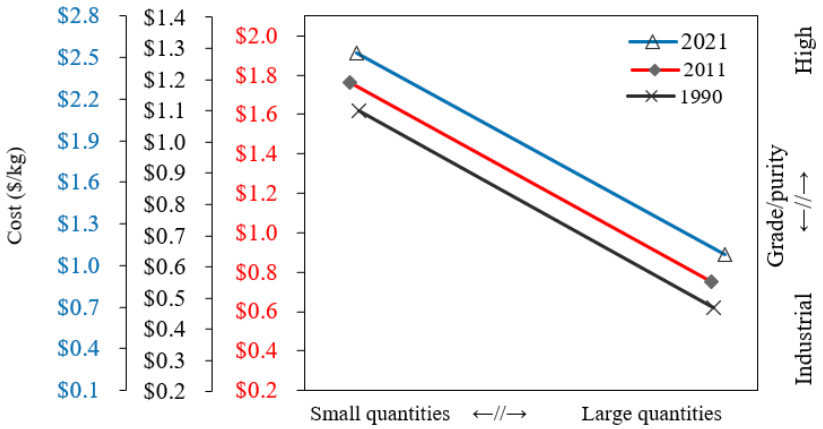


Figure 27. Cost of solar salt as a function of year, quantity, and grade/purity.

## 5.2 LWR-TES Cost Functions

This subsection discusses the cost functions for the LWR use case. The data points retrieved from the steady-state models developed for LWRs under different HDRs and coupling options provide sufficient resolution to create the cost functions for the various component and system sizes.

### 5.2.1 Cost Function Results for the Individual Equipment

First, the costing data for the various sized equipment were acquired from APEA and then used to create a cost function for each piece of equipment. The costing data for the molten salt storage media and storage tanks were the only components analyzed outside of APEA, following the methodology outlined in Section 5.1.2. Table 22 summarizes the cost function constants for the various components in the LWR-TES coupling use cases, the MAPE for each cost function, and the superset model that each piece of equipment falls under.

Figure 28 combines the cost function curves for various LWR-TES use case components. The red line in the turbine data indicates the start of extrapolated data beyond 20MWe (cost database limit of APEA).

Table 22. Summary of cost function constants for the various LWR-TES use case components.

| Equipment | ***A*** | ***D'*** | ***X*** | MAPE | Notes | BOP or Superset |
|---|---|---|---|---|---|---|
| Turbine | 3,086,300.0 | 16.34 MW | 0.7155732 | 0.4% | | BOP/Discharge |
| Condenser | 5,146,000.0 | 163.7 $MW_{th}$ | 0.5269188 | 9.3% | | BOP/Discharge |
| Cond. Feedwater Pump | 1,019,000.0 | 0.2075 MW | 0.4262537 | 2.6% | 101 to 230 kPa | Charge/Discharge |
| C-IHX | 2,892,100.0 | 72.57 $MW_{th}$ | 0.9881200 | 2.0% | | Charge |
| D-IHX | 3,513,100.0 | 72.57 $MW_{th}$ | 0.9805190 | 4.3% | | Discharge |
| BOP Pump (>400 kWe) | 284,600.0 | 0.3338 MW | 0.6202303 | 5.4% | 6 to 3600 kPa | BOP |
| BOP Pump (<100 kWe) | 108,400.0 | 0.0716 MW | 0.3106622 | 3.1% | 7 to 1200 kPa | Discharge |
| FWH Pump | 91,900.0 | 0.01251 MW | 0.3449450 | 4.9% | <20 kWe | Charge |
| Cold Molten-Salt Pump | 139,100.0 | 0.0001335 MW | 0.3993631 | 11.1% | | Storage |
| Hot Molten-Salt Pump | 139,100.0 | 0.0001335 MW | 0.3993631 | 11.1% | | Storage |
| Tanks | 1,544,148.0 | 218.1 $MWh_{th}$ | 0.9000000 | N/A | Carbon-steel | Storage |
| Molten Salt | 17,484,069.0 | 9888480 kg | 0.9000000 | N/A | Hitec® | Storage |

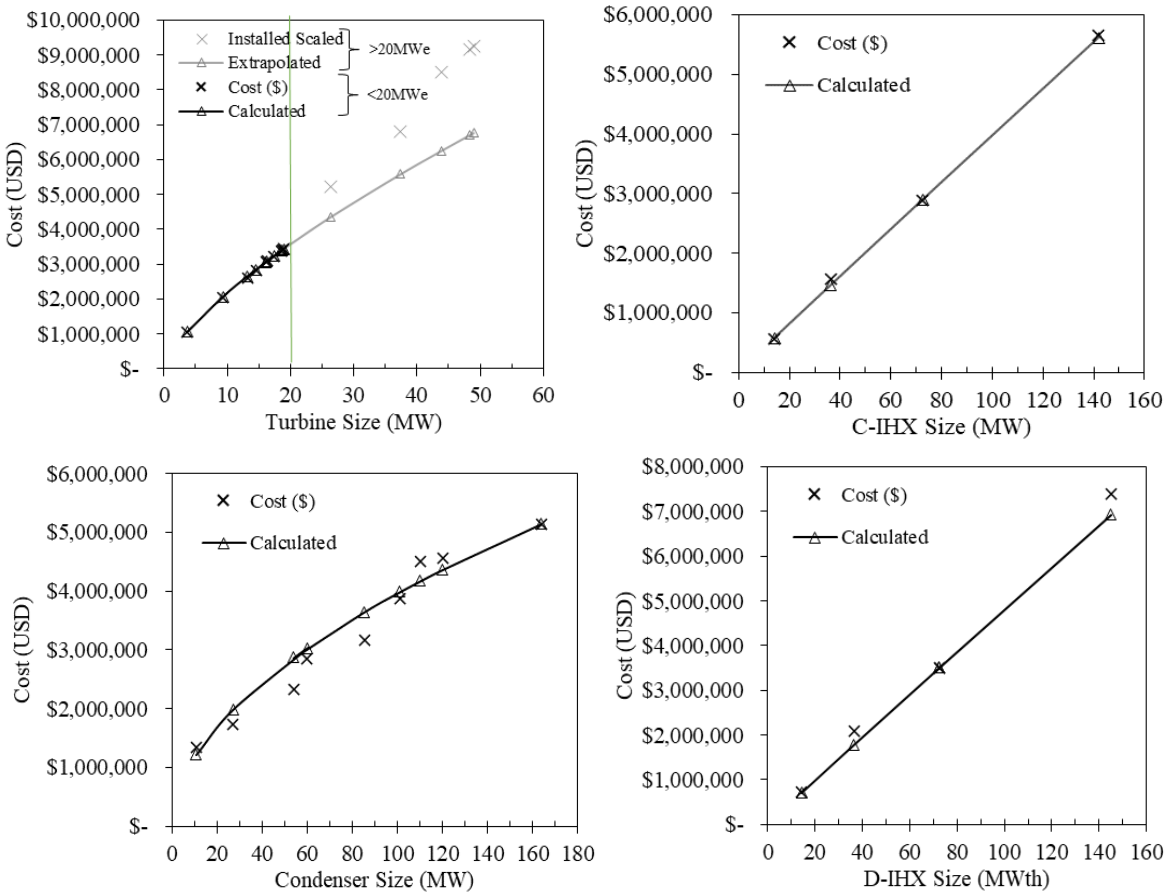

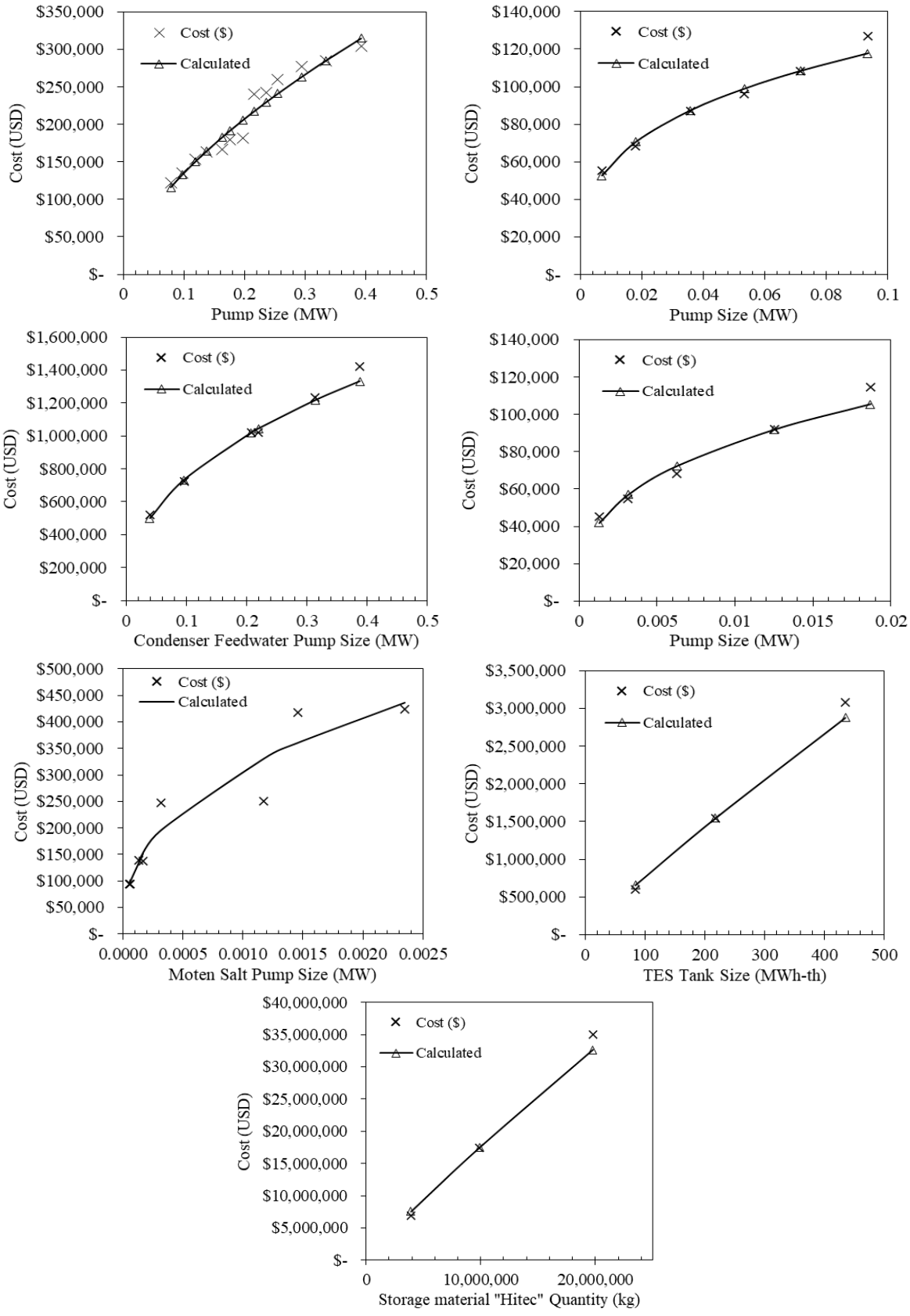


Figure 28. Cost function curves for the various LWR-TES use cases components.

### 5.2.2 Superset Cost Functions

As discussed in Section 5.1.1, the subset of cost functions from the individual pieces of equipment were then used to create three superset models: the (1) charge model, (2) storage model, and (3) discharge model. Figure 29 shows a process flow diagram of an A-LWR with its groupings being used to derive the superset cost functions. A single cost function for each of these three supersets was created by combining the cost functions for the individual-pieces-of-equipment subsets that fall under each of these supersets. Figure 30 combines the curves for the three superset cost functions as a function of system size. The secondary x-axis links the system size to the proportional HDR for each, and hence to the cost. Table 23 summarizes the cost function constants for the three superset models in the LWR-TES coupling use cases and gives the MAPE for each cost function.

Table 23. Cost function constants for the three superset models for the LWR-TES use cases.

| Superset model | A | D' | X | MAPE |
|---|---|---|---|---|
| Charge | 2,964,480.3 | 72.57 $MW_{th}$ | 0.95986969 | 0.2% |
| Storage | 36,452,122.8 | 435.42 $MWh_{th}$ | 0.83976343 | 4.2% |
| Discharge | 10,896,427.1 | 72.57 $MW_{th}$ | 0.69183838 | 0.8% |

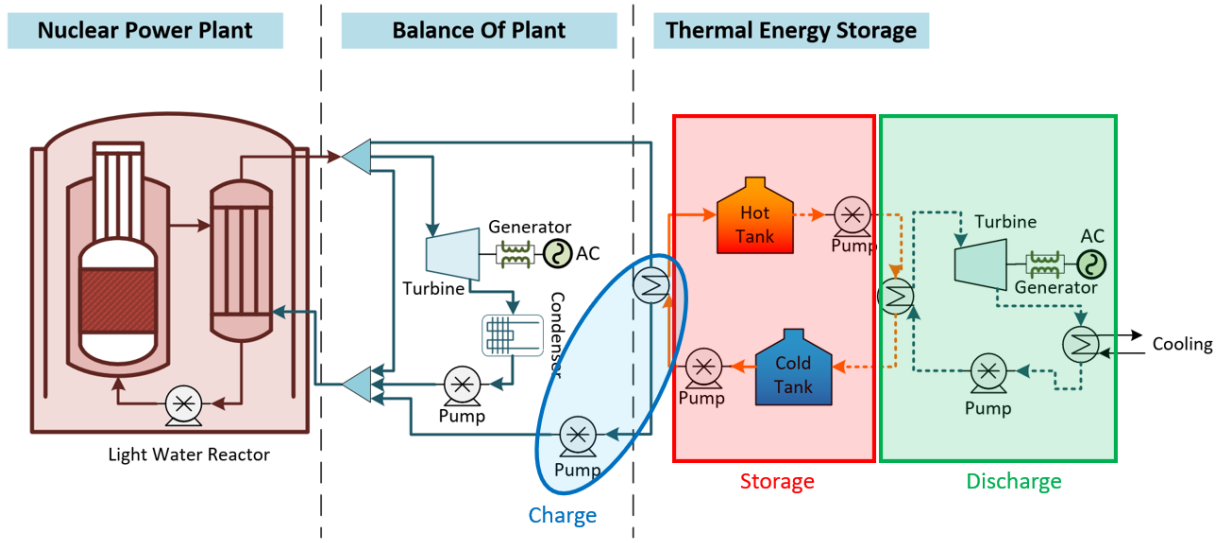


Figure 29: Component groupings in an A-LWR to derive the superset cost functions.

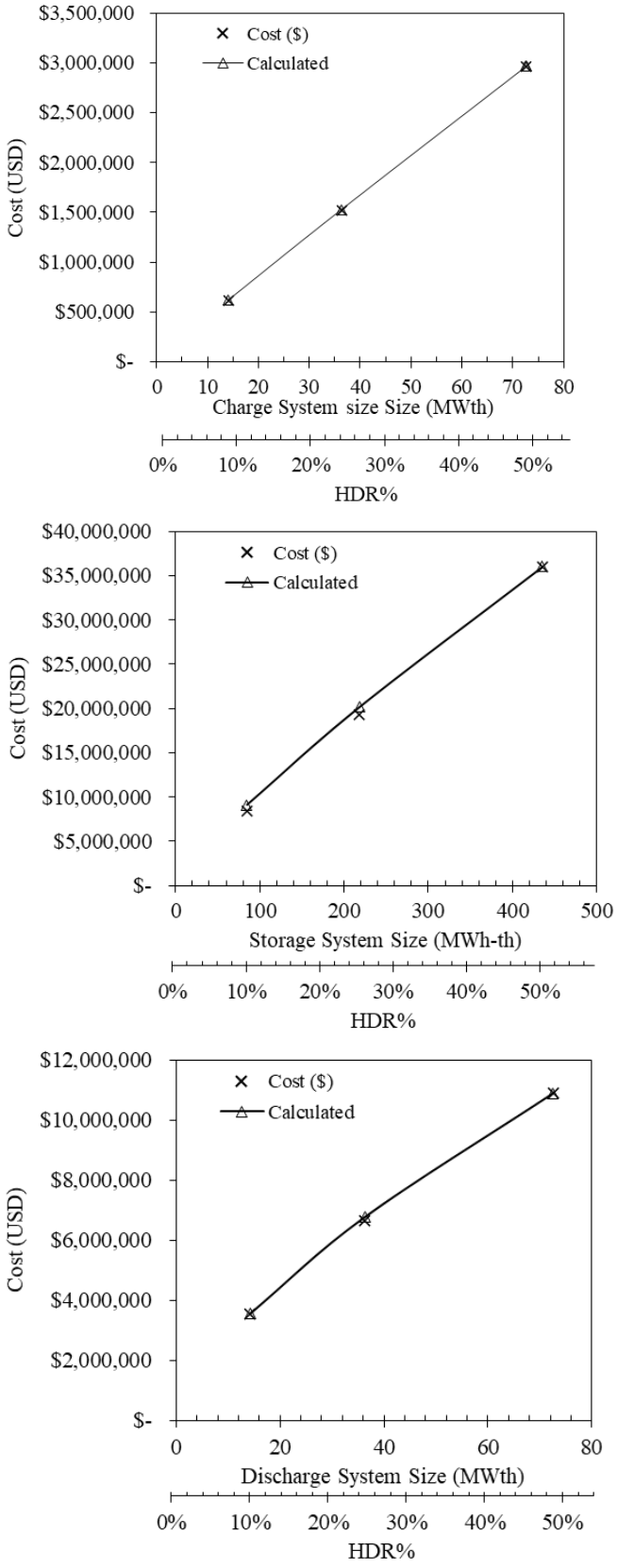


Figure 30. Cost functions curves for the superset models for the A-LWR-TES use cases.

### 5.2.3 Additional Analysis

Using the cost functions for the individual components shown in Section 5.2.1, a preliminary system size and cost summary was developed for the TES-LWR coupling, as well as the reference (i.e., no TES) case. As the models were sized to deliver an additional 3.67–18.57 MWe in electric output (depending on the HDR) over various durations, the equipment size and the additional capital installed cost accrued by adding the TES system are summarized in Table 24. The table also includes the sizing and installed cost analysis results for the tanks and molten-salt storage media under each of the three HDR values.

Table 24. System size and cost summary for the refence case, and the various equipment needed for A-LWR-TES- coupling at three different HDRs.

| | Equipment size (MW, MWh, kg) | | | | Calculated equipment cost (USD) | | | |
|---|---|---|---|---|---|---|---|---|
| | Ref. | 50% HDR | 25% HDR | 10% HDR | Ref. | 50% HDR | 25% HDR | 10% HDR |
| Turbine* | 49.02 | 18.57 | 9.32 | 3.67 | $6,774,127 | $3,382,169 | $2,065,010 | $1,059,432 |
| Condenser** | 110 | 54.05 | 26.99 | 10.61 | $4,173,439 | $2,870,044 | $1,990,552 | $1,217,067 |
| Cond. Feedwater Pump | 0.396 | 0.2195 | 0.09573 | 0.03883 | $1,342,189 | $1,043,715 | $732,767 | $498,798 |
| C-IHX | - | 72.57 | 36.35 | 14.11 | | $2,892,100 | $1,460,588 | $573,367 |
| D-IHX | - | 72.57 | 36.29 | 14.27 | | $3,513,100 | $1,780,670 | $713,046 |
| BOP Pump (<400 kWe) | 0.216 | - | - | - | $217,266 | | | |
| BOP Pump (<100 kWe) | - | 0.0358 | 0.018 | 0.007 | | $87,400 | $70,590 | $52,640 |
| FWH Pump | - | 0.006261 | 0.003127 | 0.001276 | | $72,380 | $56,966 | $41,815 |
| Cold Molten Salt Pump | - | 0.0003133 | 0.0001657 | 0.0000616 | | $195,561 | $151,637 | $102,136 |
| Hot Molten Salt Pump | | 0.001175 | 0.0001335 | 0.00005249 | $0 | $331,549 | $139,100 | $95,813 |
| Tanks | - | 435.42 | 218.1 | 84.66 | | $2,876,844 | $1,544,148 | $658,884 |
| Molten Salt | - | 19774800 | 9888480 | 3888000 | | $32,623,219 | $17,484,069 | $7,547,090 |

* The turbine equipment cost for the 50%, 25%, and 10% HDR cases represents only the additional cost realized for the additional turbine capacities added due to the additional heat dispatched from TES (i.e., TES power cycle turbine for coupling option 1, or the oversizing turbine capacity value for coupling option 3).

* The total power generated by the NPP during the TES discharge cycle is the sum of the reference turbine capacity and one of the HDR turbine capacity values.

** The condenser equipment costs for the 50%, 25%, and 10% HDR cases represent only the additional costs realized for the extra condenser capacities added due to the additional heat dispatched from TES (i.e., TES power cycle condenser for coupling option 1, or the oversizing condenser capacity value for coupling option 3).

** The total condenser power during the TES discharge cycle is the sum of the reference condenser capacity and one of the HDR condenser capacity values.

Figure 31 provides curves and equations that can be used to estimate the size of any of the three superset models (charge, storage, or discharge systems) as a function of HDR. This information can aid in estimating the system size for an HDR other than the three standard ratios employed in this study. The charge, storage, and discharge system size for a targeted HDR can then be applied to the superset cost functions in order to estimate the total installed cost of each case. Alternatively, the secondary x-axis in the curves under Figure 30 can be used to estimate the superset model size on the primary x-axis and then determine the total installed cost of the superset system from the y-axis.

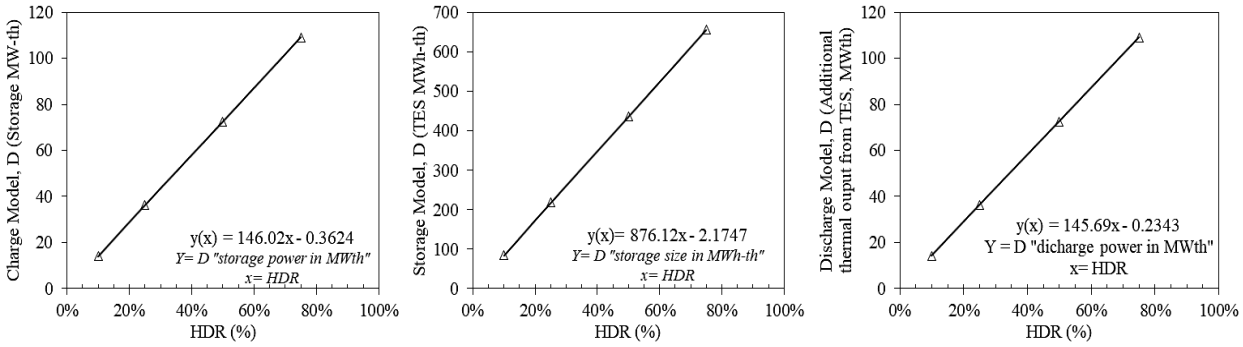


Figure 31. A-LWR superset model (charge, storage, and discharge) sizing curves as a function of HDR.

## 5.3 HTGR-TES Cost Functions

This subsection discusses the cost functions for the HTGR use case. The data points retrieved from the steady-state models developed for the HTGR under different HDRs and coupling options provide enough resolution to create the cost functions for the various component and system sizes.

### 5.3.1 Cost Function Results for the Individual Equipment

First, the costing data for the various-sized equipment were acquired from APEA, then used to create a cost function for each piece of equipment. The costing data for the molten-salt storage media and storage tanks were analyzed outside APEA, following the methodology outlined in Section 5.1.2. Table 25 summarizes the cost function constants for the various components in the HTGR-TES coupling use cases, the MAPE for each cost function, and the superset model that each piece of equipment falls under. Figure 32 combines the cost function curves for various HTGR-TES use case components.

Table 25. Summary of the cost function constants for the various HTGR-TES use case components.

| Equipment | ***A*** | ***D'*** | ***X*** | MAPE | Notes | BOP or Superset |
|---|---|---|---|---|---|---|
| Turbine | 2,237,600.0 | 11.26 MW | 0.7192345 | 0.4% | | BOP/Discharge |
| Condenser | 4,577,000.0 | 92.18 $MW_{th}$ | 0.6415093 | 9.3% | | BOP/Discharge |
| Cond. Feedwater Pump | 1,063,000.0 | 0.195 MW | 0.4689908 | 4.3% | | Charge/Discharge |
| C-IHX | 7,738,000.0 | 41.58 $MW_{th}$ | 0.2859381 | 4.9% | | Charge |
| D-IHX | 12,817,200.0 | 91.03 $MW_{th}$ | 0.9920155 | 9.6% | | Discharge |
| BOP Pump (>400 kWe) | 1,034,400.0 | 1.369 MW | 0.3178757 | 2.4% | | BOP |
| BOP Pump (<400 kWe) | 296,100.0 | 0.2346 MW | 0.4388273 | 3.7% | | Discharge |
| FWH Pump | 270,100.0 | 0.1399 MW | 0.6130092 | 8.5% | | Charge |
| Cold Molten-Salt Pump | 131,600.0 | 0.000301001 | 0.3168514 | 7.5% | | Storage |
| Hot Molten-Salt Pump | 383,200.0 | 0.0002509 | 0.5096359 | 7.4% | | Storage |
| Tanks | 1,930,291.2 | 272.64 $MW_{th}$ | 0.9000000 | 5.4% | Carbon-Steel | Storage |
| Molten Salt | 4,767,363.9 | 4410720 kg | 0.9000000 | 5.4% | Solar Salt® | Storage |

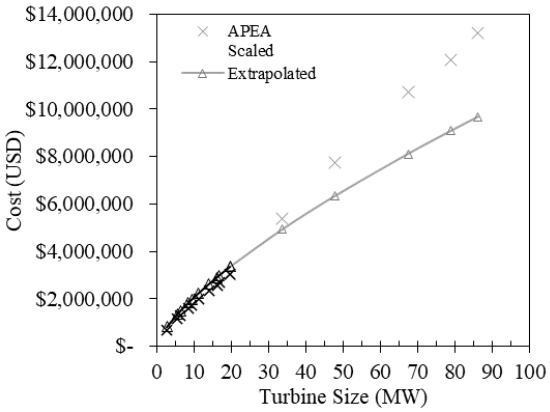
APEA
Scaled
Extrapolated
Cost (USD)
Turbine Size (MW)

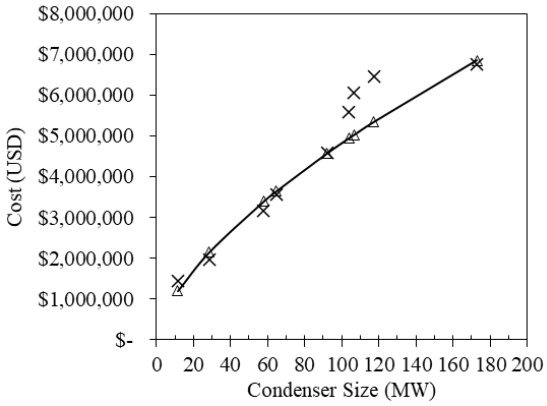
Cost (USD)
Condenser Size (MW)

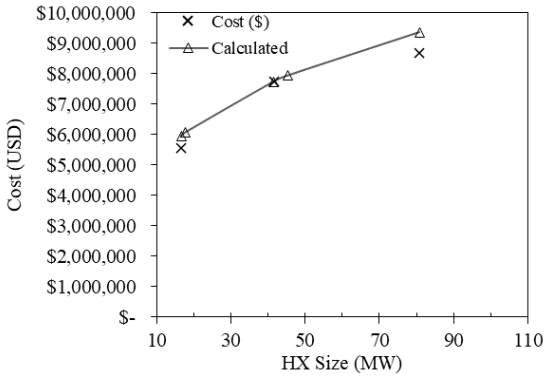
Cost ($)
Calculated
Cost (USD)
HX Size (MW)

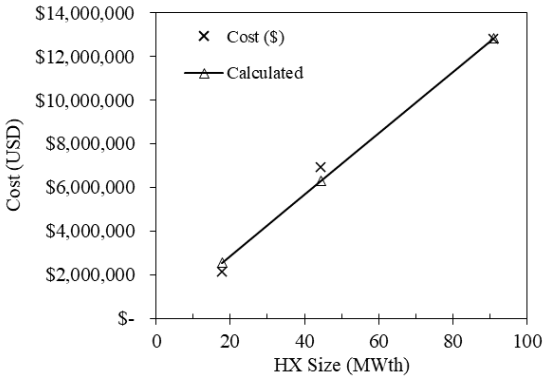
Cost ($)
Calculated
Cost (USD)
HX Size (MWth)

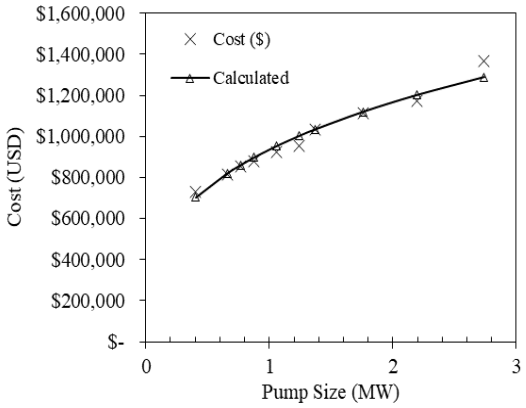
Cost ($)
Calculated
Cost (USD)
Pump Size (MW)

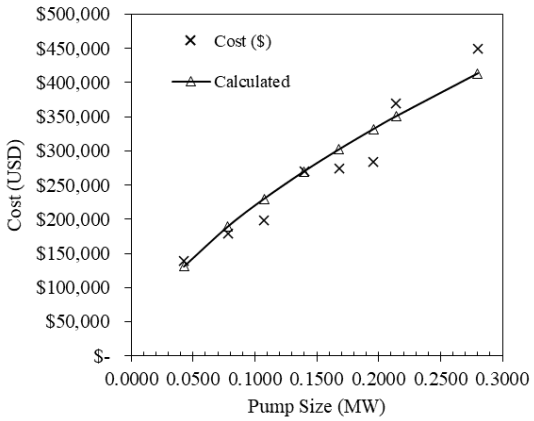
Cost ($)
Calculated
Cost (USD)
Pump Size (MW)

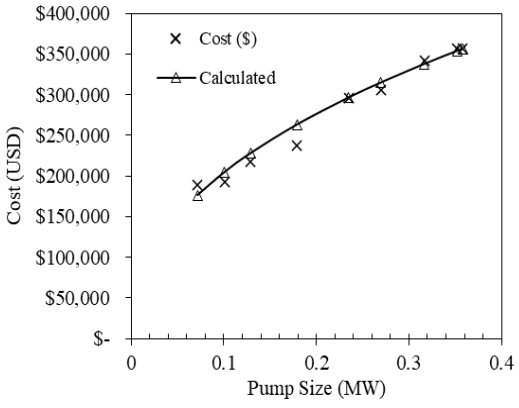
Cost ($)
Calculated
Cost (USD)
Pump Size (MW)

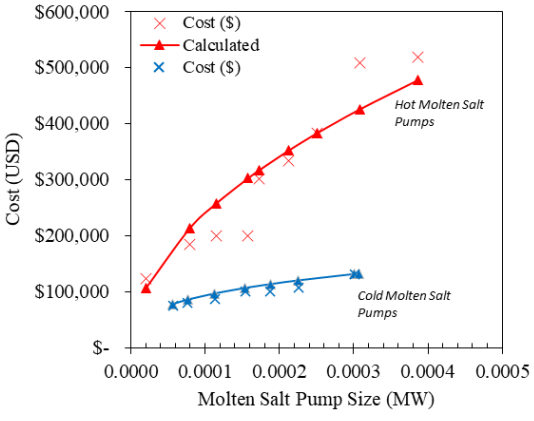
Cost ($)
Calculated
Cost ($)
Hot Molten Salt Pumps
Cold Molten Salt Pumps
Cost (USD)
Molten Salt Pump Size (MW)

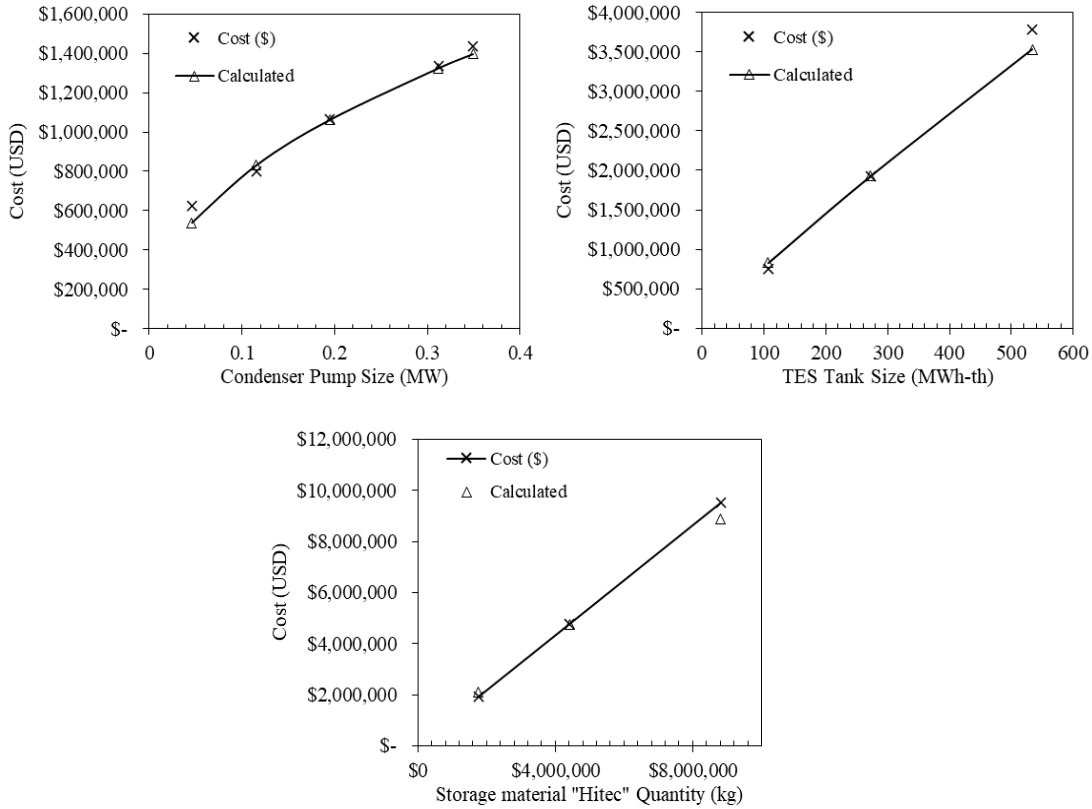


Figure 32. Cost function curves for the various HTGR-TES use case components.

### 5.3.2 Superset Cost Functions

As discussed in Section 5.1.1, the subsets of cost functions from the individual pieces of equipment were then used to create three superset models: the (1) charge model, (2) storage model, and (3) discharge model. A single cost function for each of these three supersets was created by combining the cost functions for the individual-pieces-of-equipment subsets that fall under each of these supersets. Figure 33 combines the curves for the three superset cost functions as a function of system size. The secondary x-axis links the system size to the proportional HDR for each, and hence to the cost. Table 31 summarizes the cost function constants for the three superset models in the HTGR-TES coupling use cases and gives the MAPE for each cost function.

Table 26. Cost function constants for the three superset models for the HTGR-TES use cases.

| Superset model | A | D' | X | MAPE |
|---|---|---|---|---|
| Charge | 9,969,119.3 | 88.95 $MW_{th}$ | 0.2949494 | 0.1% |
| Storage | 12,864,236.1 | 533.71 $MW_{th}$ | 0.8817904 | 0.1% |
| Discharge | 22,149,510.8 | 88.95 $MW_{th}$ | 0.8165095 | 0.5% |

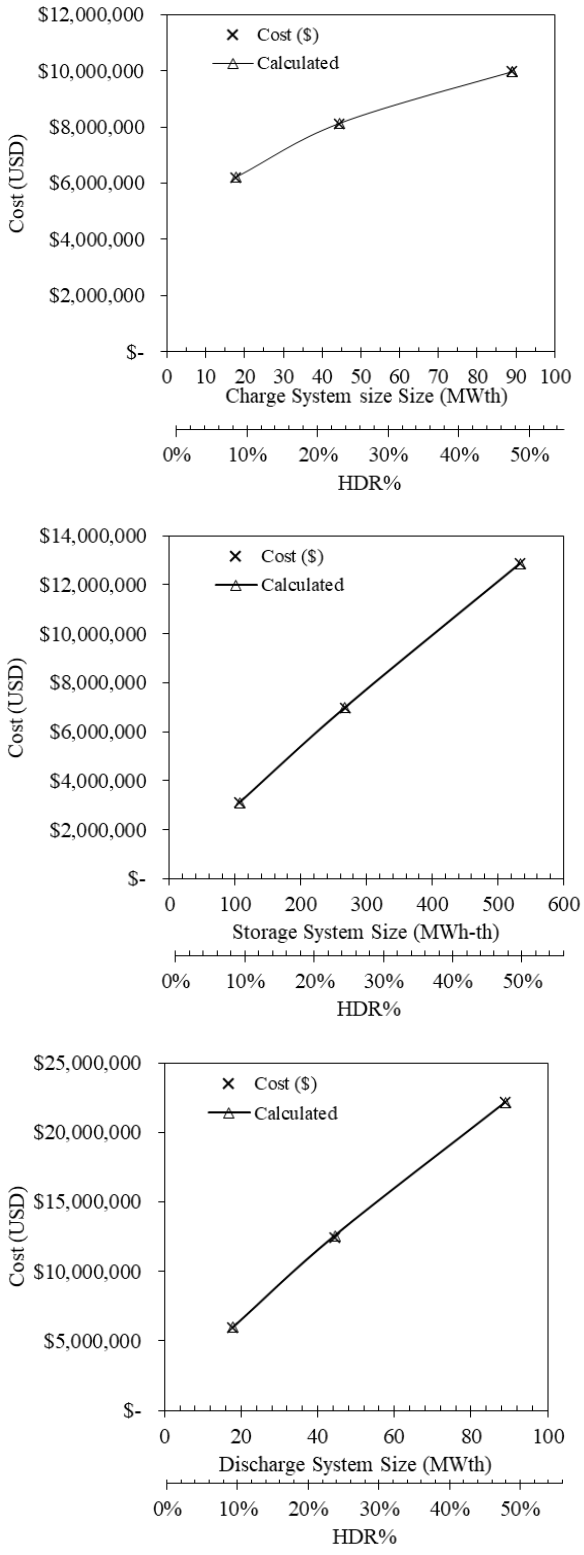


Figure 33. Cost functions curves for the superset models for the HTGR-TES use cases.

### 5.3.3 Additional Analysis

Using the cost functions for the individual components shown in Section 5.3.1, a preliminary system size and cost summary was developed for the HTGR-LWR coupling, as well as the reference (i.e., no TES) case. As the models were sized to deliver an additional 6.391–31.84 MWe in electric output (depending on the HDR) over various durations, the equipment size and the additional capital installed cost accrued by adding the TES system are summarized in Table 32. The table also includes the sizing and installed cost analysis for the tanks and molten-salt storage media under each of the three HDR values.

Table 27. System size and cost summary for the refence case, and the various equipment needed for HTGR-TES-H coupling at three different HDRs.

| | Equipment size (MW, MWh, kg) | | | | Calculated equipment cost (USD) | | | |
|---|---|---|---|---|---|---|---|---|
| | Ref. | 50% HDR | 25% HDR | 10% HDR | Ref. | 50% HDR | 25% HDR | 10% HDR |
| Turbine* | 87 | 31.84 | 15.93 | 6.391 | $9,737,532 | $4,725,740 | $2,871,804 | $1,488,924 |
| Condenser** | 117.4 | 57.48 | 28.75 | 11.49 | $5,345,145 | $3,380,606 | $2,167,594 | $1,203,520 |
| Cond. Feedwater Pump | 0.453 | 0.235 | 0.1155 | 0.04589 | $1,578,388 | $1,160,211 | $831,496 | $539,335 |
| C-IHX | - | 88.95 | 44.48 | 17.79 | | $9,617,520 | $7,888,621 | $6,070,171 |
| D-IHX | - | 88.95 | 44.48 | 17.79 | | $12,526,644 | $6,298,784 | $2,537,731 |
| BOP Pump (<400 kWe) | 1.369 | - | - | - | $1,034,400 | | | |
| BOP Pump (<100 kWe) | - | 0.3577 | 0.179 | 0.07186 | | $356,310 | $262,958 | $176,178 |
| FWH Pump | - | 0.2151 | 0.1074 | 0.04286 | | $351,600 | $229,690 | $130,792 |
| Cold Molten Salt Pump | - | 0.000307247 | 0.0001537 | 0.00005688 | | $132,459 | $106,358 | $77,621 |
| Hot Molten Salt Pump | | 0.000157684 | 0.00007886 | 0.0000202 | $0 | $302,431 | $212,452 | $106,123 |
| Tanks | - | 533.7 | 266.88 | 106.74 | | $3,533,131 | $1,893,549 | $830,016 |
| Molten Salt | - | 8821440 | 4410720 | 1764504 | | $8,896,216 | $4,767,364 | $2,090,163 |

* The turbine equipment cost for the 50%, 25%, and 10% HDR cases represents only the additional cost realized for the additional turbine capacities added due to the additional heat dispatched from TES (i.e., TES power cycle turbine for coupling option 1, or the oversizing turbine capacity value for coupling option 3).

* The total power generated by the NPP during the TES discharge cycle is the sum of the reference turbine capacity and one of the HDR turbine capacity values.

** The condenser equipment costs for the 50%, 25%, and 10% HDR cases represent only the additional costs realized for the extra condenser capacities added due to the additional heat dispatched from TES (i.e., TES power cycle condenser for coupling option 1, or the oversizing condenser capacity value for coupling option 3).

** The total condenser power during the TES discharge cycle is the sum of the reference condenser capacity and one of the HDR condenser capacity values.

Figure 34 shows curves and equations usable to estimate the size of any of the three superset models (charge, storage, or discharge systems) as a function of HDR. This information can aid in estimating the system size for HDRs other than the three standard ratios employed in this study. The charge, storage, and discharge system size for a targeted HDR can then be applied to the superset cost functions to estimate the total installed cost of each case. Alternatively, the secondary x-axis in the curves under Figure 33 can be used to estimate the superset model size on the primary x-axis and then determine the total installed cost of the superset system from the y-axis.

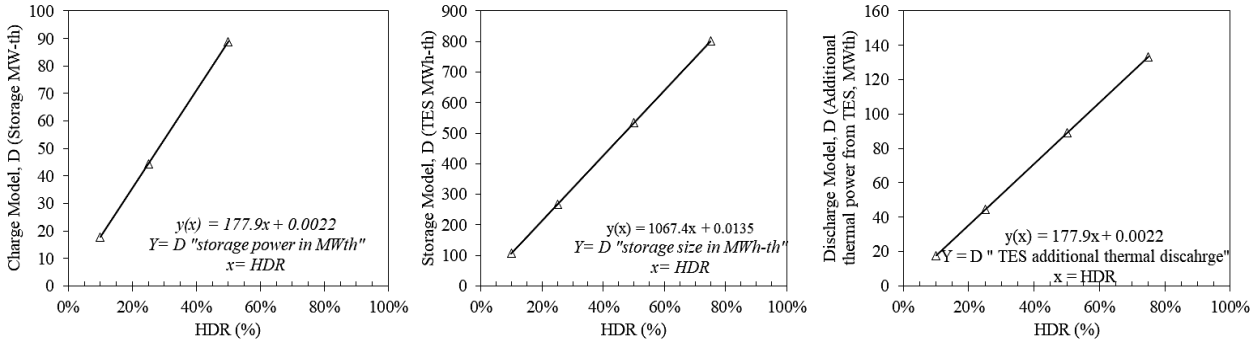


Figure 34. HTGR superset model (charge, storage, and discharge) sizing curves as a function of HDR.

## 5.4 System and Dispatch Optimization Using HERON

RAVEN [20] and its dispatch optimization plugin HERON were used to perform an optimization of the presented energy storage systems. The signal processing and synthetic history capabilities of RAVEN were used to take the unpredictable behavior of electricity markets into account in the system's optimization. An ARMA model was used to analyze and reproduce price signals from the PJM market and will be discussed in more detail in a follow up future work. Using these data, stochastic optimization of the models was performed via HERON at two different levels: the components' capacities and their dispatch. The main optimization consisted of finding the optimal component capacities to maximize the net present value (NPV) of the portfolio. To compute this NPV, a secondary optimization was necessary; namely, the dispatch of the fixed-capacity components in the portfolio was optimized each hour over the system's lifetime.

The focus of this TEA is to compare the economic advantages of one choice of thermal energy storage design over another. This can be accomplished using a differential NPV analysis, reducing the need for NPP cost data and thus eliminating the uncertainty surrounding those data. The following equation shows the calculation conducted for this analysis, with the NPV of the studied system being compared to a baseline case:

$$\Delta NPV = NPV(System) - NPV(baseline)$$

In the current analysis, the baseline case is selected based on the following assumptions for the current use of NPPs: (1) the system consists only of a nuclear power plant selling its power to the grid and (2) the calculation of the NPV of this baseline system is then used as a reference to assess whether a particular storage system design coupled with the nuclear power plant is more economically interesting.

### 5.4.1 HERON Case Setup

The goal of the TES use case is to analyze several reactor types, integrated with different TES technologies, that operate in different markets and regions. Figure 35 shows a matrix of the potential studies that would be carried out under the TES use case in the future including additional reactor types, such as molten salt reactor (MSR), or additional markets such as NYISO (New York Independent System Operator) and CAISO (California Independent System Operator).

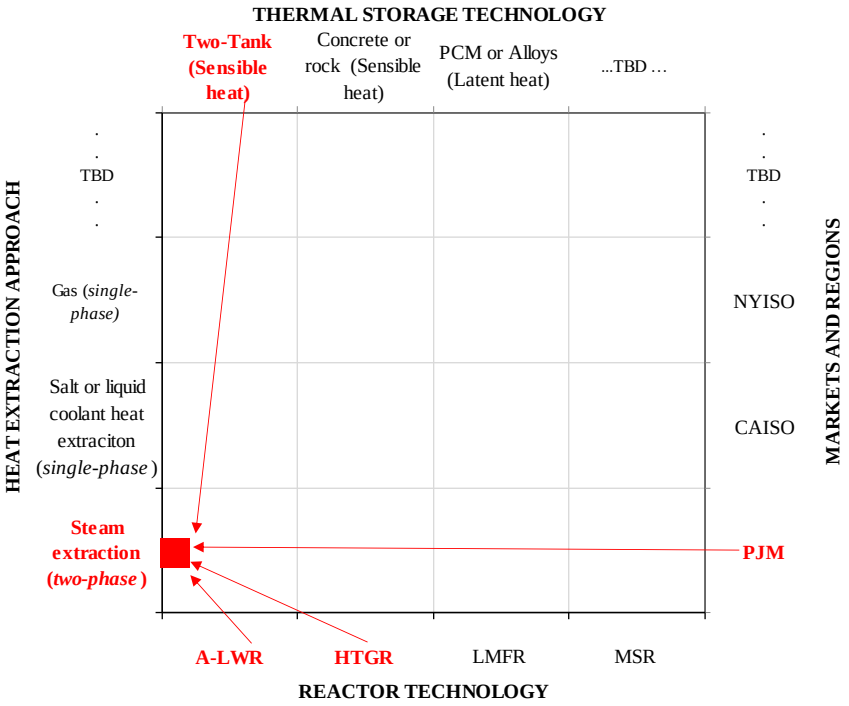


Figure 35. TES use case matrix for current and future studies.

The cases selected for this study focused on the A-LWR and HTGR systems, both of which have a Rankine power cycle for electricity generation. As mentioned in Section 3.1.3, the primary heat transfer fluid (steam) is diverted from the main steam header and used to transfer heat to the working fluid within the TES systems (i.e., molten salt). So far, the analyzed coupling of the TES system to the NPP is of the type referred to in Section 3.2.1 as option 1, and superset cost functions acquired from Aspen HYSYS for both the reactor types were used. HERON makes use of the Extensible Markup Language (XML) for its input structure, similar to RAVEN. The HERON input.xml file defines the interaction between the individual components of the case being analyzed. Figure 36 shows the process flow diagram used to set up the HERON input.xml file. The steam generator could potentially provide reactor heat to two components, and this heat is either used to generate electricity sold to the grid or to provide heat to TES for storage purposes. The components in yellow are the supersets for which the cost functions were derived. These cost functions are provided as inputs in the cashflow section of the code for each component.

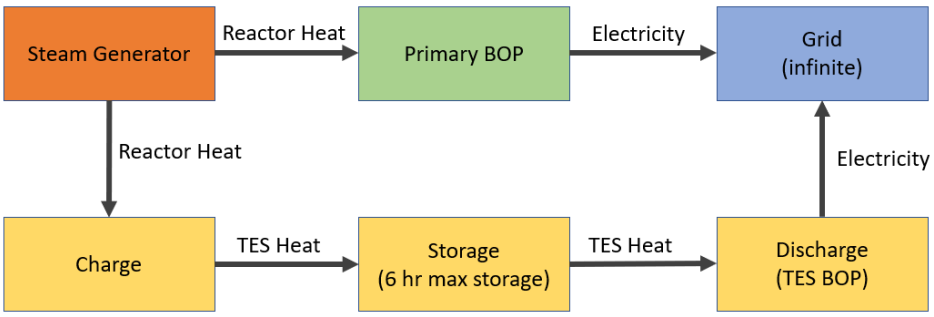


Figure 36. Process flow diagram of the energy transfer between different components.

For each component, the capacity can be provided as either a single value or as a range. The steam generator, primary BOP and grid all have fixed values, whereas the charge, storage, and discharge components have a range over which they can be optimized. The BOP and discharge components also correspond to a specific efficiency as they convert thermal energy to electricity via a Rankine cycle. Information on the local marginal price, which is used to determine whether to store the reactor heat for future use or convert it into electricity and sell it to the grid, is provided by the ARMA file. The location of this file is also given within the HERON input file. The goal of the optimizer is to iterate through possible component capacities and locational marginal price values and then converge to a design that provides the highest economic benefit, which for this case was specified in terms of mean NPV.

Once the HERON input file is set up, it is executed via a command line executable. HERON parses the input file and generates three new files required for RAVEN. The outer.xml file, which contains information pertaining to the system capacity optimization, allows users to tweak settings in RAVEN's gradient descent optimizer. The second file is the inner.xml file, which contains information on the dispatch optimization. This file is rarely changed by the user. The final required file is the heron.lib file, which contains the cashflow and case information required during RAVEN's runtime.

### 5.4.2 HERON Dispatch Analysis

Preliminary analysis of the HERON-optimized dispatch indicated that the mean NPV is highest for NPP systems without an integrated TES. This could be due to the following reasons:

1) The specific market chosen for this analysis may not have enough price volatility for an integrated system to recoup the TES system's capital expenditures (CAPEXs) and maximize its profit.
2) The pinch point caused by steam condensation, as mentioned in Section 4, limits the maximum temperature up to which the molten salt can be heated. This leads to a larger TES system, thus increasing its CAPEX and that of the overall system.

To support the claim made in the first statement, the TES CAPEXs were reduced to 75% and 50% of their calculated values. At 75% CAPEX, the HTGR system with an integrated TES system proved the most economical, whereas the A-LWR still gravitated toward the no-TES setup. This is primarily because the TES system is more expensive in the LWR setup, due to the type of salt used and the maximum temperature at which it operates. At 50% CAPEX, however, application of an integrated TES system to both the reactor types is the optimal choice.

To overcome the limitations of the pinch point, heat transfer would have to occur between the single-phase fluid within the primary loop and the heat storage medium. This could be accomplished in the case of the HTGR and LMFR by tapping into the primary coolant loop. Analyses are currently being conducted to model such systems and perform dispatch optimizations by using HERON to address the limitations. The results of these studies will be provided in a follow-up work.

## 6. MODELICA TRANSIENT MODELING OF A-LWR IES

To keep up with the other modeling efforts of this project, development within HYBRID for this use case has focused on implementing the three cases of the LWR-type SMR candidate systems. HTGR and LMFR models will be completed in future work. This development is occurring such that modeling can take advantage of object-oriented programming within Modelica to swap reactor systems and storage materials in order to change from a LWR type to a HTGR and then a LMFR. The purpose of developing and implementing Modelica models is to understand the dynamic behavior of these IES and to evaluate systems' controls. The reasons behind the reactor, TES media, and integration selection have already been discussed in this report. In this section, the specific implementation of each case within Modelica is described, focusing on the integration techniques, BOP modeling, and control methods used. For further background on the development of the reactor models and TES model, see [21] and [22].

The control systems discussed in the following sections were all developed based on system power dispatch control. Given a power setpoint, three operating regimes may be able to occur in cases 1 and 3. When the power requirement is lower than the nominal reactor electrical output, the system will operate in charging mode and direct thermal energy into the TES. When the power requirement exceeds the nominal reactor electrical output, the system will operate in discharging mode and meet the power requirement by dispatching energy from the TES. Standby operation occurs when electrical demand is equal to the nominal reactor electrical output. Note that standby operation occurs much more frequently during economically driven operation than in load-driven operation.

In case 2, only the charging and buffer operation modes are employed. During economic operation with a sufficiently large energy storage capacity, it is possible that the system might only charge—and not discharge any energy from the TES. During buffer operation, which is the expected operation mode, the system charges and discharges simultaneously. The TES discharges to meet the given power demand. To maximize the economic benefit of the NPP, reactor heat should charge at nominal conditions. Note that due to anticipated economic challenges, case 2 is not presently pursued for LWRs.

Some terms must be introduced to consistently discuss the IES deployment scenarios. In all these cases, the thermal integration point for heating the TES is the C-IHX. The flow depositing heat across the C-IHX is referred to as "bypass" while hot and "condensate" when flowing out of the C-IHX. The mass flow in the C-IHX on the TES side is the "charging" flow. The thermal dispatch integration point is the D-IHX. The mass flow in the D-IHX on the TES side is the "discharging" flow, and the steam flow on the other side is the "TES feed" and "TES steam."

## 6.1 Case 1: Standalone NPP-TES Coupled with a Secondary Power Generation Cycle

In the first case, the TES dispatches energy to produce electricity via an independent BOP. To control this kind of system based on power dispatch, the system must operate in each of the three modes. The intent of this use case is to maintain constant nominal reactor heat output such that the dynamic control mechanisms can be determined.

### 6.1.1 LWR Control Scheme

During standby mode, the TES control systems would operate zero flow on both the charging and discharging sides. There are nine controlled elements within the case 1 IES, as seen in Figure 37. The A-LWR operates via natural circulation, so there is no primary-side pumping mechanism with which to alter the primary-side flow. The primary side controls the primary coolant pressure via mechanisms outside the consideration of IES operation. The pressurizer operates via nominal methods in all operating paradigms. Control rods on the primary side will also operate according to the nominal method of controlling average coolant temperature. Within the primary BOP, the controllable mechanisms include the turbine bypass valve (TBV), turbine control valve (TCV), feedwater heating valve (FHV), and feedwater control pump (FWCP). The independent TES BOP will also have a separate TCV, FHV, and FWCP set denoted with a "D-" (standing for discharge) before the name (i.e., the D-TCV, D-FHV, and D-FWCP), and this set must be controlled. This naming convention should also aid in analysis of case 3. The TES model used is sized so that constantly operating pumps can produce the flow necessary to meet 100% of the TES charge/discharge demand. Internally, a charging control valve (CCV) and a discharging control valve (DCV) moderate the TES fluid flows.

To meet demand, control for the NPP-integrated BOP must be able to operate during all three operational modes. The overarching system demand is the primary input for the control systems. A summary of the BOP control methods is given in Table 28. Turbine output is the primary operational setpoint and will be controlled via the TBV. Note that this TBV is independent of a pressure relief valve that ensures over-pressurization does not occur. The TCV operates to maintain steam pressure at the outlet of the steam generator. The FHV position meets feedwater temperature during all operational

modes. To maintain feed mass flow, the FWCP changes its speed to increase or decrease the pumping power. The fact that the components combine in a non-linear system enables the overall system conditions to be met. The goal of the FHV, TCV, and FWCP subsystem is to provide a constant heat sink to the primary side in order to avoid impacting reactor conditions whenever possible.

The TES BOP is a relatively simpler system. Feedwater is sourced directly from the TES BOP condenser and pumped through the D-FWCP, which operates to maintain steam pressure. The D-TCV opens to meet the electrical demand (i.e., the system demand less the nominal BOP production) in conjunction with the D-FCV. The D-FCV effectively operates to meet large changes in demand, while the D-TCV makes smaller adjustments to the power output.

Within the TES, the CCV changes position such that the charging flow meets a reference hot tank temperature. Similarly, the DCV changes position to meet the reference cold tank temperature. Both valves have two additional mechanisms that aid in modal operation. The first is an anticipatory signal that forces open the valves to let some mass through at the initiation of charging/discharging. This counteracts the fact that, according to the valve logic, simply not opening is a mathematically acceptable way to meet the reference temperatures. The second mechanism is a safety mechanism that forces the valves to close when there is a lack of source media (meaning that the CCV looks at the cold tank level and the DCV looks at the hot tank level). This is done by multiplying the opening value by a fraction if the level becomes too low.

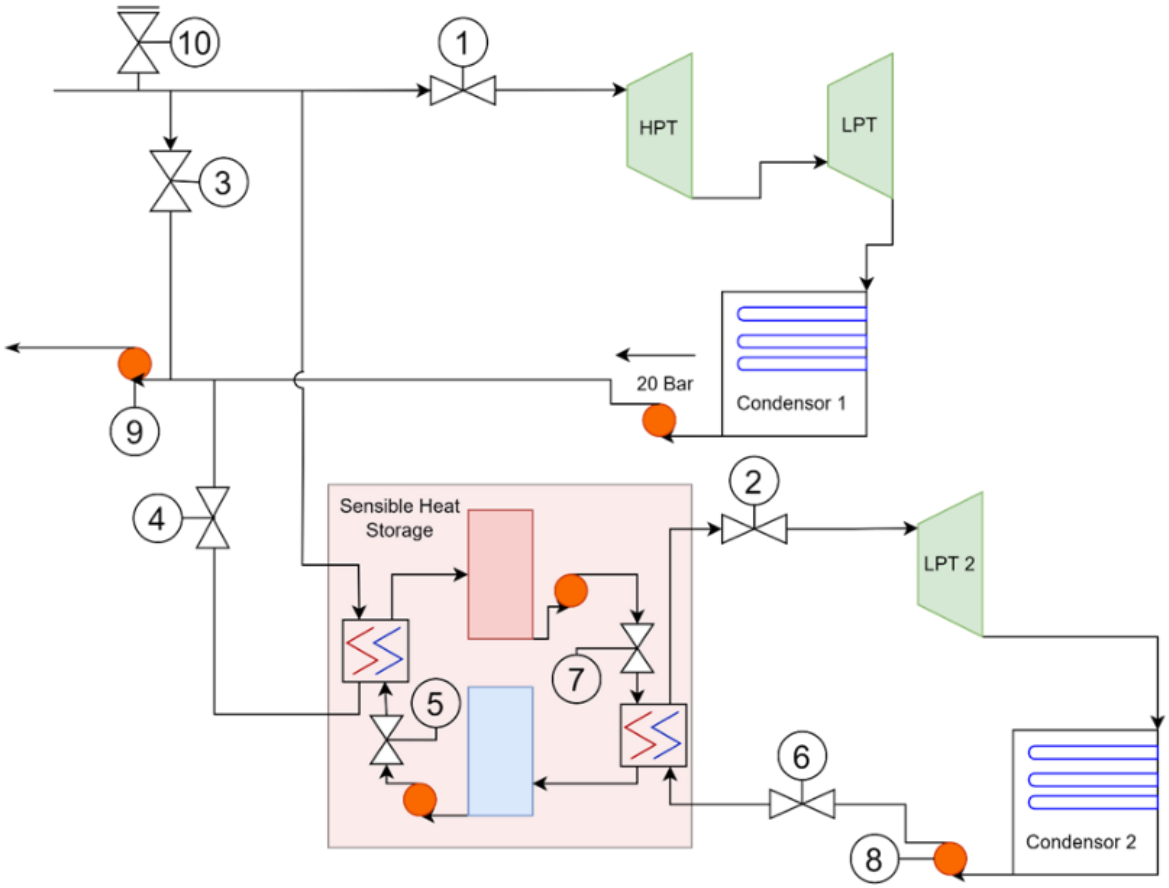


Figure 37. Block diagram of the case 1 Modelica model.

Table 28. Case 1 control methods summary.

| Label | Name | Controlling | Setpoint |
|---|---|---|---|
| 1 | Turbine Control Valve (TCV) | Steam Inlet Pressure (HPT) | 34 bar |
| 2 | Discharge Turbine Control Valve (D-TCV) | Power (LPT 2) | If demand power > Q_nominal = demand power – Q_nominal else is 0. |
| 3 | Feedwater Heating Valve (FHV) | Feedwater Temperature | 148°C |
| 4 | Turbine Bypass Valve (TBV) | Power (HPT and LPT) | If demand power > Q_nominal = Q_nominal else is demand power. |
| 5 | Charging Control Valve (CCV) | SHS Hot Tank Temperature | 240°C |
| 6 | Discharging Feedwater Control Valve (D-FCV) | Power (LPT 2) | If demand power > Q_nominal = demand power – Q_nominal else is 0. |
| 7 | Discharging Control Valve (DCV) | SHS Cold Tank Entry Temperature | 180°C |
| 8 | Discharging Feedwater Control Pump (D-FWCP) | Steam Inlet Pressure (LPT 2) | 12 bar |
| 9 | Feedwater Control Pump (FWCP) | Reactor Secondary Mass Flow | 67 kg/s |
| 10 | Pressure Relief Valve | Pressure Overloads | Release at 150 bar |

### 6.1.2 Aspen HYSYS® Comparison with Case 1 Dymola Model

The Dymola models can be run into a quasi-steady state at their charging or discharging state. This allows for a cursory comparison with the Aspen HYSYS® models in these two modes, ensuring that the system sizing is appropriate in the Modelica model. For case 1, comparisons between the parameters of interest at these two states are shown in Table 29 and Table 30. Good agreement is seen between the Aspen HYSYS® and Dymola® models in almost every condition. Notable differences occur between the molten salt mass flow rates in discharge mode. Dymola dynamically adjusts molten salt mass flows to maintain temperatures in the two storage tanks, and consequently these mass flows vary significantly—even in a quasi-steady-state demand profile. The other significant difference between the two model conditions is that a non-zero flow (3.16 kg/s) must be maintained in charging for the TES BOP cycle, which produces a power in zero-discharge of 1.45 MW. The BOP cycle is controlled in order to maintain an overall power output equivalent to that in the Aspen HYSYS® case.

In Dymola, as is explained in Section 6.1.1, the control system dispatches the thermal storage in order to control the power level. As a result, the HDR drifts away from the 50% value used in the Aspen HYSYS®. Having specified the size of the system, in the quasi-steady charge state, however, the HDR achieved is close to 50% at 47.8%. Finally, the condenser in Dymola is assumed perfect and is not modeled further. These values have been left blank in Table 29 and Table 30.

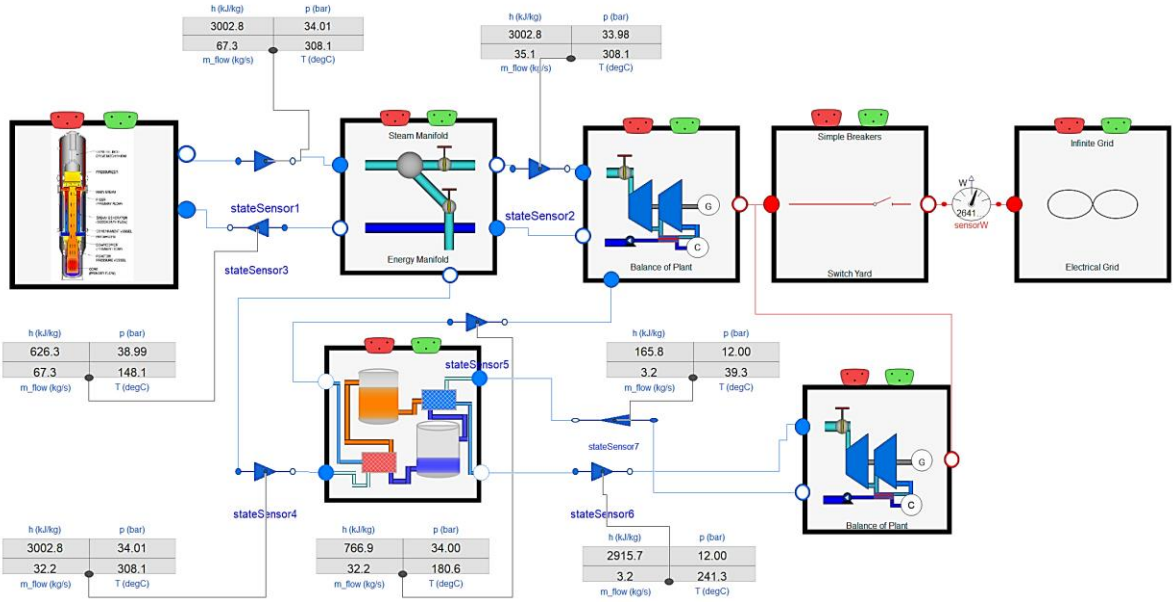


Figure 38. Modelica process flow diagram of an A-LWR-TES coupling with a standalone secondary TES power generation cycle (first coupling method) and a HDR of close to 50%, showing the active charge cycle and inactive hot standby discharge cycle in hot standby mode.

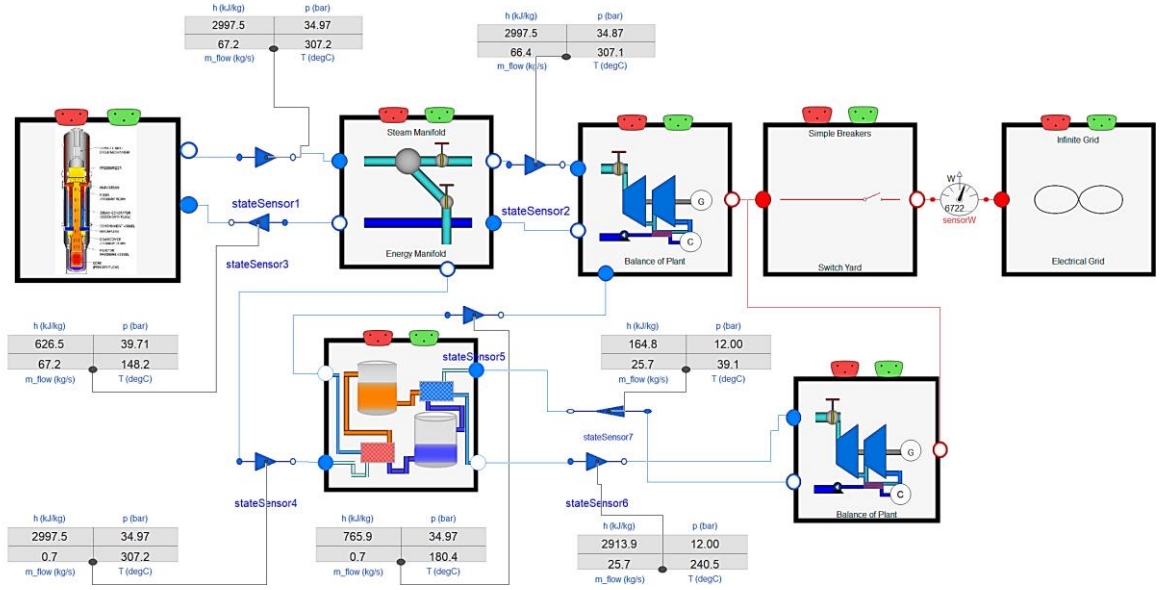


Figure 39. Modelica process flow diagrams of an A-LWR-TES coupling with a standalone secondary TES power generation cycle (first coupling method), showing the primary power generation cycle with an inactive charging cycle, as well as the active discharge cycle and secondary power generation cycle.

Table 29. Comparison between the Aspen HYSYS® and Dymola® BOP and operating conditions of an A-LWR-TES coupling with a secondary power generation cycle and a HDR of 50%.

| | | ----------Aspen HYSYS®---------- | | | ----------Dymola®---------- | | |
|---|---|---|---|---|---|---|---|
| Equipment | Cycle | Mass flow rate (kg/s) | Inlet temperature (°C) | Exit temperature (°C) | Mass flow rate (kg/s) | Inlet temperature (°C) | Exit temperature (°C) |
| Charge HX (C-IHX) | Charge | 33.53 (steam)<br>915.5 (salt) | 306.9 (steam)<br>180 (salt) | 195.7 (water)<br>238.7 (salt) | 32.20 (steam)<br>889.32 (salt) | 308.1 (steam)<br>180.04 (salt) | 180.6 (water)<br>241.11 (salt) |
| Discharge HX (D-IHX) | Discharge | 26.83 (steam)<br>915.5 (salt) | 36.75 (water)<br>238.87 (salt) | 218 (stream)<br>180 (salt) | 25.7 (steam)<br>1126.8 (salt) | 39.10 (water)<br>240.41 (salt) | 240.50 (stream)<br>179.94 (salt) |
| Cold tank pump | Charge | 915.5 | 180 | 180 | 889.32 | 180.04 | 241.11 |
| Hot tank pump | Discharge | 915.5 | 238.7 | 238.7 | 1126.8 | 240.41 | 240.41 |
| TES power cycle pump | Discharge | 26.83 | 36.69 | 36.75 | 25.70 | 39.10 | 39.10 |
| FWH pump | Charge | 33.53 | 195.7 | 195.7 | 32.20 | 180.6 | 180.6 |
| NPP BOP pump | Charge | 30.39 | 36.86 | 37.05 | 31.33 | 41.50 | 41.50 |
| BOP condenser | Charge | 30.39 | 41.68 | 36.86 | 31.33 | 41.50 | 41.50 |
| BOP condenser pump | Charge | 1230 | 26.67 | 26.67 | - | - | - |
| TES condenser | Discharge | 26.86 | 41.67 | 36.69 | 25.70 | 39.00 | 39.00 |
| TES condenser pump | Discharge | 1300 | 26.66 | 26.67 | - | - | - |
| BOP turbine | Charge | 30.39 | 306.9 | 41.68 | 31.33 | 289.55 | 41.50 |
| BOP turbine | Discharge | 55.81 | 306.9 | 41.68 | 56.23 | 306.1 | 41.50 |
| TES turbine | Discharge | 26.83 | 218 | 41.67 | 25.66 | 240.13 | 39.02 |
| Molten salt | - | - | 238.7 (cold) | 180 (hot) | - | 240.4 (cold) | 179.94 (hot) |
| Cold/hot tanks | - | - | 238.7 (cold) | 180 (hot) | - | 240.4 (cold) | 179.94 (hot) |

Table 30. Comparison between the Aspen HYSYS® and Dymola® BOP power levels and turbine pressure drops of an A-LWR-TES coupling with a secondary power generation cycle and a HDR of 50%.

| | | ----------Aspen HYSYS®---------- | | | ----------Dymola®---------- | | |
|---|---|---|---|---|---|---|---|
| Equipment | Cycle | Mass Flow rate (kg/s) | Power (MW) | Pressure Drop (Bar) | Mass Flow rate (kg/s) | Power (MW) | Pressure Drop (Bar) |
| BOP turbine | Charge | 30.39 | 26.42 | 33.91 | 31.33 | 24.97 | 18.96 |
| TES turbine | Charge | - | - | - | 3.16 | 1.45 | 1.389 |
| Power Combined | Charge | - | 26.42 | 33.91 | - | 26.42 | - |
| BOP turbine | Discharge | 55.65 | 48.39 | 33.91 | 56.23 | 48.66 | 33.95 |
| TES turbine | Discharge | 26.84 | 18.99 | 33.91 | 25.66 | 18.56 | 11.73 |
| Power Combined | Discharge | - | 67.38 | 33.91 | - | 67.22 | - |

### 6.1.3 Transient Shakedown Results

The A-LWR-TES coupled system was run through severe cyclical ramping to establish expectations for how the system should respond to dynamic dispatching. The shakedown test forced the system to periodically ramp from full charging mode to a brief standby period. This was followed by a discharging

period, before the system demand immediately reverted back to full charging mode. By using such an aggressive demand profile, the model can be pushed to its extreme operating points, and it is possible to obtain initial evaluations of how a system may respond.

Figure 40–Figure 47 show the key results generated by the shakedown simulation of the A-LWR-TES. Figure 40 shows the imposed demand on the system and the corresponding electric generation. Aside from small demand misses immediately before and after demand ramps, the system was capable of meeting demand at all three power levels. Figure 41 shows the electricity production, by source, throughout the simulation. The BOP electricity fluctuated at each of the three levels as the system attempted to over-produce during times of TES discharge, and the TES operated via batch dispatch of heat. Figure 42 shows the feedwater temperature throughout the simulation. Feedwater temperature is a parameter of interest, as it sets the main steam generator conditions and can dramatically impact primary coolant conditions. Brief changes in feedwater temperature occur during these system changes, due to changes in system flow throughout the system. These alterations are brief, and by-and-large the control system responds and reestablishes the appropriate feedwater temperatures. Figure 43 shows the steam generator mass flow rate, which is also related to feedwater temperature. As the total steam mass flow rate suddenly increases or decreases due to pressure changes within the system, the feedwater temperature will correspondingly decrease or increase. This is due to the heating power within the feedwater system being much lower than the potential for heat acceptance by the feedwater (and is supplied by the steam generator). Thus, changes in the steam flow rate will result in feedwater temperature changes. Figure 44 shows that these changes in feed conditions do result in primary-side impacts within the nuclear core via coolant feedback mechanisms, but the control rods respond effectively and maintain the reactor power within +/- 5% of nominal power throughout the simulation.

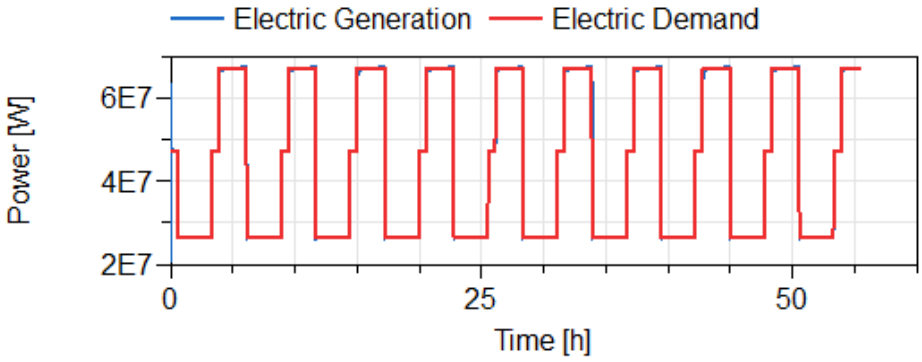


Figure 40. Electric demand and power production curves for the A-LWR-TES.

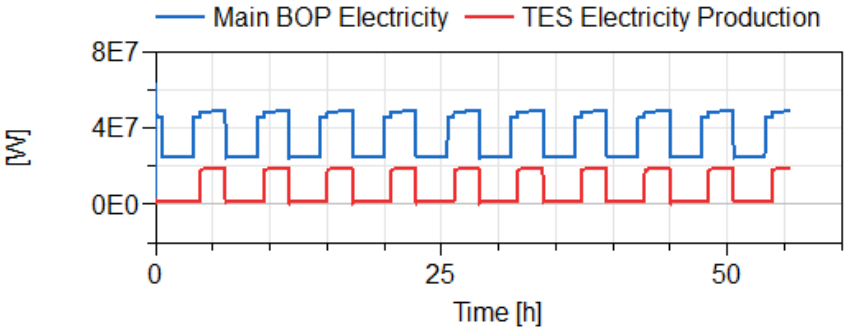


Figure 41. Power production from the primary BOP and TES BOP for the A-LWR-TES.

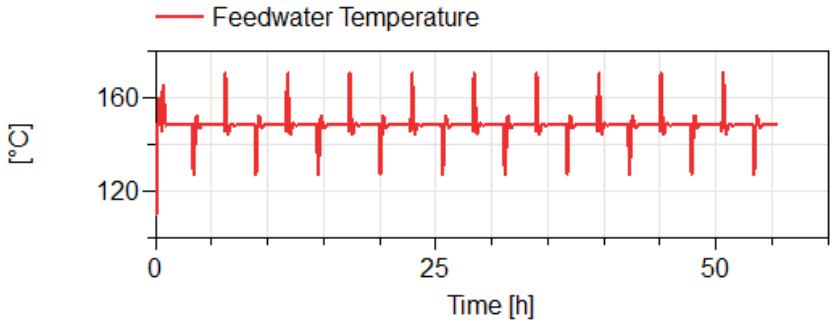


Figure 42. Feedwater temperature data for the A-LWR-TES.

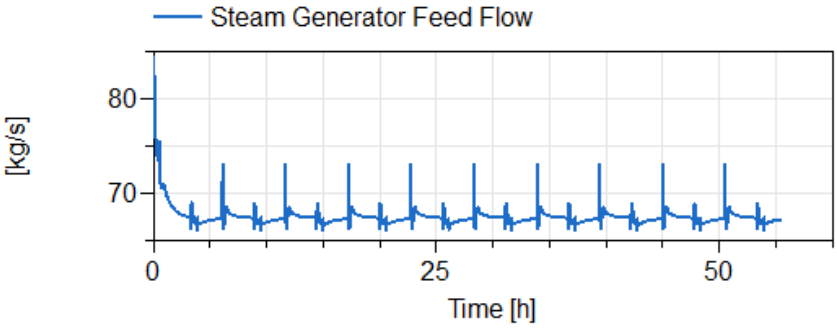


Figure 43. Steam generator mass flow rate for the A-LWR-TES.

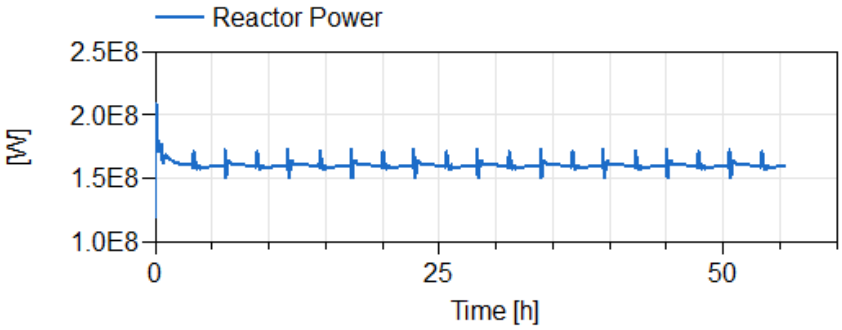


Figure 44. Reactor thermal power, mainly maintained within +/- 5% for the A-LWR-TES.

Figure 45 shows how much the valves had to cycle throughout this shakedown test in order to meet power demands while maintaining steam pressure. Additional cycling may be an issue, and having a good measure is important for future degradation studies. Figure 46 shows the relative steam charging and discharging mass flow rates. The impact of this is also seen in Figure 47, in which the tank levels are seen, revealing that the current shakedown test is charging too much relative to the amount of system discharging, thus causing the hot tank level to rise. During a shakedown test, perfectly even charging and discharging should not be expected. Only during extended (7+ days) dispatch should this be necessary.

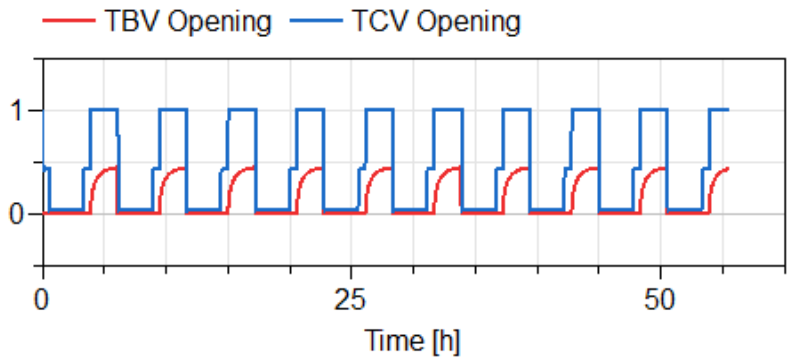


Figure 45. Valve opening profiles throughout the for the A-LWR-TES simulation (0 = closed and 1 = opened).

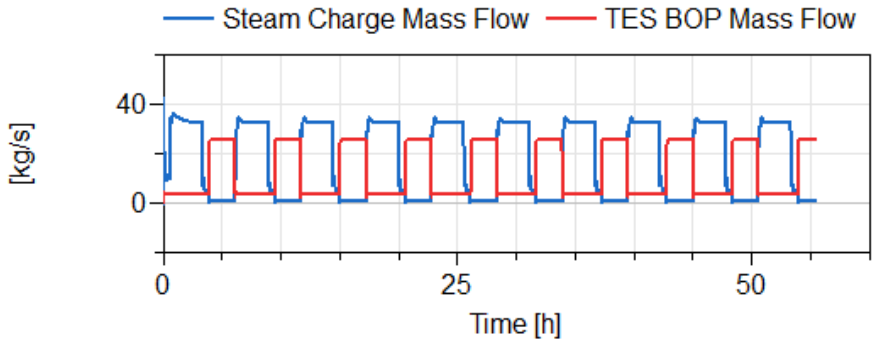


Figure 46. Steam charging mass flow rate and BOP production steam mass flow rate for the A-LWR-TES.

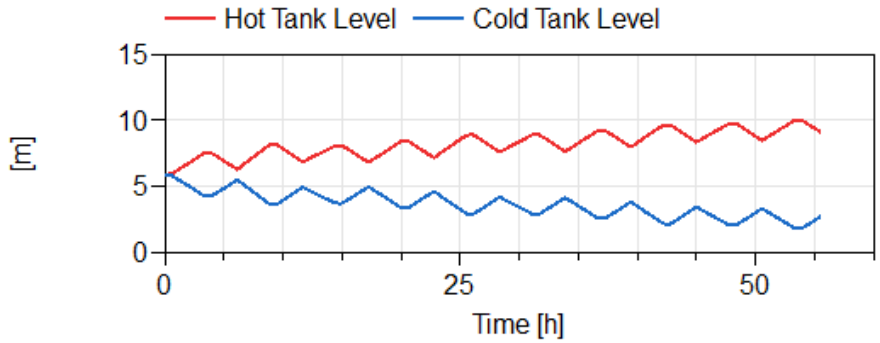


Figure 47. Tank levels throughout the for the A-LWR-TES simulation.

### 6.1.4 HERON Dispatch Demand Results

A sample HERON dispatch was taken from a debug run and slightly adjusted for use as an economic dispatch profile to demonstrate the linkage between HERON and HYBRID tools. Because of how the HERON evaluation is set up, there can be significant differences between the initial HYBRID model and HERON run outcomes. Namely, HERON seeks to optimize the size of separate subsystems based on their respective cost curves, which can lead to significant variation—specifically within the TES BOP system. In this case, the shakedown testing matched the initial HYSYS modeling, producing about 20 MWe from the TES BOP. Based on the cost curve, HERON expanded the size of the BOP to be able to produce 51 MWe. The BOP was expanded some to accommodate this change within the model.

Other adjustments that may be accounted for in future HERON runs include a minimum power rate from the TES BOP, which was set at 2 MWe in this case; changing the thermal-to-electric conversion efficiency in BOPs, based on the power rate; and, finally, setting a (now conventional within the IES team) 50% thermal bypass from the primary BOP. A minimum power rate on the TES BOP stems from two sources. The first is a modeling limitation: transient models tend to be computationally difficult when systems alter their operation mode too much. By requiring a minimum power rate, the entire TES BOP can always generate at least some power, and no zero-flow errors arise. The second is an as-of-yet poorly characterized but well-understood need to maintain at least hot standby conditions within a turbogenerator system. Because modeling is based on enthalpy and entropy calculations, the thermal and rotational ramping limits are avoided in turbogenerator modeling, and a simplifying assumption is used to simply maintain minimum power generation.

Power level changes were mainly scheduled to be 10-minute ramps, so a change from hour x to hour x+1 occurs from hour x:55:00 to hour x+1:05:00. Slightly longer ramps were implemented for hours 11 and 20, when the power was shifting from maximum discharge to maximum charge in order to allow the control systems appropriate time to keep up with the system. Figure 48 shows the difference in the dispatch profile when shorter ramps are imposed on the system. Note that while this figure covers hours 0 to 23, the plots that follow occur after a 2-hour period of steady-state nominal operation, and thus are plotted from hours 3 to 26.

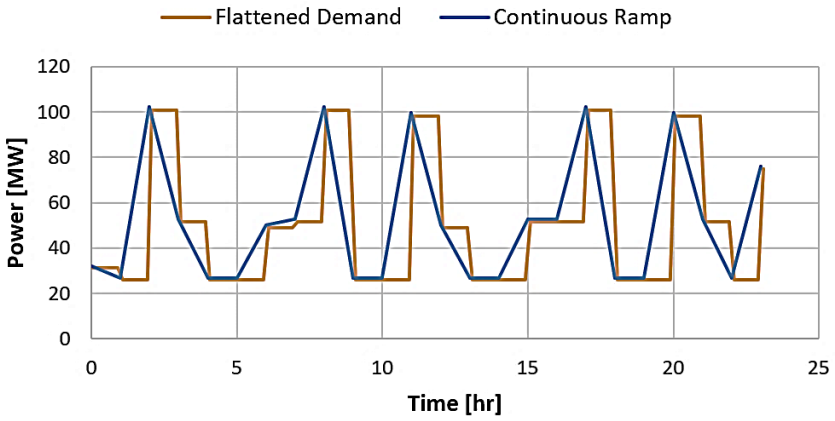


Figure 48. HERON dispatch demand, showing continuous ramp (linear connection between hourly setpoints) demand and ten-minute inter-hour ramping demand.

Figure 49 shows the IES electricity demand and production throughout the simulation. This value is generally matched, with the exception of some minor misses during peaking operation. This small mismatch may be due to an overestimation within the dispatch modeling of the nominal system efficiency. Figure 50 shows the TES BOP demand and dispatch profiles, which match up very well. The TES BOP, a much simpler system, meets the demand very well. Figure 51 shows the impact on reactor power as a result of this mode of operation. For the same reasons discussed in giving the shakedown results, the reactor power changes due to feedback, but system controls maintain +/- 5% operating conditions.

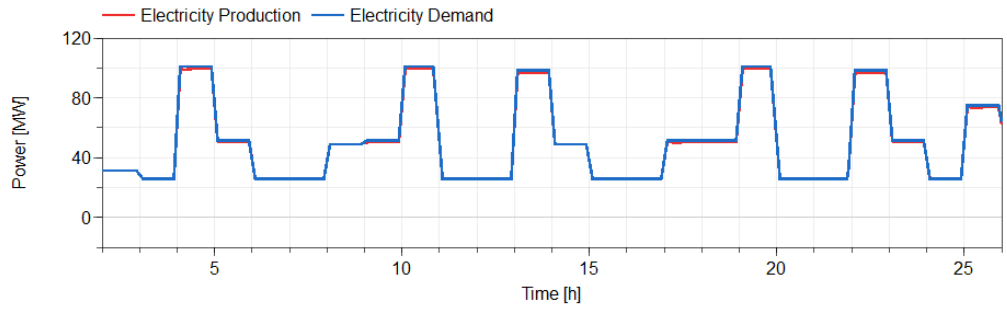


Figure 49. Electricity production vs. demand throughout a 24-hour dispatch test.

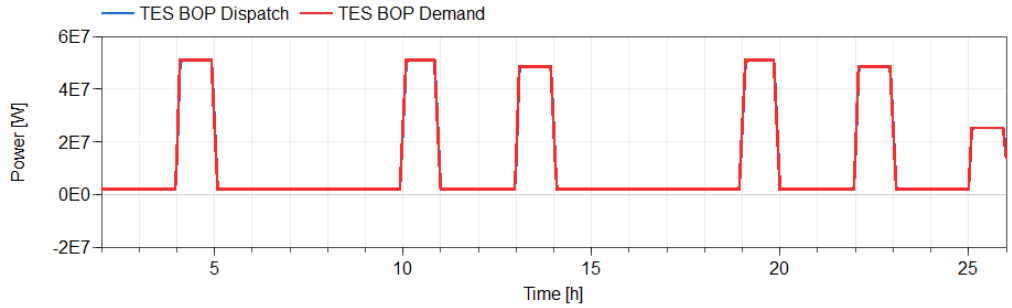


Figure 50. TES BOP dispatch throughout a 24-hour dispatch test.

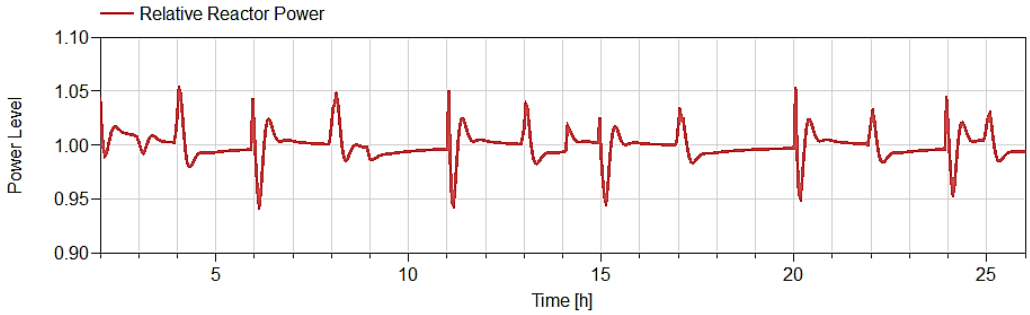


Figure 51. Relative reactor power throughout the dispatch test. The power is generally maintained within +/- 5% of nominal power.

Figure 52 shows the tank levels throughout this simulation. Overall, the system discharges more heat than was charged. The initial HERON simulation estimated that these values should be within 10% of each other. As stated previously, the addition of minimum thermal dispatch from the system is the likely reason and will be looked at in future analyses. Figure 53 shows the TES BOP efficiency declining during times of lower energy production. It should be noted that the integrated energy efficiency is much higher than the default average of the values in Figure 53, as the low efficiency correlates with a much smaller heat dispatch than does the higher efficiency value. Thus, the higher efficiency has a larger impact on full-length efficiency.

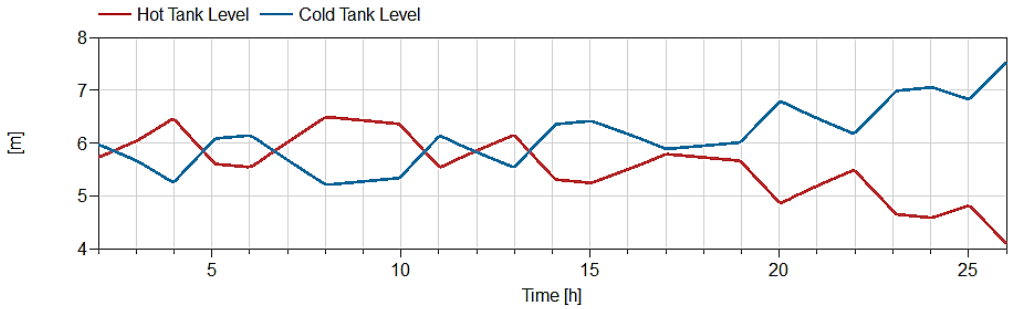


Figure 52. Hot and cold tank levels throughout the dispatch. On this sample day, more energy was discharged from the TES than was sent to the TES.

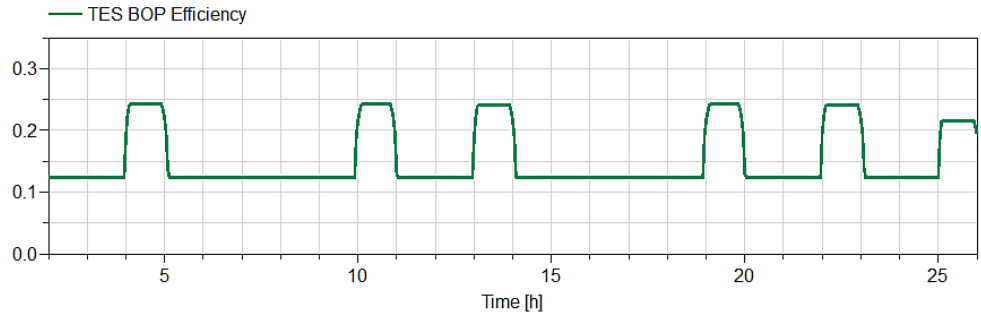


Figure 53. TES BOP thermal-to-electric conversion efficiency. Hot-standby minimum operating conditions are significantly less efficient than nominal operating conditions. The operating conditions, even under a highly expanded BOP size, align with steady-state modeling results.

## 6.2 Case 2: Directly Coupled NPP-TES System

As mentioned in Section 3.1.2, this case was not fully modeled for the A-LWR case due to its low financial potential. For this analysis, it was assumed that no changes would be made to the primary heat exchangers of the designs—as such, the efficiency loss of a system that transfers heat from liquid water to boil steam, and then condenses that steam to heat storage, followed by boiling to produce a new source of steam becomes too much loss to overcome. In the future, it may be possible to investigate whether molten salt could replace the steam in the primary steam generator, and then conduct the analysis for an A-LWR system; however, at present, more losses would occur in a latent-heat-to-sensible-heat-to-latent-heat conversion system than could be analyzed.

## 6.3 Case 3: Integrated NPP-TES Coupled with an Oversized Primary Turbine

This section shows the case 3 system design and offers a comparison with the HYSYS and system shakedown testing results. Future work will include a HERON dispatch for this kind of system. Case 3 reveals some different phenomena in the system BOP—phenomena that occur as the low-pressure turbine is supplied with steam from both the high-pressure turbine and the TES discharge.

### 6.3.1 Control Scheme

The control scheme in case 3 is adjusted slightly from the one in case 1, as there is no longer a separate turbogenerator system for TES dispatch. The D-TCV and D-FCV are currently a redundant pair of valves that both operate to meet electric power demands that exceed the nominal demand. This choice was made as a result of modeling experience having shown that two valves work better than one. Outside

of this change, the TBV, TCV, CCV, DCV, FWCP, and FHV all operate just the same as in case 1. The TBV continues operating to control the electrical output of the system. The TCV maintains the steam pressure, the FWCP maintains the feedwater mass flow rate, the FHV controls the feedwater temperature, and the CCV and DCV control the hot and cold tank temperatures. The setpoints for those control actions are summarized in Table 31, with placements shown in Figure 54.

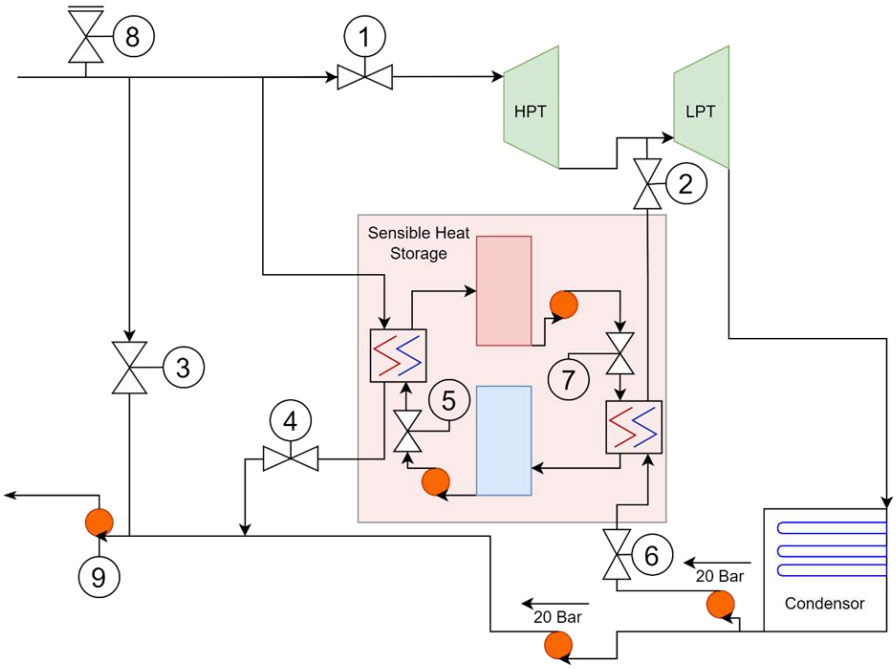


Figure 54. Block diagram describing the case 3 Modelica IES construction.

Table 31. Summary of the case 3 control setpoints.

| Label | Name | Controlling | Setpoint |
|---|---|---|---|
| 1 | Turbine Control Valve (TCV) | Steam Inlet Pressure (HPT) | 34 bar |
| 2 | Discharge Turbine Control Valve (D-TCV) | Power (Peaking) | If demand power > Q_nominal = demand power else is 0. |
| 3 | Feedwater Heating Valve (FHV) | Feedwater Temperature | 148°C |
| 4 | Turbine Bypass Valve (TBV) | Power (HPT and LPT) | Demand Power |
| 5 | Charging Control Valve (CCV) | SHS Hot Tank Temperature | 240°C |
| 6 | Discharging Feedwater Control Valve (D-FCV) | Power (Peaking) | If demand power > Q_nominal = demand power else is 0. |
| 7 | Discharging Control Valve (DCV) | SHS Cold Tank Entry Temperature | 180°C |
| 8 | Pressure Relief Valve | Pressure Overloads | Release at 150 bar |
| 9 | Feedwater Control Pump (FWCP) | Reactor Secondary Mass Flow | 67 kg/s |

### 6.3.2 Aspen HYSYS® Comparison with the Case 3 Dymola Model

As with case 1, the Dymola model is run under quasi-steady-state conditions that are assumed equivalent to the Aspen HYSYS® in terms of both charge and discharge. Table 32 and Table 33 give a comparison of the notable parameters in both models.

In this case, the difficulty in comparing the two models stems from the difference in the turbine configuration setups. The Dymola model more accurately reflects the proposed design, with the discharge steam being fed into an oversized LPT, whereas Aspen HYSYS models the oversized portion of the LPT as a separate turbine. This leads to discrepancies in the values (see Table 32 and Table 33). One result of the varied representations in the two models is that the discharge salt mass flow rate in Dymola differs from that in Aspen HYSYS®. The lower pressure upon entry into the LPT means that maintaining the same power from the discharge circuit requires a greater enthalpy rise in the steam side of the D-IHX. This requires a greater mass flow rate of Hitec to achieve the new enthalpy rise.

Again, it is worth noting that Dymola will not operate at zero-flow. For the case 3 model, the steam mass flow that must be maintained in the discharge loop in charge mode in the Dymola model is 2.51 kg/s.

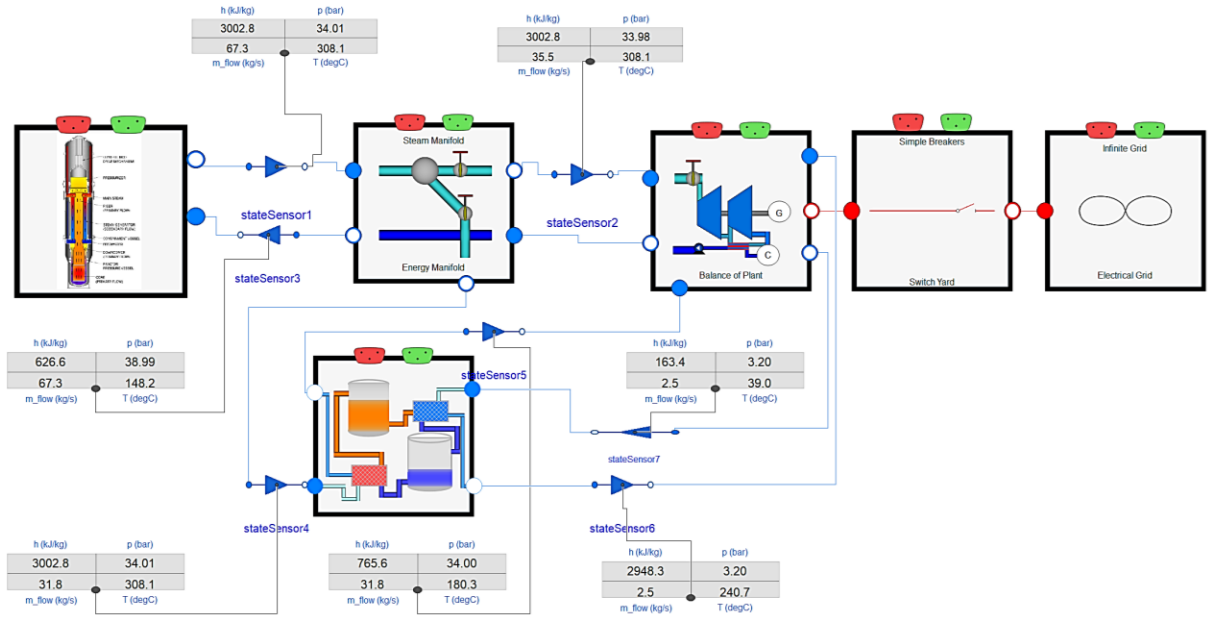


Figure 55. Modelica process flow diagram of an A-LWR-TES coupling with an oversized BOP cycle (the third coupling method) and a HDR of 50%, showing the active charge cycle and the inactive hot standby discharge cycle in hot standby mode.

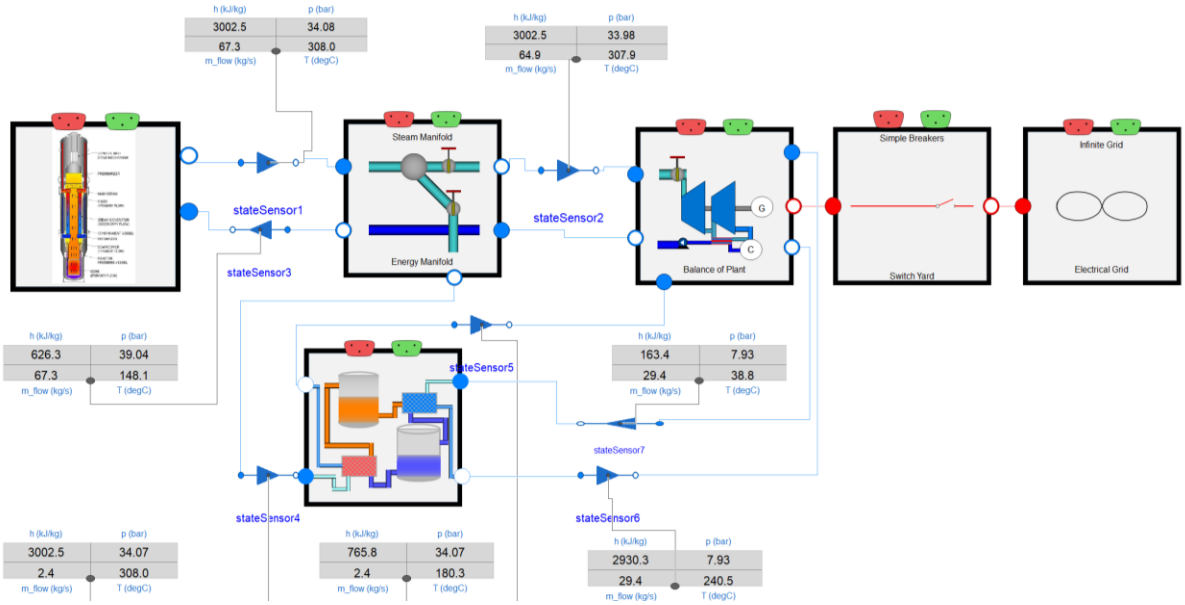


Figure 56. Modelica process flow diagram of an A-LWR-TES coupling with an oversized BOP cycle (the third coupling method) and a HDR of 50%, showing the BOP condition during the discharge cycle.

Table 32. Comparison between the Aspen HYSYS® and Dymola® BOP and operating conditions for an A-LWR-TES coupling with an oversized BOP cycle at a HDR of 50%.

| | | ----------Aspen HYSYS®---------- | | | ----------Dymola®---------- | | |
|---|---|---|---|---|---|---|---|
| Equipment | Cycle | Mass flow rate (kg/s) | Inlet temperature (°C) | Exit temperature (°C) | Mass flow rate (kg/s) | Inlet temperature (°C) | Exit temperature (°C) |
| Charge HX (C-IHX) | Charge | 33.53 (steam)<br>915.5 (salt) | 306.9 (steam)<br>180 (salt) | 195.7 (water)<br>238.7 (salt) | 31.8 (steam)<br>975.2 (salt) | 308.1 (steam)<br>179.9 (salt) | 180.3 (water)<br>240.5 (salt) |
| Discharge HX (D-IHX) | Discharge | 26.83 (steam)<br>915.5 (salt) | 36.75 (water)<br>238.87 (salt) | 218 (stream)<br>180 (salt) | 29.4 (steam)<br>1301.0 (salt) | 38.80 (water)<br>240.4 (salt) | 240.5 (stream)<br>179.7 (salt) |
| Cold tank pump | Charge | 915.5 | 180 | 180 | 975.2 | 179.9 | 179.9 |
| Hot tank pump | Discharge | 915.5 | 238.7 | 238.7 | 1301.0 | 240.4 | 240.4 |
| NPP BOP pump | Discharge | 55.65 | 36.69 | 36.75 | 54.47 | 39.00 | 38.59 |
| FWH pump | Charge | 33.53 | 195.7 | 195.7 | 31.8 | 180.3 | 180.3 |
| NPP BOP pump | Charge | 30.39 | 36.86 | 37.05 | 31.33 | 39.00 | 38.59 |
| BOP condenser | Charge | 30.39 | 41.68 | 36.86 | 33.77 | 39.02 | 39.00 |
| BOP condenser pump | Charge | 1230 | 26.67 | 26.67 | - | - | - |
| TES condenser | Discharge | 82.49 | 41.67 | 36.69 | 83.89 | 39.02 | 39.02 |
| TES condenser pump | Discharge | 3733 | 26.66 | 26.67 | - | - | - |
| BOP turbine_1* | Charge | 30.39 | 306.9 | 41.68 | 31.33 | 285.2 | 133.1 |
| BOP turbine_2 (LPT)** | Charge | - | - | - | 33.84 | 133.1 | 39.02 |
| BOP turbine_1* | Discharge | 55.65 | 306.9 | 41.68 | 54.47 | 300.81 | 189.91 |
| BOP turbine_2 (LPT)** | Discharge | 26.84 | 218 | 41.67 | 83.89 | 189.91 | 39.02 |
| Molten salt | - | - | 238.7 (cold) | 180 (hot) | - | 240.5(cold) | 179.9(hot) |
| Cold/hot tanks | - | - | 238.7 (cold) | 180 (hot) | - | 240.5(cold) | 179.9(hot) |

Table 33. Comparison between the Aspen HYSYS® and Dymola® BOP power levels and turbine pressure drops for an A-LWR-TES coupling with an oversized BOP cycle at a HDR of 50%.

| | | ----------Aspen HYSYS®---------- | | | ----------Dymola®---------- | | |
|---|---|---|---|---|---|---|---|
| Equipment | Cycle | Mass flow rate (kg/s) | Power (MW) | Pressure drop (Bar) | Mass flow rate (kg/s) | Power (MW) | Pressure drop (Bar) |
| BOP HPT turbine_1 | Charge | 30.39 | 26.42 | 33.91 | 31.33 | 9.70 | 12.82 |
| BOP LPT turbine_2 | Charge | - | - | - | 33.84 | 16.72 | 2.89 |
| BOP Combined | Charge | - | 26.42 | 33.91 | - | 26.42 | - |
| BOP HPT turbine_1 | Discharge | 55.65 | 48.39 | 33.91 | 54.47 | 13.39 | 20.23 |
| BOP LPT turbine_2 | Discharge | 26.84 | 18.99 | 11.91 | 83.89 | 53.76 | 7.73 |
| BOP Combined | Discharge | - | 67.38 | 33.91 | - | 67.15 | - |

* Aspen model: BOP Turbine 2 (LPT) represents only the additional power generated from the BOP turbine train due to the additional heat dispatched from TES.
**Dymola models: BOP Turbine 2 (LPT) represents the full oversized LPT, with flow entering from both the discharge circuit and the high-pressure turbine.

According to current HERON work, only case 1 involved a HERON dispatch run. In lieu of HERON dispatch runs for the other cases in the current study, some shakedown test results are given in the following section. Additional optimized HERON dispatch runs will be evaluated in future work.

### 6.3.3 Case 3 Shakedown Test Results

As with the case 1 shakedown test, the case 3 shakedown test involved cyclical demand changes to move the system from charging to nominal power to discharging and back to charging again. The impacts of this operation can be observed in Figure 57–Figure 62. Figure 57 shows that the case 3 system can be established physically, such that demand can be met even with challenging ramp rates between various power levels.

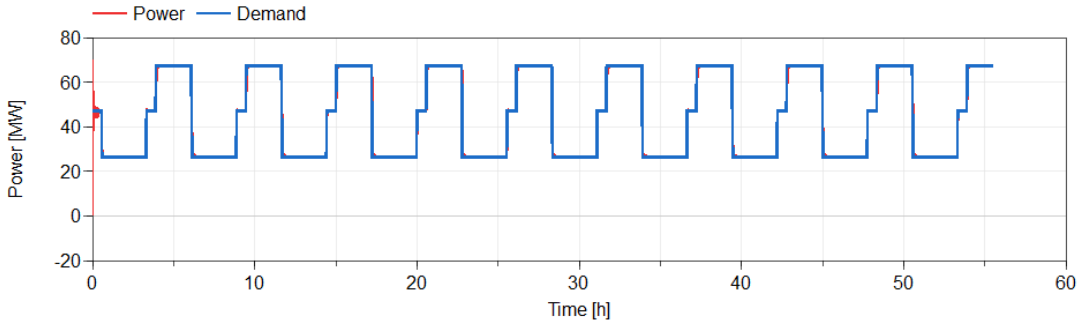


Figure 57. Power vs. demand in the case 3 shakedown test.

Figure 58 shows, on a single plot, the interaction between the feedwater temperature and the relative reactor power level. As feedwater temperatures increase or decrease, the opposite impact is seen on the reactor power level, due to the kinetics feedback associated with the corresponding increase or decrease in moderator temperature. While the control rods also move, the coolant temperature is the input to the control rod controlling algorithm. Thus, the feedback occurs first. The power shifts are more profound in case 3 than in case 1, at times exceeding +/- 10%.

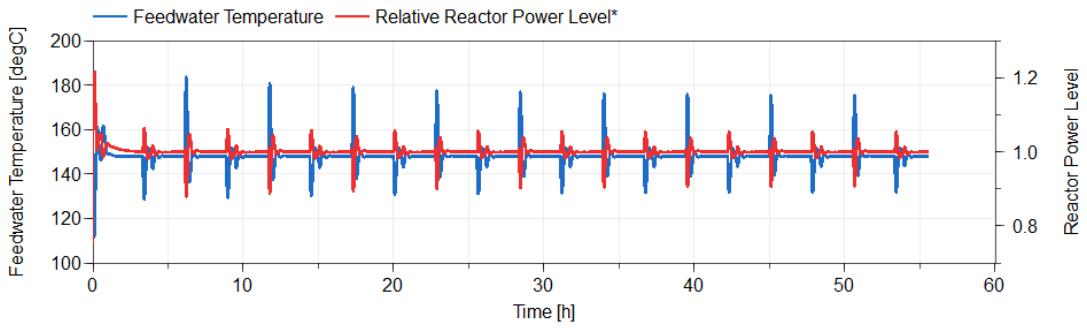


Figure 58. Feedwater temperature and relative reactor power level. Note the proportional and opposite behaviors.

Figure 59 shows the amount of cycling of various valves within the system. As noted in previous sections, this could lead to additional degradation within these components. Capturing this behavior may be very valuable. Figure 60 shows the hot and cold tank levels. The most interesting result is that a fully consistent cycle does not appear to be reached, even toward the end of the cycle. This is likely due to the extreme non-linearity of this integrated system, which could lead to a variety of precise setpoints (e.g., different valve position combinations) that meet the controller requirements.

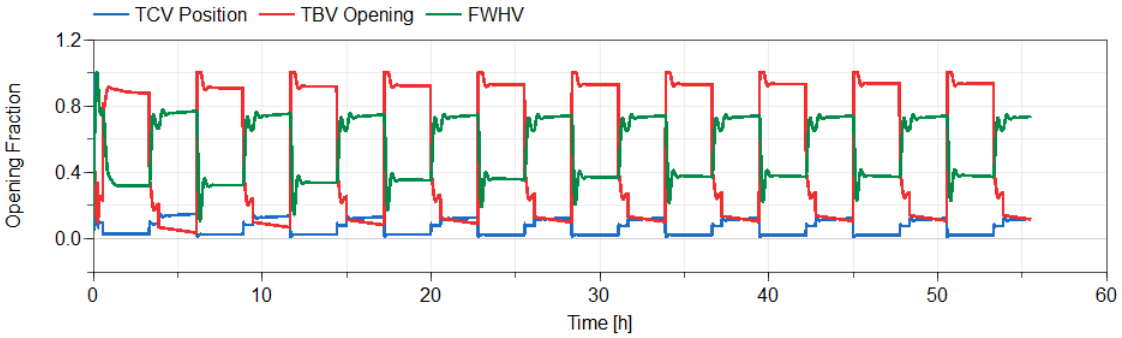


Figure 59. Various valve opening positions that cycle to various operating points, depending on the current system demand.

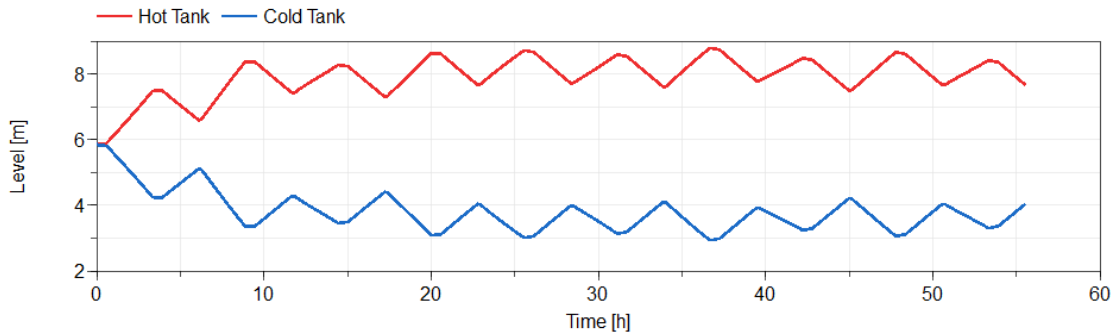


Figure 60. Hot and cold tank levels throughout the simulation.

Figure 61 and Figure 62 show how conditions within the low-pressure turbine change in accordance with different operating conditions. The pressure at the inlet of the LPT increases during discharge as the mass flow across the turbine more than doubles. This is an important design characteristic that must be taken into account in a deployed system. In Figure 62, the temperature change associated with changing operating modes is also observed. The temperature is lowest during charging, which is also when we see

the lowest pressure. As the saturation temperature decreases with pressure, this is an expected phenomenon. The opposite is true—with the temperature rising by nearly 50°C between the charging and discharging modes—as the pressure increases due to increase in net steam flow as steam flows from the TES discharge. Additional temperature rise occurs in discharge mode as the steam entering from the TES discharge is superheated, which may not be the case of the steam exiting the HPT. This is another system operating characteristic that should be evaluated before deployment in order to ensure that this thermal cycling behavior does not cause excess strain on the turbine.

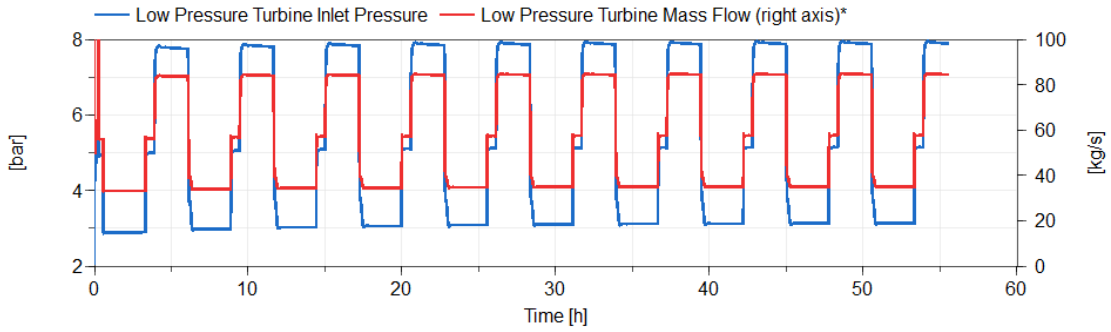


Figure 61. Low-pressure turbine inlet pressure and mass flow rate. Operating during discharge mode, when there is an increase in the mass flowing through the turbine, causes system pressure changes.

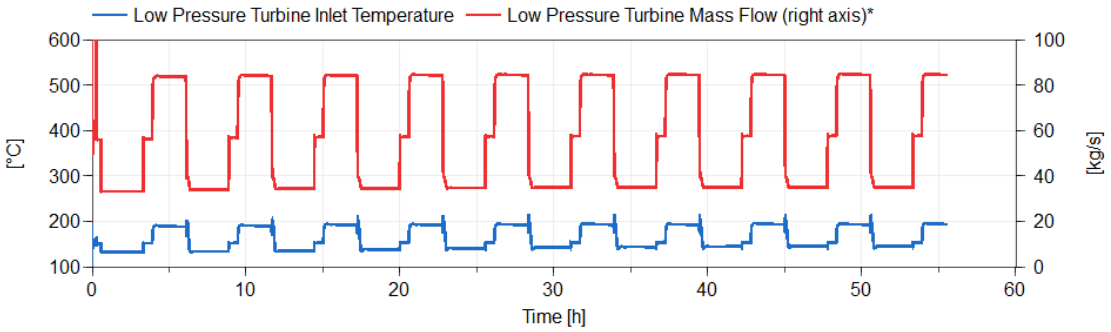


Figure 62. Low-pressure turbine inlet temperature and mass flow rate. Discharge operations cause temperature increases within the turbine.

# 7. CONCLUSIONS

This study evaluated three different TES coupling options for thermal power extraction from the A-LWR-type SMR (NuScale), HTGR (Xe-100), and LMFR (PRISM) candidates in order to enable flexible and hybrid plant operation. Using Aspen HYSYS, steady-state systems-level BOP models were developed to demonstrate the system design, optimum equipment sizing, and operating conditions for different coupling options involving various HDRs. The LWR and HTGR use cases were studied for three thermal energy bypass ratios and three different coupling options. The LMFR use case was studied for 50% thermal energy bypass for one coupling option. To conduct full-scale TEA of the various coupling options, the components in each model were sized using Aspen EDR, when applicable. Details on the sized components from the fully balanced LWR and HTGR models were fed back to APEA, operating conditions were reassigned based on optimum sizing, and the cost conditions for the individual pieces of equipment in relation to different system sizes were acquired. HTGR was found to have significant advantages over A-LWR when comparing the maximum temperature achievable by the TES—mainly due to the higher steam saturation temperature at the higher pressure. The cost functions from the individual-pieces-of-equipment subset were then used to generate superset models for the charge, storage, and discharge systems. Lessons learned and system design considerations to be taken into account in all

similar TES systems were discussed in detail. To date, the design discussed herein is specific to a few selected advanced reactors (A-LWR, HTGR, and LMFR). However, the coupling approach is intended to be generic such that it is valuable to A-NPPs and other reactor types that employ a steam turbine system for power generation. Thus far, dynamic modeling has been completed for the A-LWR.

In summary, the study successfully developed useful models and technical approaches to determine the capital and operating expenses of system components for use in the HERON/HYBRID TEA, determined accurate steady-state conditions for the selected examples that were then utilized to conduct Transient Process models and Control Schemes adopted in Modelica, demonstrated the capability to use HERON data within HYBRID transient physical models, and proved that the cases investigated to date are physically feasible in terms of dynamic operation.

The overall results obtained in this use case do not yet support any sweeping conclusions about the application of TES within a nuclear IES. The tools are in place to evaluate a variety of advanced reactor and TES technologies, as well as other potential markets. To date, the analysis team has focused on familiar systems to demonstrate the tools and analysis methods that could be more broadly applicable as more cases are studied using HERON for economic analysis, as well as HYBIRD modeling to establish and evaluate physical models.

# 8. FUTURE WORK

Investigation of additional reactor technologies: Additional LMFR models for the first coupling option with additional HDRs (25% and 10%), as well as for the third coupling option, will be created and their cost functions developed. The optimal system size and heat dispatch results will be generated from HERON, followed by transient-state modeling and optimized control schemes determined using HYBRID.

Investigation of heat extraction approaches: Other coupling methods, including single-phase to single-phase heat transfer will be investigated for a few selected reactor technologies. This would enable higher operating temperatures for the TES systems, thus reducing their size and CAPEX.

Heat dispatch optimization and investigation into additional markets and regions: HERON analyses will be conducted for the modified integrations between the various reactor types and TES systems, along with their respective cost functions. Additional markets such as California Independent System Operator (CAISO) and New York Independent System Operator (NYISO) will also be evaluated to gauge the electricity price volatility in those markets and evaluate whether those markets would be optimal for setting up advanced reactors coupled to TES systems.

Expansion of HYBRID models and scaling mechanisms: HYBRID modeling must expand with the technologies investigated in the future of this TES use case analyses. Additionally, within the models, it would be beneficial to introduce scaling mechanisms that allow for a single HYBRID Modelica model to operate at any power level assigned to it by HERON. Additionally, feedback needs to occur between HYBRID and HERON to inform the economic analyses of modeling limitations such as hot standby operating requirements. Thus far, HYBRID modeling has shown good agreement with the necessary demand profiles, based on the control systems established. As more advanced reactor concepts are investigated, control scheme analysis must continue to ensure that necessary operating conditions can be met. The HTGR and LMFR reactor models exist within HYBRID; these models will be integrated with TES models to evaluate candidate so the need for this work will be to integrate those models with storage to create the IES.

# 9. ACKNOWLEDGEMENTS

This work was supported by the DOE-NE IES program, with work conducted at INL under DOE Operations contract no. DE-AC07-05ID14517.

# 10. REFERENCES


[1] Saeed, R. M., K. L. Frick, A. Shigrekar, D. Mikkelson, and S. Bragg-Sitton. 2022. "Mapping thermal energy storage technologies with advanced nuclear reactors." *Energy Conversion and Management* 267:115872. https://doi.org/10.1016/j.enconman.2022.115872.

[2] Saeed, R. M., A. Shigrekar, K. L. Frick, and S. M. Bragg-Sitton. 2022. "Phenomenon Identification and Ranking Table Analysis for Thermal Energy Storage Technologies Integration with Advanced Nuclear Reactors." INL/EXT-21-65459. Idaho National Laboratory, Idaho Falls, Idaho. https://www.osti.gov/biblio/1875124.

[3] Frick, K., J. M. Doster, and S. Bragg-Sitton. 2018. "Design and operation of a sensible heat peaking unit for small modular reactors." *Nuclear Technology* 205(3):415-441. https://doi.org/10.1080/00295450.2018.1491181.

[4] Idaho National Laboratory. "HERON." Accessed September 2022. https://github.com/idaholab/HERON/wiki.

[5] Frick, K. L, A. Alfonsi, C. Rabiti, and D. M. Mikkelson. 2022. "Hybrid User Manual." INL/MIS-20-60624, revision 1. Idaho National Laboratory, Idaho Falls, Idaho. https://www.osti.gov/servlets/purl/1863262.

[6] Frick, K., C. T. Misenheimer, J. M. Doster, S. D. Terry, and S. Bragg-Sitton. 2018. "Thermal Energy Storage Configurations for Small Modular Reactor Load Shedding." *Nuclear Technology* 202(1):53-70. https://doi.org/10.1080/00295450.2017.1420945.

[7] Wang, K., Z. Qin, W. Tong, and C. Ji. 2020. "Thermal Energy Storage for Solar Energy Utilization: Fundamentals and Applications." In *Renewable Energy - Resources, Challenges and Applications* edited by M. A. Qubeissi, A. El-Kharouf, and H. S. Soyhan. London: IntechOpen. https://doi.org/10.5772/intechopen.91804.

[8] Hoffman, H. W., and S. I. Cohen. 1960. "Fused Salt Heat Transfer–Part III: Forced—convection Heat Transfer in Circular Tubes Containing the Salt Mixture NaNO2-NANO3 -KNO3." ORNL-2433. Oak Ridge National Laboratory, Oak Ridge, Tennessee. http://doi.org/10.2172/4181833.

[9] Knighton, L. T., A. Shigrekar, D. S. Wendt, K. Frick, R. D. Boardman, A. A. Elgowainy, A. Bafana, H. Tun, and K. R. Reddi. 2021. "Energy Arbitrage: Comparison of Options for use with LWR Nuclear Power Plants." INL/EXT-21-62939. Idaho National Laboratory, Idaho Falls, Idaho.

[10] Kolb, G. J., C. K. Ho, T. R. Mancini, and J. A. Gary. 2011. "Power Tower Technology Roadmap and Cost Reduction Plan." SAND2011-2419. Sandia National Laboratories, Albuquerque, New Mexico. http://stage-ste.psa.es/documents/CR%203%202011%20SANDIA%20Power%20Tower.pdf.

[11] Glatzmaier, G. 2011. "Developing a cost model and methodology to estimate capital costs for thermal energy storage." NREL/TP-5500-53066. National Renewable Energy Laboratory, Golden, Colorado. https://www.nrel.gov/docs/fy12osti/53066.pdf.

[12] U. S. Bureau of Labor Statistics. "Producer Price Index by Industry: Chemical Manufacturing (PCU325325)." FRED, Federal Reserve Bank of St. Louis. Accessed September 2022. https://fred.stlouisfed.org/series/PCU325325.

[13] U.S. Nuclear Regulatory Commission. "Application Documents for the NuScale Design." Accessed March 24, 2022. https://www.nrc.gov/reactors/new-reactors/smr/nuscale/documents.html.

[14] NuScale Power, LLC. 2020. “Chapter Ten, Steam and Power Conversion System, PART 2 – TIER 2.” Revision 5. *NuScale Standard Plant Design Certification Application* https://www.nrc.gov/docs/ML2022/ML20224A499.pdf.

[15] Brits, Y., and J. Crowell. 2020. “X-Energy: Xe-100 Reactor The Key To An Integrated Energy System, Reliable Baseload, Agile Load Following, Industrial Applications.” In “Flexible Nuclear Energy for Clean Energy Systems.” NREL/TP-6A50-77088. NICE Future. https://www.nice-future.org/assets/pdfs/x-energy.pdf.

[16] Kearney, D. W. et al. 2003. “Overview on Use of a Molten Salt HTF in a Trough Solar Field.” NREL/PR-550-40028. *NREL Parabolic Trough Thermal Energy Storage Workshop* Golden, Colorado. https://www.nrel.gov/docs/fy03osti/40028.pdf.

[17] U. S. Nuclear Regulatory Commission. 1987. "PRISM$_{TM}$ - Preliminary Safety Information Document.” Volume II, Chapters 5-8. GEFR-00793. https://www.nrc.gov/docs/ML0828/ML082880395.pdf.

[18] Triplett, B., E. Loewen, and B. Dooies. 2012. "PRISM: A Competitive Small Modular Sodium-Cooled Reactor." Nuclear Technology 178(2):186-200. https://doi.org/10.13182/NT178-186.

[19] Boerema, N., G. Morrison, R. Taylor, and G. Rosengarten. 2012. “Liquid sodium versus Hitec as a heat transfer fluid in solar thermal central receiver systems.” *Solar Energy* 86(9):2293-2305. https://doi.org/10.1016/j.solener.2012.05.001.

[20] Idaho National Laboratory. “RAVEN.” Accessed September 2022. https://github.com/idaholab/raven.

[21] Frick, K. 2019. “Status report on the NuScale module developed in the Modelica framework.” INL/EXT-19-55520. Idaho National Laboratory, Idaho Falls, Idaho. https://doi.org/10.2172/1569288.

[22] Mikkelson, D., A. Shigrekar, S. Hancock, K. Frick, and A. Epiney. 2022. “Delivery of dynamic thermal energy storage models and advanced reactor concept models to the HYBRID repository.” INL/RPT-22-68222. Idaho National Laboratory, Idaho Falls, Idaho. https://doi.org/10.2172/1881858.

# APPENDIX A

# NuScale Detailed Model